Fakultät für Mathematik, Informatik und Naturwissenschaften | RWTH AACHEN UNIVERSITY

Excitatory/inhibitory imbalance in schizophrenia: a multimodal approach

Von der Fakultät für Mathematik, Informatik und Naturwissenschaften der RWTH Aachen University zur Erlangung des akademischen Grades einer Doktorin der Naturwissenschaften genehmigte Dissertation

vorgelegt von

Mariia Suslova, M.Sc.

aus

St. Petersburg, Russland

Berichter:

Prof. Dr. Martin Zenke

Prof. Dr. Marc Spehr

Jun.-Prof. Dr. Arnim Gaebler

Prof. Dr. Angelika Lampert

Tag der mündlichen Prüfung*: 03.06.2025*

Contents

Zusammenfassung 4

Summary 5

Abbreviations 6

1. Introduction 7

1.1 Overview of schizophrenia 7

1.2 Etiology of schizophrenia 8

1.3 Excitatory/Inhibitory imbalance 9

1.4 Sodium channels in the context of schizophrenia 10

1.4.1 Function and structure of the VGSC 10

1.4.2 Expression patterns of VGSC 15

1.4.3 NaV1.2 function and localization 16

1.4.4 NaV1.2 implication in neuropsychiatric disorders 17

1.4.5 Schizophrenia-associated variants in NaV1.2 17

1.5 NMDAR hypothesis of schizophrenia 18

1.6 Experimental approaches to study schizophrenia 22

1.6.1 Utilising HEK cells in studying schizophrenia-related mutations in NaV1.2 channel 23

1.6.2 Modelling schizophrenia with iPSC-derived neurons 23

1.7 Aim of the project 27

2. Materials and methods 28

2.1 Molecular biology / Generation of the NaV1.2 variants 28

2.2 HEK cell culture 28

2.3 Reprogramming of the PBMCs / Generation of iPS cells 28

2.4 Differentiation of iPS cells into CNS neurons 29

2.5 Electrophysiology 31

2.5.1 Voltage clamp recordings in HEK cells 31

2.5.2 Current clamp recordings in iPSC-derived neurons 32

2.5.3 Voltage clamp recordings in iPSC-derived neurons 32

2.6 Data analysis 33

2.7 Immunostaining 34

2.8 Real-time polymerase chain reaction 35

2.9 Calcium imaging 36
3 Results 37
3.1 Effect of schizophrenia-associated mutations in NaV1.2 37
3.1.1 R850P and V1282F alter voltage dependence of activation, S1656P abolishes the activation current 37
3.1.2 R850P alters voltage dependence of inactivation 39
3.1.3 R850 affects subthreshold depolarization 40
3.1.4 R850P modifies the use-dependent block 41
3.1.5 R850P impacts recovery from fast inactivation 43
3.2 Two new iPS cell lines of patients with schizophrenia 45
3.3 Testing glutamatergic neuronal differentiation on iPS cells 49
3.4 Proof of principle of NMDAR recordings in iPSC-derived neurons 51
3.5 Testing GABAergic differentiation on iPS cells 55
4 Discussion 58
4.1 Effect of NaV1.2 variants 58
4.1.1 R850P variant causes diverse LoF effects on NAV1.2 electrophysiology .. 58
4.1.2 V1282F variant has a moderate effect on NaV1.2 function 60
4.1.3 S1656P variant results in a non-functional sodium channel 60
4.1.4 Other findings, implicating NaV1.2 in pathogenesis of schizophrenia or psychosis 62
4.1.5 Implication of NaV1.1, 1.3, and 1.6 in schizophrenia 63
4.1.6 NaV1.2 loss-of-function implication in E/I imbalance 64
4.2.1 Modulation of NaV1.2 as a potential mechanism of E/I imbalance 65
4.1.7 Interactions between sodium channels and NMDARs 66
4.2 Modelling schizophrenia using iPSCs 67
4.2.1 Establishment of schizophrenia patient iPS cell lines 67
4.2.2 Glutamatergic neuronal differentiation and schizophrenia pathology 67
4.2.3 Electrophysiological characterization of iPSC-derived neurons 68
4.2.4 GABAergic differentiation in iPSCs 68
4.2.5 Possible origins of NMDAR dysfunction in schizophrenia 68
4.2.6 iPSC-based models of schizophrenia 69
4.3 Limitations 71
5 Conclusion and outlook 73

6 References 74
7 List of figures 82
8 List of tables 83
9 Declaration of authorship 84
10 Appendix 85

Zusammenfassung

Schizophrenie (SZ) ist eine komplexe Störung, welche gemeinsam die normale Gehirnfunktion beeinträchtigen und die soziale Funktionsfähigkeit sowie die Lebensqualität der Patient*innen erheblich beeinflussen. Die Ätiologie der Störung ist multifaktoriell und umfasst genetische, neurobiologische und umweltbedingte Faktoren. Forschungen haben ein Ungleichgewicht zwischen exzitatorischer und inhibitorischer (E/I) Neurotransmission als einen zentralen Bestandteil der Pathophysiologie der SZ hervorgehoben. Diese Dysregulation kann auf Anomalien im Glutamatsystem zurückzuführen sein, einschließlich Funktionsstörungen in spannungsgesteuerten Natriumkanälen (VGSCs) wie NaV1.2 oder in N-Methyl-D-Aspartat-Rezeptoren (NMDARs), die beide eine wesentliche Rolle bei der Aufrechterhaltung der neuronalen Erregbarkeit und der Netzwerkintegrität spielen.

Spannungsgesteuerte Natriumkanäle sind entscheidend für die neuronale Erregbarkeit, und Varianten im SCN2A-Gen (kodierend für NaV1.2) werden mit SZ in Verbindung gebracht. Diese Mutationen, die oft zu einem Funktionsverlust (LoF) führen, verändern die Schalteigenschaften des Kanals und können potenziell zu einem exzitatorischen/inhibitorischen Ungleichgewicht beitragen. In dieser Arbeit habe ich folgende, spezifische, mit Schizophrenie assoziierte SCN2A-Varianten charakterisiert: R850P, V1282F und S1656P. Mittels Patch-Clamp-Elektrophysiologie konnte ich zeigen, dass alle drei Varianten einen Funktionsverlust für NaV1.2 bewirken.

Um die NMDAR-Hypothese der SZ weiter zu untersuchen, generierte ich induzierte pluripotente Stammzellen (iPSCs) aus SZ-Patienten und differenzierte sie zu Neuronen, um die NMDAR-Funktionsstörungshypothese der SZ zu erforschen. Ich etablierte Protokolle, um die NMDAR-Funktion direkt mittels Patch-Clamp und Calcium-Imaging zu untersuchen, mit dem Ziel, das E/I-Gleichgewicht in patientenspezifischen Zellmodellen zu bewerten.

Die Ergebnisse zeigen, dass NaV1.2 LoF-Varianten zum E/I-Ungleichgewicht bei SZ beitragen und dass die Etablierung patientenspezifischer iPSC-Modelle wertvolle Einblicke in NMDAR-bezogene Mechanismen bieten und eine Plattform zur Erprobung potenzieller pharmakologischer Interventionen darstellen könnte. Dieser duale Ansatz deutet darauf hin, dass die Modulation von VGSCs zusammen mit gezielten NMDAR-Therapien ein therapeutisches Potenzial zur Behandlung der Symptome der Schizophrenie haben könnte.

Summary

Schizophrenia (SZ) is a complex disorder that collectively disrupt normal brain function, significantly impacting patients' social functioning and quality of life. The disorder's etiology is multifactorial, involving genetic, neurobiological, and environmental factors. Research has emphasized an imbalance in excitatory and inhibitory (E/I) neurotransmission as a core component of SZ pathophysiology. Dysregulation in this balance may stem from abnormalities in the glutamate system, including dysfunctions in voltage-gated sodium channels (VGSCs / NaV) like NaV1.2, or in N-methyl-D-aspartate receptors (NMDARs), both of which play crucial roles in maintaining neuronal excitability and network dynamics.

Voltage-gated sodium channels play a crucial role in neuronal excitability, and variants in SCN2A gene (encoding NaV1.2) are associated with SZ. These variants, often resulting in loss-of-function (LoF) effects, have been shown to alter channel kinetics, potentially leading to excitatory/inhibitory dysregulation. In this thesis, I characterized specific schizophrenia-linked SCN2A variants — R850P, V1282F, and S1656P using HEK293T cells as a heterologous expression system. Employing patch clamp electrophysiology, I demonstrated that all three of them have loss-of-function effects on NaV1.2 function.

To further investigate the NMDAR hypothesis of SZ, I generated induced pluripotent stem cells (iPSCs) from patients with SZ and established the protocols to differentiate them into central cortical neurons and directly examine NMDAR function via patch clamp and calcium imaging, aiming to assess E/I balance in patient-specific cellular models.

The respective findings underscore that NaV1.2 LoF variants may contribute to E/I imbalance in SZ, and the establishment of patient-specific iPSC models could offer valuable insights into NMDAR-related mechanisms of SZ. These cellular models may provide a platform for testing potential pharmacological interventions. This dual approach suggests that VGSC modulation, along with targeted NMDAR therapies, may hold therapeutic potential in managing the symptoms of schizophrenia.

Abbreviations

AIS Axon Initial Segment

AP Action Potential

ASD Autism Spectrum Disorder

BMP Bone Morphogenetic Protein

cAMP Cyclic Adenosine MonoPhosphate

CNS Central Nervous System

DMEM Dulbecco's modified eagle medium

E/I Excitatory/inhibitory

EDTA EthyleneDiamineTetraacetic Acid

eGFP Enhanced Green Fluorescent Protein

ESC ExtraCellular Solution

FGF Fibroblast Growth Factor

fMRI Functional Magnetic Resonance Imaging

GABA Gamma-Aminobutyric Acid

GAD67 Glutamic acid decarboxylase 67

GoF Gain-Of-Function

HEK Human Embryonic Kidney

HEPES 4-(2-hydroxyl)-1-piperazineethanesulfonic acid

ICS IntraCellular Solution

ID Intellectual Disability

iPSC Induced Pluripotent Stem Cells

LoF Loss-Of-Function

MEF Mouse Embryo Fibroblast

MMN Mismatch Negativity

NMDAR N-Methyl-D-Aspartate receptor

NO Nitric Oxide

NPC Neural Progenitor Cell

(d)PBS (Dulbecco's) Phosphate-Buffered Saline

(q)PCR (Quantitative) Polymerase Chain Reaction

PBMC Peripheral Blood Mononuclear Cell

PCP Phencyclidine

PET Positron Emission Tomography

PPI PrePulse Inhibition

RA Retinoic Acid

RMP Resting Membrane Potential

SHH Sonic Hedgehog

SNP Single Nucleotide Polymorphism

SRR Serine Racemase

SZ Schizophrenia

$V_{1/2}$ Half maximal activation or fast/slow inactivation voltage

VGSC Voltage-gated sodium channel

VSD Voltage-Sensing Domain

WNT Wingless

WT Wild-Type

1. Introduction

1.1 Overview of schizophrenia

Schizophrenia (SZ) is a complex and severe mental disorder characterized by various disturbances of perception, cognition and emotions. It is characterized by symptoms that can be divided into three groups. Positive symptoms consist of hallucinations, delusions, impulsivity and aggression (Hoptman 2015). Negative symptoms include avolition (decreased activity), anhedonia, asociality, blunted affect and alogia (decreased speech) (Correll and Schooler 2020). Lastly, cognitive symptoms involve deficits in memory, executive function, and attention.

Schizophrenia reduces life expectancy by around 20% and is associated with further psychiatric and somatic comorbidities such as diabetes, cardiovascular diseases, etc. (Kahn et al. 2015; Laursen, Nordentoft, and Mortensen 2014). Due to the resulting functional impairment, it represents one of the most debilitating diseases. Importantly, the patients have severe difficulties maintaining social relationships, employment and independent life (Harvey 2014).

The risk factors of schizophrenia are a combination of genetic, neurobiological, environmental, and psychosocial influences. Early-life contributors include pregnancy and birth complications, maternal malnutrition, and advanced paternal age (Malaspina et al., 2001; Mcgrath et al., 2014). The male sex also contributes to onset probability and severity of the disease (Räsänen et al. 2000). Additionally, urban environment, migration status and social adversities are proven risk factors (Kahn et al. 2015).

Schizophrenia also has a strong genetic component, with recent genomic studies identifying many specific DNA variants linked to the disorder. It is now understood to be polygenic, i.e. involving numerous risk alleles. Some of the identified risk alleles or genes overlap with those of other neuropsychiatric disorders like bipolar disorder, intellectual disability, and autism spectrum disorder. Key genetic findings include *de novo* variants, rare copy number variations, rare single nucleotide variants, small insertions/deletions, tandem repeats, and common single nucleotide polymorphisms (SNPs) that vary in their contribution to the disease risk (Rees, O'Donovan, and Owen 2015).

Psychotic symptoms in schizophrenia usually emerge between ages 18 and 25, with earlier, subtler signs often appearing in the prodromal phase. These include delayed developmental milestones, reduced childhood IQ, and cognitive decline shortly before psychosis onset. The prodromal phase is a key period for potential early intervention (Insel 2010).

Despite the large burden schizophrenia is putting on patients, health system and economy, so far there is no clear understanding of the underlying molecular mechanisms of the disease. Moreover, no available therapy could ease all positive, negative and cognitive

symptoms for a sufficiently big fraction of patients. One of the reasons may be the large complexity of genetic and environmental factors causing the disease. Another reason is the general issue of studying psychiatric diseases – the living human brain tissue is not available for experiments on the cellular level and animal models cannot represent the full mental phenotype of the disease.

1.2 Etiology of schizophrenia

Due to the complexity and heterogeneity of schizophrenia, consensus regarding its origin remains elusive. Over time, the understanding of schizophrenia has been evolving, with new theories emerging to account for its diverse manifestations.

In the 1950s, the contrasting effects of amphetamine and neuroleptics on both psychotic patients and healthy individuals inspired the dopaminergic hypothesis of schizophrenia. Amphetamine or cocaine, acting as dopamine receptor agonists, were observed to cause psychosis closely resembling paranoid schizophrenia. Conversely, chlorpromazine and other neuroleptic medications, which block dopamine receptors, demonstrated efficacy in alleviating psychotic symptoms (Willner 1997).

However, the dopaminergic hypothesis does not fully explain all aspects of the disorder. Despite supporting evidence from animal studies, post-mortem research, and clinical drug effects, the dopamine hypothesis of schizophrenia lacks strong genetic backing (McCutcheon, Krystal, and Howes 2020). Positron Emission Tomography (PET) studies on dopamine levels in patients with schizophrenia are not consistent for all investigated brain regions. Moreover, around 30% of individuals do not respond to dopamine-blocking antipsychotic medications (Kahn et al. 2015). Additionally, dopamine dysregulation alone may not fully account for the cognitive and negative symptoms of schizophrenia (Correll and Schooler 2020). While antipsychotic medications that target dopamine receptors are indeed effective in treating positive symptoms of schizophrenia in around 60-70% of patients, they are less effective for negative and cognitive symptoms (Insel 2010). This suggests that the dopaminergic dysregulation is likely secondary to abnormalities in other systems, particularly the glutamatergic system, and is significantly influenced by environmental factors.

The next milestone in understanding schizophrenia pathology was the glutamatergic hypothesis. The effect of the noncompetitive glutamate antagonist, phencyclidine (PCP) provided one of the first supporting evidence. In healthy individuals, it induced symptoms similar to those of schizophrenia, while in patients it worsened their symptoms, suggesting a role for glutamate dysregulation in the disorder (S. H. Snyder 1980). Another drug with a similar effect was ketamine. Like PCP, it is a noncompetitive blocker of N-Methyl-D-Aspartate receptor (NMDAR) (Lahti et al. 1995). Therefore, dysregulation of glutamatergic neurotransmission was assumed to be at the core of the disease pathophysiology.

Understanding the interactions among schizophrenia etiological factors is crucial for developing more effective strategies for prevention, early intervention, and treatment of schizophrenia. Moreover, the considerable heterogeneity of the clinical phenotype as well as

the polygenetic architecture may suggest the existence of distinct pathophysiological mechanisms.

1.3 Excitatory/Inhibitory imbalance

A shared principle of main hypotheses on schizophrenia pathogenesis suggests that overall disruptions in the delicate balance between excitatory and inhibitory neurotransmission (E/I imbalance) contribute to the cognitive, affective, and perceptual disturbances observed in the disorder.

One possible way E/I imbalance can contribute to the pathophysiology of schizophrenia is the abnormality in the cortical circuit refinement. This is of particular importance during early adulthood when the onset of schizophrenia commonly occurs. During this stage, cortical circuits undergo significant developmental changes, involving the pruning of excitatory synapses, the proliferation of inhibitory circuits, and the remodeling of pyramidal dendrites. These processes play a crucial role in fine-tuning the balance between excitatory and inhibitory activity in the cortex. However, disruptions during this critical period such as excessive excitatory pruning and the following reduced interneuron activity may contribute to the manifestation of schizophrenia, as it exacerbates pre-existing neurodevelopmental deficits (Ahmad et al. 2018).

Pharmacological, clinical, and genetic evidence highlights the involvement of NMDARs in schizophrenia. Subanesthetic doses of NMDAR antagonists can induce schizophrenia-like symptoms in healthy individuals (Javitt and Zukin 1991; S. H. Snyder 1980), and the symptoms of anti-NMDAR encephalitis resemble those of schizophrenia (Dalmau et al. 2019). Genetic studies have further identified SNPs and rare exonic variants in genes associated with the NMDAR complex as linked to schizophrenia (Rees, O'Donovan, and Owen 2015).

Dysfunction of NMDARs on GABAergic interneurons is particularly implicated in the disorder's pathophysiology. There is substantial evidence that reduced NMDAR function in these interneurons leads to excitation/inhibition imbalance (Belforte et al. 2010; Hyun, Inoue, and Hayashi-Takagi 2020). Moreover, NMDAR antagonists at subanesthetic doses preferentially affect GABAergic interneurons, further disrupting E/I balance (Lisman et al. 2008).

Gamma-Aminobutyric Acid (GABA) is the brain's primary inhibitory neurotransmitter, and its dysfunction can lead to E/I imbalance. Deficits in GABA synthesis, release, and signaling have been implicated in schizophrenia, contributing to cortical hyperactivity and impaired synchronization of neural networks (de Jonge et al. 2017; Xu and Wong 2018). *Postmortem* studies have demonstrated decreased glutamic acid decarboxylase (GAD67) and parvalbumin (calcium-binding protein found in fast-spiking GABAergic interneurons) levels, as well as a reduction in the axon terminal density of chandelier interneurons in patients with schizophrenia (Hashimoto et al. 2003; Pierri et al. 1999). Reduced GABAergic inhibition may contribute to hyperactivity in cortical circuits and impaired synchronization of neural networks, leading to cognitive deficits and psychotic symptoms. Further evidence of E/I

imbalance in schizophrenia comes from MR spectroscopy studies demonstrating increased glutamate/glutamine or altered GABA levels in schizophrenia (Marsman et al. 2014; Merritt et al. 2016).

In this project, I assessed various aspects of E/I imbalance in schizophrenia from different perspectives.

1.4 Sodium channels in the context of schizophrenia

Given the complexity of excitatory and inhibitory pathways in the brain, there are numerous ways in which E/I imbalance could emerge. Voltage-gated sodium channels (VGSCs) are the key players in the generation and propagation of action potentials (APs), which are fundamental to excitation. Variants in the genes encoding VGSCs, are associated with various neuropsychiatric diseases, including schizophrenia (Fromer et al. 2014; Hoischen, Krumm, and Eichler 2014). In animal studies, it was shown that sodium channel blockers are helpful in alleviating PCP-induced cognitive dysfunction (Large et al. 2011). Consequently, VGSCs, especially those expressed in the central nervous system (CNS), are plausible targets for research into pathologies related to E/I imbalances.

1.4.1 Function and structure of the VGSC

An action potential—a signal carrying changes in the membrane potential of a cell—arises from the voltage-dependent opening of Na+ and K+ channels. Sodium channels are responsible for the rapid depolarization the membrane potential (Fig. 1a). The membrane potential shifts towards the Na^+ Nernst potential due to a short-term increase in sodium conductivity. Subsequently, there is a rapid decrease in Na^+ conductivity followed by an increase in K^+ conductivity, causing the membrane potential to move back towards the potassium equilibrium potential. The whole process takes only a few milliseconds and cells are able to generate several action potentials in series. This electrical pathway is utilized to swiftly transmit information in complex organisms and induce specific effects on the target organ, such as neuronal excitation or muscle cell contraction.

Figure 1b describes the states of a sodium channel: the voltage-dependent opening of the channel, the rapid inactivation, and the selective conductivity for sodium ions. Sodium channel current is associated with the short-lived open state. Opening and closing of several hundred channels are involved in a single action potential (Bagal et al. 2015).

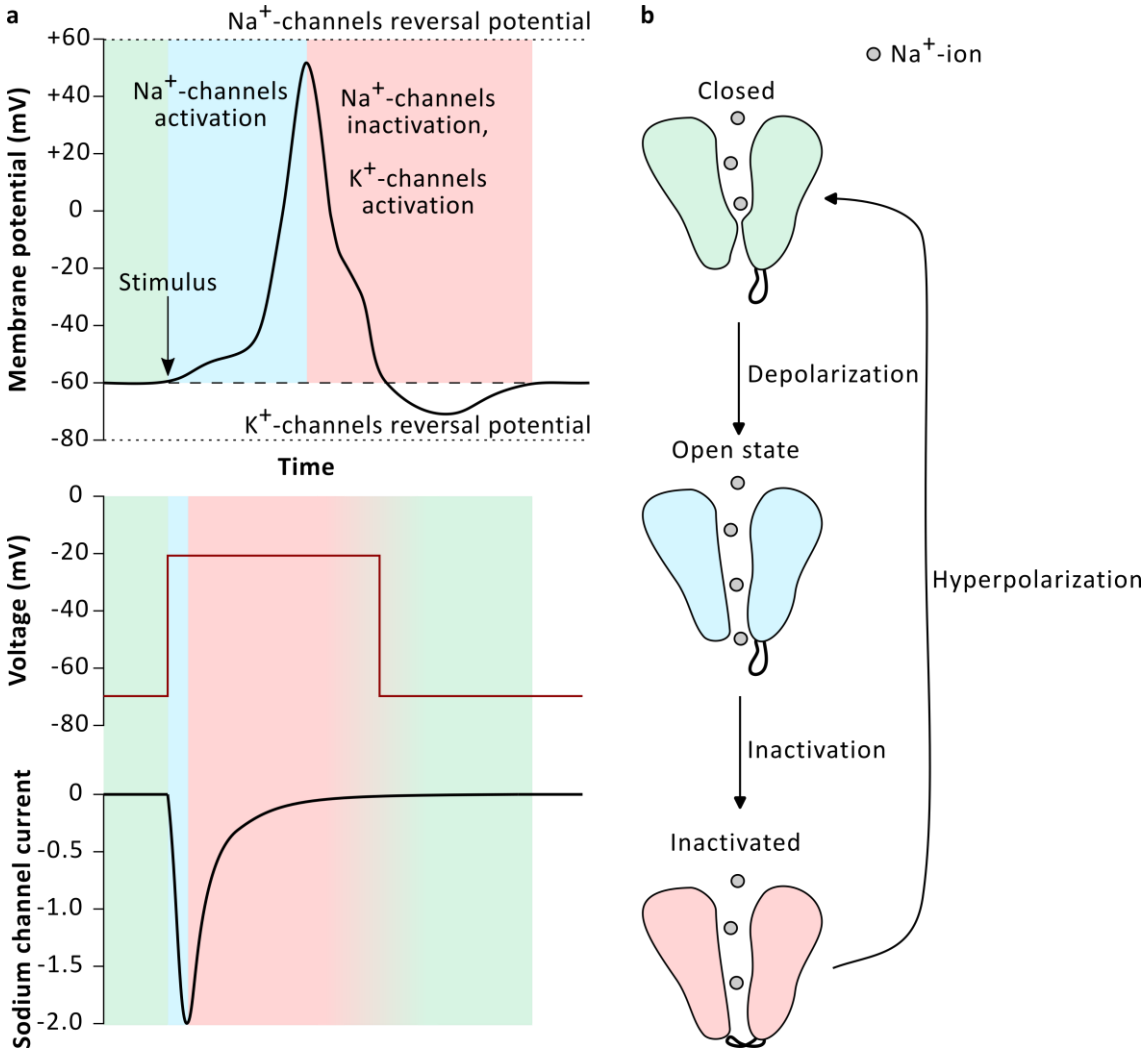

Figure 1. Sodium channel involvement in the action potential generation. ***(a)*** *Schematic depiction of an action potential (top) and sodium current in response to a rectangular depolarization of the membrane potential (bottom).* ***(b)*** *Simplified model of voltage-gated sodium channel states. Based on* (Bagal et al. 2015).

The discovery of sodium channel proteins was made possible through the use of neurotoxins that bind to them with high affinity. Specifically, α-scorpion gating-modifier toxins from *Leiurus quinquestriatus* were used to label sodium channel protein subunits in the mammalian brain. This process identified two subunits: a large α-subunit (260 kDa) and a smaller β-subunit (33–36 kDa). Further research used saxitoxin, a pore blocker, to solubilize and purify a complex of the α-subunit with two β subunits (β1 and β2) from rat brain. This complex was shown to function as a voltage-gated sodium channel when reconstituted into phospholipid vesicles or planar phospholipid bilayers. All three subunits were found to be hydrophobic membrane glycoproteins. Homolog α subunits were identified in sodium channels from electric eel electroplax and mammalian skeletal muscle. A significant advancement was the cloning and sequencing of cDNA encoding the α subunits. This process was based on amino acid sequences and antibodies from purified sodium channels, initially from electric eel and then from mammalian brain, skeletal muscle, and heart. The primary

structures of these channels provided crucial insights for extensive structure-function studies over the next three decades (Catterall 2023).

The α-subunit consists of approximately 2000 amino acids arranged in 24 transmembrane segments across four homologous domains (DI to DIV), with each domain containing six segments (S1-S6) (Figure 2). These domains are connected to each other via intracellular loops. The conserved transmembrane domains share about 50% identical amino acid sequences, while the intracellular loops vary significantly. Segments S1-S4 form a voltage-sensing domain (VSD) located distally from the pore in the center and S5 and S6 are pore-forming helixes (Fig. 2, 3a). When looking from the extracellular space, the DI-DIV domains form a rather symmetric structure (Fig. 3b). The intracellular linker between Domains III and IV acts as the inactivation gate.

The β1 and β2 subunits were also cloned and sequenced, revealing them as single membrane-spanning cell adhesion molecules with a large extracellular N-terminal domain and a short intracellular C-terminal domain. Later studies identified related β3 and β4 subunits.

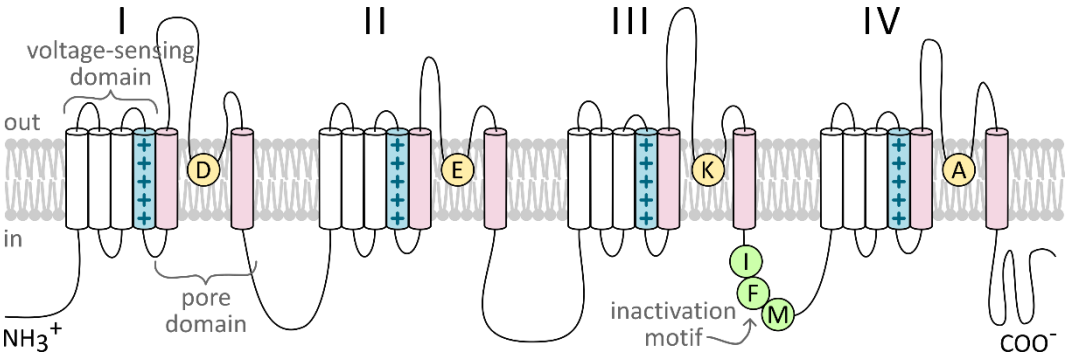

Figure 2. VGSC topology model, highlighting selectivity filter in yellow, pore-forming helixes in pink, and voltage-sensing helixes in blue. Based on (Catterall 2023)

In 2017, a first high-resolution eukaryotic sodium channel structure was published (Shen et al. 2017), starting a series of fine-tuning structural discoveries in sodium channels. In further detail, VGSC possess the following essential features and components.

Selectivity filter:

The selectivity filter is responsible for the high selectivity of the channel for sodium ions over all other relevant cations. It is made of four amino acids positioned on transmembrane loop between S5 and S6, shown on the Figure 2 in yellow circles. Voltage-gated sodium channels have the selectivity filter made of an aspartate (D), glutamate (E), lysine (K), and alanine (A); (therefore called "DEKA-filter") facing the extracellular space (Heinemann et al. 1992). Point mutations of these amino acids change the selectivity, increasing its affinity for monovalent organic or inorganic cations (Schlief et al. 1996; Sun et al. 1997), or for calcium ions (Heinemann et al. 1992). VGSCs studied to date exhibit similar conductivity properties, suggesting a shared selectivity filter (Catterall 2000). Epithelial or

bacterial sodium channels have other selectivity filter motifs – (G/S)XS or EEEE motifs, respectively (Ren et al. 2001; Sheng et al. 2000).

Voltage sensor and Voltage-Dependent Activation:

VGSC possess an activation gate that opens in response to a depolarizing voltage change. The voltage dependence of sodium channel activation is caused by the outward motion of positively charged amino acids located on S4 helixes in the electric field. This initiates a conformational change that leads to pore opening. Driven by the electrochemical gradient, Na^+ ions flow into the cell, generating an inward current along with further membrane depolarization.

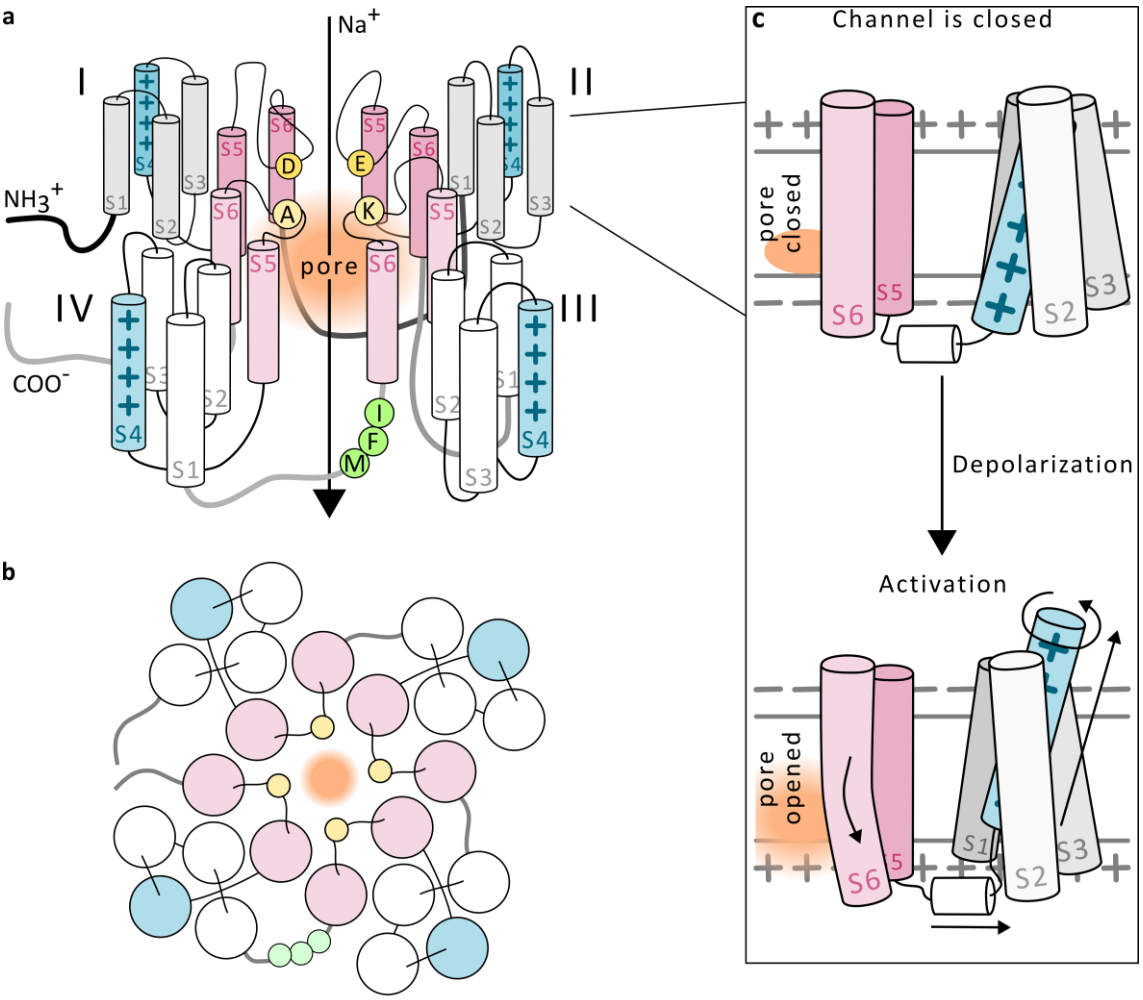

Figure 3. VGSC structure and activation schemes: ***(a)*** *Topological model of NaV, highlighting selectivity filter in yellow, pore-forming helixes in pink, and voltage-sensing helixes in blue.* ***(b)*** *Top view of the NaV1.2 topology scheme.* ***(c)*** *Schematic representation of NaV activation: upon membrane depolarization, the positively S4-helix moves towards the extracellular space, which causes movement of the S4-S5 helical linker and allows the S6 helix to bend and open the pore.*

In more details, 12 positively charged residues within the S4 segments act as voltage sensors. Upon activation, S4 segments move outwards within the membrane electric field (Kostritskii and Machtens 2023; Shen et al. 2017). This movement of the voltage sensor is currently described as a “sliding-helix mechanism”. Helixes of S1-S3 segments form a scaffold, within which the S4 segment undergoes a complex movement, involving rotation and sliding, and translates out by approximately 10 Å (Vargas et al. 2012). This transition of S4 helix leads to a movement of the S4-S5 helical linker, finally allowing the S6 helix to bend and open the pore (Fig. 3c). Activation of VSDI-III is enough for the channel to be conductive; the VSD-IV movement is delayed and is necessary for fast inactivation (Hellier 2014).

Inactivation:

Within just 1-5 ms after opening of the channel (for some isoforms), it transitions to an inactivated state, allowing the membrane to repolarize. Sodium channel inactivation is divided into fast (milliseconds) and slow (seconds) components. In this state, the channel is not conductive, and a hyperpolarization is needed before it can be activated again.

The fast inactivation is crucial for the rapid repolarization in the action potential. The intracellular loop between domains 3 and 4 is responsible for the rapid closing. The amino acids I1488, F1489 and M1490 (NaV1.2 numeration) in this loop are essential for the process, this sequence is called the IFM-motif (Fig. 2). This motif is very conserved in all human NaV isoforms. Currently, the consensus is that the mechanism of inactivation is allosteric: the IFM-motif binds to its receptor site that is formed by the DIV-S6 helix and the S4-S5 linkers of DIII and DIV (Fig. 4a,b). Consequently, the pore is blocked by the DIV-S6 segment that is pushed by the hydrophobic residues at the IFM-motif binding site (Clairfeuille et al. 2019; Jiang, Zhang, and Xia 2022; Rühlmann et al. 2020).

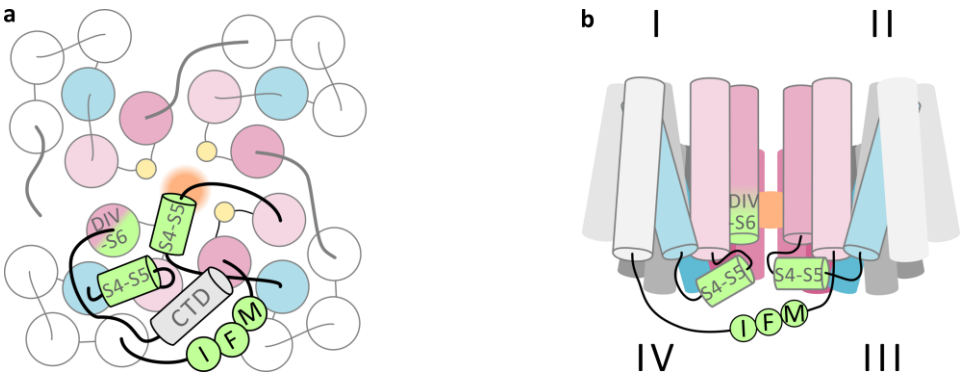

*Figure 4. Inactivation particle reception cite and the IFM-motif of VGSCs highlighted in green **(a)** bottom view; **(b)** side-bottom view.*

Slow inactivation (Vilin et al., 2001; O'Reilly et al., 2001) appears after prolonged depolarization. It is probably related to a complex channel rearrangement in order to protect the cell against repetitive stimuli. Currently, it is assumed that it appears as a result of a pore collapse (Payandeh 2018). However, no exact mechanism is known yet.

β subunits: By 2001, β-subunits were recognized as crucial modulators of VGSCs, influencing gating states, current density, and expression patterns of VGSCs (Isom, 2001). Additionally, β-subunits can elicit new gating states, such as resurgent currents, and regulate the channel's sensitivity to mechanical stimuli, varying by channel subtype (Körner et al., 2018; Maroni et al., 2019). β-subunits also mediate cell-cell contacts through homophilic interactions of their extracellular Ig-domain, contributing to intercellular communication and recruitment of VGSCs at the nodes of Ranvier (Malhotra et al., 2000).

In vivo, β-subunit effects are significant: SCN1B-null mice show cardiac, neurological, and nociceptive abnormalities, while SCN2B- and SCN3B-null mice exhibit altered VGSC density and seizure susceptibility (Chen et al., 2002; Lopez-Santiago et al., 2007, 2011). Mutations in these proteins can lead to epilepsy, Brugada syndrome, and neuropathic pain (Alsaloum et al., 2019). The α-β interaction varies across VGSC subtypes, indicating a complex and evolutionarily conserved mechanism (Molinarolo et al., 2018).

Neuromodulation: The function of sodium channels can be modulated intracellularly via the phosphorylation of amino acids in the DI-DII linker. This can affect the peak current, the voltage and time dependence of activation and deactivation and the persistent current. The modulation can also occur via the activation of muscarinic acetylcholine receptors m1, m3, and m5 (Cantrell et al. 1996), via dopamine and serotonin receptors (Yin et al. 2017), via the coexpression of G proteins (Mattheisen, Tsintsadze, and Smith 2018) and via hypoxia and nitric oxide (Cannon 2017).

1.4.2 Expression patterns of VGSC

There are 9 members of human VGSCs identified and functionally characterized in mammals. Their names, respective genes and major expression tissues for humans are summarized in the Table 1: Voltage-gated sodium channel isoforms – protein name, gene name, protein size and predominant tissue expression. (Goldin 2002; Körner et al. 2024).

Table 1: Voltage-gated sodium channel isoforms – protein name, gene name, protein size and predominant tissue expression. (Goldin 2002; Körner et al. 2024)

Name	Gene	Size, AA	Tissue
NaV1.1	*SCN1A*	2009	CNS, PNS
NaV1.2	*SCN2A*	2005	CNS, PNS
NaV1.3	*SCN3A*	1951	CNS, PNS
NaV1.4	*SCN4A*	1836	Skeletal muscle
NaV1.5	*SCN5A*	2016	Heart
NaV1.6	*SCN8A*	1980	CNS, PNS
NaV1.7	*SCN9A*	1977	PNS
NaV1.8	*SCN10A*	1956	PNS
NaV1.9	*SCN11A*	1791	PNS

In human CNS neurons, the NaV1.1, NaV1.2, NaV1.3, and NaV1.6 are the most expressed VGSC isoforms. Their expression patterns depend on cell part, cell type, and age. Specifically, NaV1.1 and NaV1.3 are predominantly expressed in the soma, NaV1.2 in unmyelinated axons and dendrites, and NaV1.6 in myelinated axons and dendrites (Kearney et al. 2002; Westenbroek, Merrick, and Catterall 1989). Concerning the neuronal subtypes, NaV1.1 is concentrated in GABA-interneurons, while NaV1.2 and NaV1.6 are primarily found in excitatory neurons. NaV1.3 expression is limited to the embryonic stage and infancy, being replaced by NaV1.1 and NaV1.2 thereafter (Whitaker et al. 2001).

1.4.3 NaV1.2 function and localization

Voltage-gated sodium channel type 2 subunit α, also called NaV1.2, is significant in the context of schizophrenia due to its involvement in neuronal excitability and signal transmission. Studies have implicated genetic variations in the SCN2A gene, which encodes NaV1.2, in the pathophysiology of schizophrenia (Carroll et al. 2016; Fromer et al. 2014; Suddaby, Silver, and So 2019). NaV1.2 has been linked to cortical excitability and synaptic plasticity, processes believed to be disrupted in schizophrenia (P. W. E. Spratt et al. 2019; Yin et al. 2017). Understanding the role of NaV1.2 in the disorder may provide insights into its underlying mechanisms and potential therapeutic targets.

According to a comprehensive immunohistological analysis of human brain performed by Whitaker et al, NaV1.2 is expressed in cortex, hippocampus, striatum, midbrain, and nerve tracts, connecting nuclei of the brain. It is relatively equally distributed in the cortical regions with slightly stronger expression in III, V and VI layers. There is no expression observed in the soma of the cells, it was rather focused on unmyelinated axons and dendrites (see above) (Whitaker et al. 2001).

In the cortex, NaV1.2 is mainly expressed in glutamatergic excitatory neurons, although it was also found in a particular subset of murine disinhibitory interneurons (Whitaker et al. 2001; Yamagata et al. 2017). Compared to another CNS isoform NaV1.6, NaV1.2 is trafficked closer to the soma in the axon initial segment (AIS) (Hu et al. 2009). This membrane region is responsible for synaptic integration and resulting action potential initiation, moreover, it regulates the release of neurotransmitters and excitability of a particular neuron (Kole and Stuart 2012).

NaV1.2 was also found in immature Ranvier nodes of myelinated axons, were it is being replaced by NaV1.6 during maturation (Cannon 2017). Ranvier nodes are small uninsulated regions on the myelinated axons, located between the myelin sheaths. Alongside oligodendrocytes, which provide myelination, the Ranvier nodes play a crucial role in salutatory conduction—a mechanism allowing action potentials to propagate along the axon significantly faster, albeit potentially at a higher energy expenditure (Harris and Attwell 2012).

Since the expression of NaV1.2 is age-dependent, it is considered that its main role in early development is the initiation and propagation of action potentials (Kole and Stuart 2012). Around the age 1-2 years, NaV1.2 is replaced by NaV1.6, an isoform with lower

activation threshold. Therefore the role of NaV1.2 shifts towards supporting the backpropagation of action potentials (Hu et al. 2009). This term refers to the action potentials traveling in a reverse direction, from the soma towards the dendritic tree, enabling synaptic plasticity, activity-dependent gene transcription and information processing in neurons. Another surprising function of this channel is a brief conduction of calcium ions, observed in rat brains and HEK cells expressing human NaV1.2 (Hanemaaijer et al. 2020). This allows for potassium channel activation, facilitating membrane repolarization.

Another age-dependent property of NaV1.2 is a splice isoform ratio. In the fetal brain, two splice isoform, 5N and 5A were found, whereas the adult human brain only had the 5A isoform (Kasai et al. 2001). In the adult NaV1.2, the asparagine in position 209 is replaced by an aspartate. This introduces a negative charge on the extracellular loop in front of the voltage-sensing S4 segment. The neonatal isoform was found to be less excitable than the adult one, and when expressed in mice it showed less action potential firing (Gazina et al. 2015), suggesting a seizure-protecting role in early neurodevelopment.

NaV1.2 is also prominently expressed in the cerebellar cortex. In this region, it was detected in parallel fibre axons and axon terminals, at presynaptic sites in granule cell axons, granule cells axon terminals, and, occasionally, their AIS. This suggests that NaV1.2 is responsible for signal transmission from granule cells to Purkinje cells, the large GABAergic neurons of the cerebellar cortex (Martínez-Hernández et al. 2013).

1.4.4 NaV1.2 implication in neuropsychiatric disorders

Mutations in SCN2A gene encoding NaV1.2 can lead to diverse alterations in its electrophysiological properties, including voltage shifts in activation and inactivation, changes in recovery from fast and slow inactivation, and variations in peak and persistent current amplitudes. These diverse effects on channel function may contribute to a wide range of associated disorders, including epilepsy, autism spectrum disorder (ASD), intellectual disability (ID), and schizophrenia (Ben-Shalom et al. 2017; Suddaby, Silver, and So 2019; Wolff et al. 2017).

In animal studies, selective deletion of SCN2A gene in brain regions relevant for schizophrenia, resulted in alterations in prepulse inhibition test (also altered in schizophrenia patients) and decreased locomotor activity (Suzuki et al. 2024). Another study observed a spectrum of phenotypes relevant for schizophrenia, such as social and behavioral impairments and altered gamma-band activity in SCN2A-knockout mice (Tatsukawa et al. 2019). In humans, genetic study found significant enrichment of loss-of-function variants in VGSCs in schizophrenia cohort (Rees et al. 2019).

1.4.5 Schizophrenia-associated variants in NaV1.2

At the beginning of this project, 5 variants in the SCN2A gene were described in patients with schizophrenia in the literature (Carroll et al. 2016; Fromer et al. 2014; Suddaby, Silver, and So 2019). Their locations are depicted in Figure 5 and the details on the sequences and the patients are summarized in Table 2.

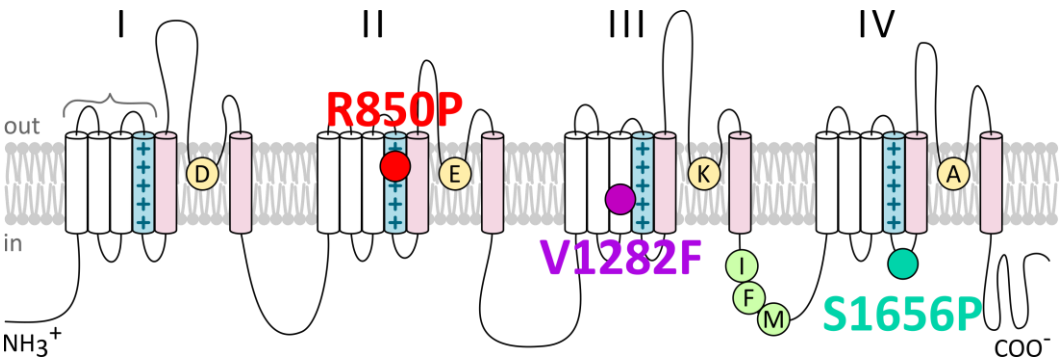

Figure 5. Topological scheme of the NaV1.2 with marked positions of the 3 schizophrenia-associated variants listed in (Suddaby, Silver, and So 2019).

The first variant introduces a stop-codon in position 169, resulting in non-functional protein (Carroll et al. 2016). The second one is located in an intron and causes a splice variant (Fromer et al. 2014). The third variant introduces an exchange of arginine to proline in position 850 on a voltage sensor domain of the DII (missense variant), reducing its positive charge (Carroll et al. 2016). The fourth variant was found in two different patients, it leads to an amino acid substitution V1282F on a transmembrane helix S3 of the DIII (missense variant). The last variant – S1656P – was found in a patient with a full SCN2A phenotype, suffering from seizures, autistic features, episodic ataxia and psychosis (Suddaby, Silver, and So 2019). It is considered as a missense variant located on the intracellular loop connecting S4 and S5 segments of the DIV.

Table 2. Locations of the variants in the Nav1.2 channel in patients with the schizophrenia phenotype (Suddaby, Silver, and So 2019).

Patient	**Protein variant**	**Mutation type**	**Domain**	**SZ remarks**
1	E169X	truncating	DII-S2	Treatment-resistant
2	N/A	Splice variant	Cytoplasmic linker	Not specified
3	R850P	missense	DII-S4	Treatment-resistant
4,5	V1282F	missense	DII-S3	Treatment-resistant
6	S1656P	missense	DIV S4-S5 linker	Full SCN2A spectrum

In this project, we aimed to electrophysiologically characterize all 3 missense variants as they did not affect the length of the protein: R850P, V1282F, and S1656P.

1.5 NMDAR hypothesis of schizophrenia

N-Methyl-D-Aspartate (NMDA) receptors represent one of the three major types of ionotropic glutamate receptors. They are expressed in nearly all glutamatergic synapses. Based on their special gating properties and regulation, they play a crucial role in synaptic plasticity, memory formation, and learning. These receptors are ligand-gated ion channels that allow the flow of calcium (Ca^{2+}), sodium (Na^{+}), and potassium (K^{+}) ions through the cell

membrane when activated by the neurotransmitter glutamate and glycine or D-serine as co-agonists (Fig. 6). NMDA receptors are unique due to their voltage-dependent activation, which requires both ligand binding and membrane depolarization to relieve the magnesium (Mg^{2+}) block of the channel (Hansen et al. 2018).

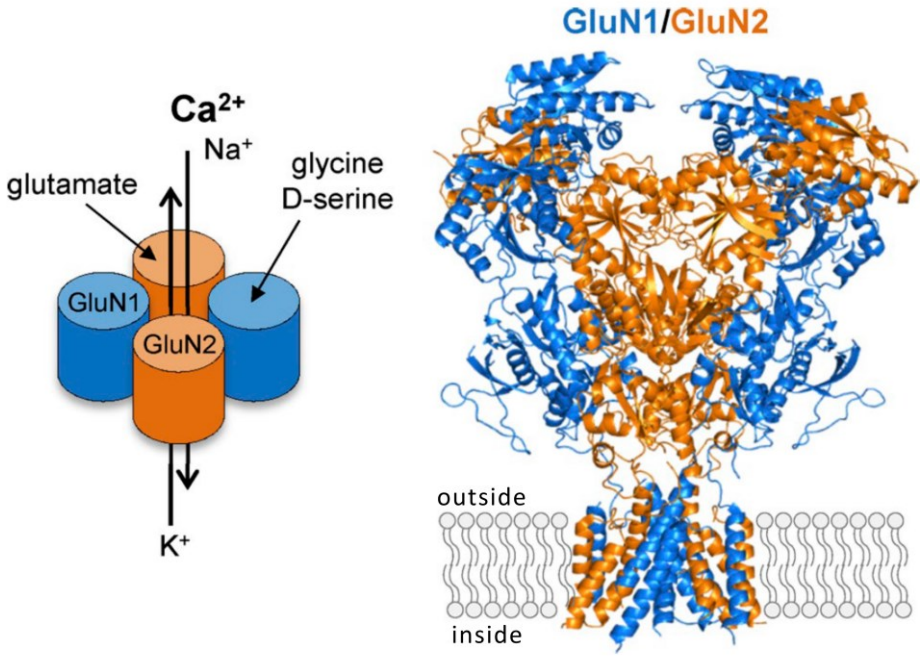

Figure 6. Subunit arrangement and 3D structure of GluN1/2 NMDA receptors, from (Hansen et al. 2018)

NMDA receptors are heterotetrameric complexes composed of multiple subunits, including GluN1, GluN2 (A-D), and GluN3 (A-B), which assemble to form functional receptors with diverse properties determined by their subunit composition. Typically, NMDARs consist of two GluN1 subunits, each containing a D-serine binding site, and two GluN2 or GluN3 subunits, which bind glutamate. These receptors are widely distributed throughout the central nervous system and play critical roles in various physiological processes, including synaptic plasticity and neuronal communication. Dysregulation or dysfunction of NMDA receptors is implicated in numerous neurological and psychiatric disorders, including schizophrenia, Alzheimer's disease, and other neuropsychiatric conditions (Lakhan, Caro, and Hadzimichalis 2013).

Pharmacological studies highlight a central role for NMDAR hypofunction, particularly in GABAergic interneurons, in the pathophysiology of schizophrenia. NMDAR antagonists such as PCP and ketamine can induce psychotic symptoms in individuals with schizophrenia and mimic core features of the disorder in healthy individuals. For example, low doses of ketamine in healthy participants produce mild psychosis, as well as negative and cognitive symptoms reminiscent of those observed in schizophrenia (Javitt and Zukin 1991). Furthermore, treatments targeting NMDAR function, such as glycine or D-serine (NMDAR co-agonists), have shown promise in alleviating schizophrenia symptoms (Labrie and Roder 2010).

Studies on large exome sequencing of schizophrenia patients showed an enrichment of both common (intronic) variants and rare exonic variants in genes encoding glutamatergic postsynaptic proteins including NMDAR – particularly GRIN2A – the gene encoding the GluN2A subunit or other proteins involved in regulation NMDAR (Fromer et al. 2014; Singh et al. 2022; Trubetskoy et al. 2022).

Another evidence is the symptomatology of anti-NMDAR encephalitis – an autoimmune condition, often present with psychosis, cognitive impairments, and catatonia, closely resembling schizophrenia symptoms (Dalmau et al. 2019).

The NMDAR hypofunction hypothesis of schizophrenia suggests widespread implications for brain function and connectivity. NMDAR dysfunction disrupts synaptic plasticity and long-range connectivity, particularly affecting cortico-cortical and cortico-subcortical networks, which underlies symptoms like disorganized thought and impaired working memory (Gao et al. 2022; Stephan, Friston, and Frith 2009). This hypofunction, especially on parvalbumin-positive interneurons, leads to reduced GABAergic inhibition, resulting in an excitatory/inhibitory imbalance that increases cortical excitability and contributes to sensory overload, hallucinations, and cognitive deficits (Fig. 7) (Gaebler et al. 2023; Nakazawa and Sapkota 2020).

Furthermore, NMDAR hypofunction has broader pathophysiological impacts. NMDARs play a crucial role in brain development, including synaptic pruning and circuit formation, and their dysfunction may lead to aberrant neurodevelopment, a hallmark of schizophrenia (M. A. Snyder and Gao 2013). Impaired NMDAR signaling also affects learning and memory processes, contributing to the cognitive impairments observed in schizophrenia (Dong et al. 2023).

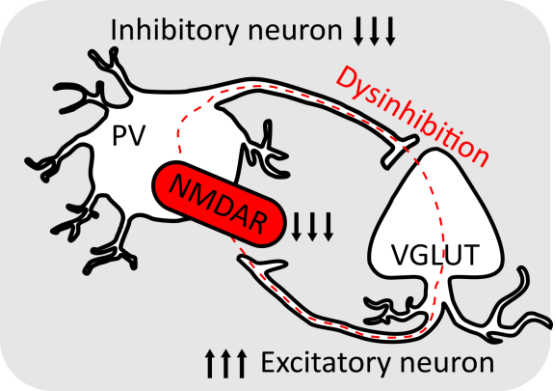

Figure 7. Scheme of E/I imbalance induced by NMDAR hypofunction in inhibitory neurons (Gaebler et al. 2023).

In mice, it was shown that reduction in NMDAR GluN1 subunit results in sensory processing disinhibition, behavioral and social abnormalities associated with schizophrenia (Duncan et al. 2004; Halene et al. 2009). Moreover, it was shown that the alterations can be observed only after per-adolescent NR1 deletion, a finding consistent with the neurodevelopmental etiology of the disease (Belforte et al. 2010).

On a patient level, reduced NMDAR expression was found in the hippocampus and prefrontal cortex in *postmortem* samples of patients with schizophrenia (Matas, John Francis William, and Toro 2021; Weickert et al. 2013). Moreover, several endophenotypes have been suggested to be closely related to NMDAR dysfunction in schizophrenia:

Prepulse inhibition (PPI) refers to the reduction in the startle reflex when a weak pre-stimulus (prepulse) precedes a stronger startle-inducing stimulus (pulse). This reduction in response is believed to reflect an individual's ability to filter out irrelevant stimuli, a process known as sensorimotor gating. An acoustic startle reflex is typically induced by a loud noise, which causes a measurable physical reaction, such as a sudden movement or jump. When this loud noise is preceded by a quieter sound, the intensity of the startle response is reduced. Deficits in PPI are commonly observed in individuals with schizophrenia, suggesting an underlying problem with sensorimotor gating in these patients. PPI can be influenced by neurotransmitter systems, including dopamine, serotonin, and glutamate (Hyun, Inoue, and Hayashi-Takagi 2020; Y. Kim, Yang, and Kim 2022). Mice with amphetamine-induced NMDAR hypofunction exhibit enhanced sensitivity to amphetamine-induced PPI disruption (Moy et al. 2006) and on rats it was shown, that decreased GluN1 subunit expression in nucleus accumbens correlates with PPI deficits (Fitzgerald & Pickel, 2015).

Mismatch negativity (MMN) reflects the brain's ability to detect deviations from expected auditory stimuli, serving as a marker of pre-attentive auditory processing. Recent research suggests that NMDA receptors play a crucial role in generating MMN, as they are involved in synaptic plasticity and the encoding of auditory information (Harms et al. 2021). MMN amplitude is significantly reduced in schizophrenia patients compared to healthy controls (Molnár et al. 2024), which could be explained by both impaired local processing at the level of the auditory cortex and dysconnectivity between auditory and prefrontal areas (Gaebler et al. 2023). Importantly, reduction of MMN similar to schizophrenia can be induced by NMDAR antagonists whereas other pharmacological agents exert only little effects at best.

Functional connectivity refers to the temporal correlation between spatially remote brain regions, reflecting how well they communicate and coordinate their activity at rest or during cognitive or sensory tasks. Genetic variants associated with NMDAR dysfunction show similar functional connectivity patterns to those induced by NMDAR antagonists, particularly in regions with high NMDAR density (Gaebler et al. 2023). Moreover, NMDAR antagonists reduce spike synchrony and effective connectivity in prefrontal networks (Zick et al. 2018). Therefore, NMDAR dysfunction may lead to disrupted neural connectivity which disrupts glutamatergic signaling and impairs the integration of neural networks. These disruptions may contribute to the cognitive deficits, hallucinations, and disorganized thoughts characteristic of the disorder.

Such endophenotypes may be useful to stratify patients according to potential NMDAR pathology, enabling a more targeted approach for diagnosis and potential therapeutic interventions (Gaebler et al., 2023).

Additionally, aberrant NMDAR-mediated synaptic plasticity and neural coordination is thought to be a key factor in the dysconnectivity hypothesis of schizophrenia. This hypothesis posits that schizophrenia arises from abnormal functional integration of brain processes (Stephan, Friston, and Frith 2009). The altered response of NMDA receptors to specific modulation results in abnormal gain control and in turn leads to a failure to optimize excitation-inhibition balance (Friston et al. 2016).

1.6 Experimental approaches to study schizophrenia

There is a variety of methods to investigate the complex neurobiological, genetic, and psychological factors of the disorder. These approaches range from genetic and molecular studies to neuroimaging and behavioral analyses.

Neuroimaging Techniques: Magnetic resonance imaging and functional magnetic resonance imaging (fMRI) are used to study the structural and functional abnormalities in the brains of individuals with schizophrenia. These techniques can reveal differences in brain volume, connectivity, and activity patterns compared to healthy controls. PET scans can measure glutamate, GABA or dopamine activity, helping to understand the role of dopamine and other chemicals in schizophrenia (Preller et al. 2024). Limitations of this approach include short time of possible observation, high costs, need for better tracer development, and ethical concerns of studying individuals experiencing acute psychotic episodes or those with severe cognitive impairments.

***Postmortem* brain studies** provide direct insights into the neurobiological abnormalities associated with the disorder. These studies allow to investigate structural, molecular, and cellular changes that occur in the brain affected by schizophrenia (de Jonge et al. 2017). However, this approach does not allow to examine neural activity nor dynamic changes in brain tissue that occur during the course of the illness. Moreover, *postmortem* brains may be affected by long-term medication or circumstances of death.

Animal models: Rodents, particularly mice, can be genetically modified to carry mutations linked to schizophrenia. These animal models exhibit behavioral traits and neural abnormalities that parallel some aspects of the human disorder. They can be used to study the effects of genetic mutations on brain development and function, to explore the environmental factors contributing to the disease, and to test new treatments (Halene et al. 2009; Mi et al. 2019). However, animal models cannot fully replicate the complexity of human psychiatric conditions, as many schizophrenia symptoms, such as hallucinations and delusions, cannot be directly observed in animals.

Large scale genetic studies (such as genome wide association studies) help to identify genetic variations associated with schizophrenia, allowing to pinpoint specific genetic markers linked to susceptibility and symptom severity (Fromer et al. 2014; Rees, O'Donovan, and Owen 2015; Xu and Wong 2018). Limitations include the complexity of the disorder, with multiple genes and environmental factors contributing, as well as the challenge of interpreting the

functional significance of identified genetic variants in the context of schizophrenia's heterogeneity.

In this project, we used experimental approaches that allow to capture patient-specific phenotypes on a protein or cellular level. This allows to investigate the very fundamental impairments that could be at the core of schizophrenia pathogenesis.

1.6.1 Utilising HEK cells in studying schizophrenia-related mutations in NaV1.2 channel

HEK (Human Embryonic Kidney) cells are advantageous due to their ease of cultivation and transfection efficiency, allowing for the expression of specific ion channel subtypes. Patch clamp electrophysiology enables the direct measurement of ion channel activity by forming a tight seal between a glass pipette and a cell membrane, facilitating the recording of ion currents with high temporal and spatial resolution. HEK cells, when transfected with recombinant ion channel proteins, serve as a versatile model system for investigating the biophysical properties, pharmacology, and regulation of ion channels.

This approach allows us to study schizophrenia-associated variants in SCN2A gene with a high precision. Given the complex electrophysiology of sodium channels, manual patch clamp is a suitable tool to assess activation, inactivation, use-dependent block and other properties of NaV1.2 of healthy individuals and schizophrenia patients.

1.6.2 Modelling schizophrenia with iPSC-derived neurons

The discovery of induced pluripotent stem cells (iPSC) by Takahashi and Yamanaka in 2006 has opened up new possibilities for cellular disease modelling (Takahashi and Yamanaka 2006). Skin fibroblasts or blood cells can be reprogrammed to regain pluripotency when exposed to specific transcription factors (OCT4, SOX2, KLF4, and c-MYC). Using small molecules to mimic early brain development processes, it is possible to guide the cells through stages similar to those seen in embryogenesis, enabling the generation of patient-specific iPSC-derived neurons.

In early brain development, neural progenitor cells (NPCs) arise from the neuroepithelial cells of the neural plate, which forms the neural tube (Fig. 8). As this tube closes, its rostral region expands into the telencephalic vesicles, which later give rise to key brain structures such as the cerebral cortex, basal ganglia, and hippocampus. The dorsal and ventral neurogenic zones within the telencephalon produce cortical excitatory pyramidal neurons and inhibitory neurons, respectively. These neurons follow distinct migratory pathways to reach their destined layers of the cortex.

This developmental process is tightly regulated by signaling molecules like Wnt, Fibroblast Growth Factor (FGF), and Retinoic Acid (RA), which guide the anterior-posterior patterning of the brain, and Bone Morphogenetic Protein (BMP), Sonic Hedgehog (SHH), and Nodal, which influence dorsal-ventral patterning. The precise regulation of these signaling pathways ensures the proper formation and migration of neurons, forming functional brain regions (Ahmad et al. 2018).

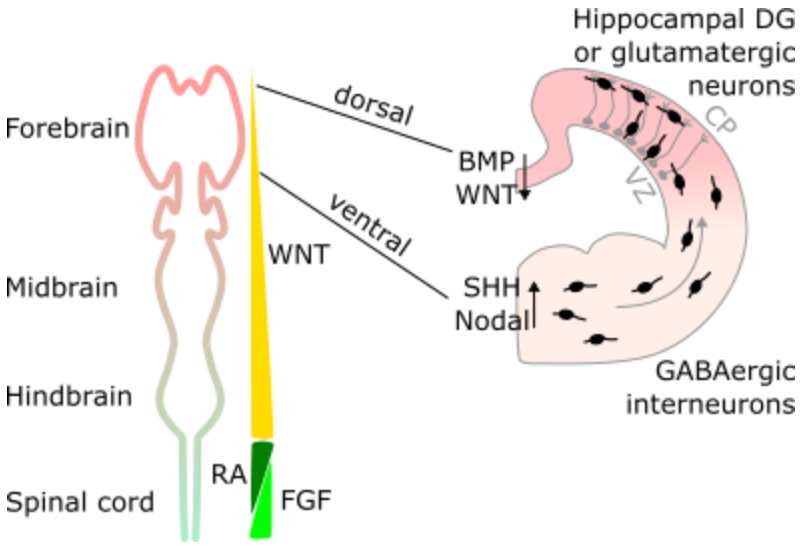

Figure 8. Key signaling pathways define neuronal fate along the anterior-posterior and dorsal-ventral axes. Neural progenitor cells in the ventricular zone (VZ) of the dorsal telencephalon give rise to excitatory, glutamatergic pyramidal neurons. These neurons utilize radial glia cells (grey) to migrate radially to the cortical plate (CP) and then populate specific cortical layers. Progenitors from the ventral neurogenic zone migrate tangentially toward the pallium, also relying on radial glial cells to reach the CP, where they differentiate into GABAergic interneurons. Adapted from (Ahmad et al. 2018).

The SMAD signaling pathway plays a significant role in maintaining the pluripotent state of iPSCs. It is activated by signals from the TGF-β/Nodal and BMP pathways, both of which inhibit neural differentiation. In order to induce iPSCs to become neural progenitor cells, it is possible to blocks these pathways: using small molecules like LDN-193189, which inhibit BMP ligands, prevents the activation of SMAD1/5/8 proteins, thereby reducing the suppressive signals that maintain pluripotency; inhibitors like SB431542 block the receptors involved in SMAD2/3 activation, further promoting CNS neural differentiation.

Additionally, XAV939, an inhibitor of the WNT/β-catenin pathway, can be employed to enhance neural differentiation by promoting CNS identity. The combination of SU5402 (an FGF receptor inhibitor) and PD0325901 (a MEK-ERK inhibitor), along with DAPT (a Notch inhibitor), can rapidly induce anterior CNS lineage differentiation from human iPSCs

This dual inhibition creates an environment for the differentiation of iPSCs into NPCs, closely mimicking early brain development and enabling the production of both excitatory and inhibitory neural cells (Fig. 9), akin to those generated in the dorsal and ventral zones of the telencephalon (Qi et al. 2017).

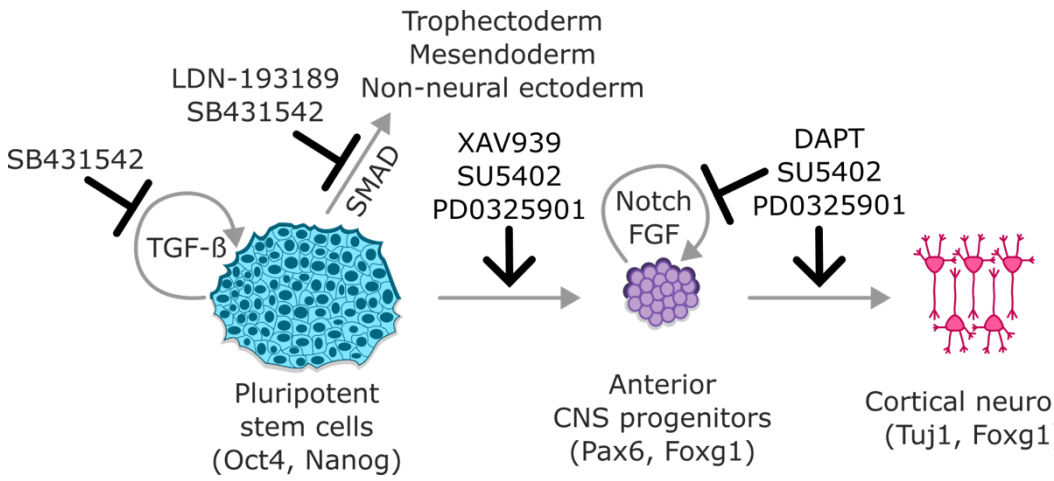

Figure 9. Scheme of differentiation utilizing dual SMAD inhibition. Adapted from (Qi et al. 2017)

Starting from 2011 (Brennand et al. 2011), different research groups have used iPSC to model schizophrenia. This approach permits to investigate the functions of living neurons genetically identical to the neurons found in the CNS of the patients. Therefore, it is possible to study exclusively genetic factors isolated from environmental effects or focusing on a particular gene variant. The studies reviewed herein collectively elucidate various molecular and cellular abnormalities associated with schizophrenia.

A recurring observation in iPSC-derived neurons from SZ patients is the dysregulation of key signaling pathways and gene expression profiles critical for synaptic refinement and long-term potentiation. For instance, studies have demonstrated perturbations in glutamate, WNT, and cyclic adenosine monophosphate (cAMP) signaling, which are essential for synaptic plasticity and neural connectivity (Brennand et al. 2011; N. S. Kim et al. 2021; Narla et al. 2017; Topol et al. 2015). Additionally, extracellular matrix organization and calcium ion binding—both of which are important for synaptic transmission—are significantly altered in iPSC-derived inhibitory neurons (J. M. Park et al. 2021; Roussos et al. 2016). Dysregulation of these molecular pathways aligns with the broader concept of E/I imbalance, suggesting that early disruptions in neurodevelopment could predispose individuals to SZ.

A major focus of iPSC studies in SZ has been the investigation of neuronal differentiation and maturation deficits. iPSC-derived neurons from SZ patients consistently show reduced neurite length and altered synaptic protein expression resulting in delayed neuronal differentiation, which contributes to a failure in forming mature synapses (Brennand et al. 2011; Grunwald et al. 2019; O. Robicsek et al. 2013; Odile Robicsek et al. 2018; Yu et al. 2014). This delayed maturation may be a key contributor to the E/I imbalance, as mature inhibitory interneurons play a crucial role in maintaining cortical homeostasis and preventing hyperexcitability.

In addition to synaptic maturation deficits, patient-derived neurons often display aberrant morphology, impaired dendritic branching, and reduced spine density—key indicators of compromised synaptic plasticity (Das et al. 2015; Forrest et al. 2017; Ishii et al.

2019; O. Robicsek et al. 2013; Sawada et al. 2020). These structural abnormalities are further compounded by mitochondrial dysfunction, which has been frequently reported in SZ iPSC models (Kathuria et al. 2020; Ni et al. 2020; Paulsen et al. 2012; O. Robicsek et al. 2013; Odile Robicsek et al. 2018; Zuccoli et al. 2023). Mitochondria play a crucial role in maintaining synaptic function by regulating calcium homeostasis and energy metabolism, and their dysfunction may directly contribute to the synaptic impairments observed in iPSC-derived neurons obtained from patients with schizophrenia.

Understanding the mechanisms that underlie E/I-imbalance in SZ not only provides insights into its pathophysiology but also opens new avenues for therapeutic intervention. iPSC models have been instrumental in identifying potential drug targets and testing pharmacological treatments that may restore E/I balance. Importantly, antipsychotic treatments such as clozapine have been tested in SZ iPSC-derived neurons, demonstrating their ability to reverse synaptic deficits and modulate signaling pathways involved in synaptic plasticity (Hribkova et al. 2022).

To the best of our knowledge, aside from the research published by Hribkova et al., no other study has investigated NMDAR dysfunction using iPSC-derived neurons from patients with schizophrenia.

1.7 Aim of the project

The aim of this project was to model and investigate two major mechanisms of excitation/inhibition (E/I) imbalance characteristic of schizophrenia at the cellular level. Schizophrenia, a complex neuropsychiatric disorder, presents symptoms linked to dysregulated neural circuits. To understand this imbalance, I utilized two distinct model systems, each designed to study different facets of excitation and inhibition in neuronal function.

Model System I: Electrophysiological Impact of Schizophrenia-Associated Mutations in NaV1.2

The first model system focused on assessing the electrophysiological effects of schizophrenia-associated mutations in the voltage-gated sodium channel NaV1.2. Using the patch clamp technique, I precisely measured the ionic currents flowing through NaV1.2 channels and determined how these mutations altered channel function. The patch clamp data provided crucial insights into how these genetic alterations impacted NaV1.2 electrophysiology. This data was further incorporated into neuronal modeling to simulate how the observed changes in NaV1.2 function influenced overall neuronal behavior. By integrating experimental and computational approaches, I sought to elucidate the role of NaV1.2 mutations in disrupting the delicate balance between excitation and inhibition in neurons, contributing to the pathophysiology of schizophrenia.

Model System II: NMDAR Function and E/I-Balance in iPSC-Derived Neurons

The second model system explored the function of N-methyl-D-aspartate receptors (NMDARs) and the E/I balance of neurotransmission in neurons derived from induced pluripotent stem cells (iPSCs) of schizophrenia patients and healthy controls. NMDARs play a critical role in synaptic transmission and plasticity, and their dysfunction has been implicated in schizophrenia. iPSC-derived neurons may allow to directly compare the cellular and molecular characteristics of neurons from affected individuals and controls. This approach could enable us to test the NMDAR hypothesis of schizophrenia, which posits that abnormalities in NMDAR signaling contribute to the disorder's symptoms. Additionally, this model may provide a platform to develop strategies for identifying patients who are likely to respond to treatments targeting NMDAR signaling, offering a potential pathway for personalized therapeutic interventions.

In summary, this project leveraged advanced electrophysiological techniques and stem cell technology to investigate the cellular mechanisms underlying the E/I imbalance in schizophrenia. By combining experimental data with computational models, I aimed to provide a comprehensive understanding of how genetic mutations and receptor dysfunctions contributed to the disorder. This data could inform the development of more effective treatments and improve the quality of life for individuals affected by schizophrenia.

2. Materials and methods

2.1 Molecular biology / Generation of the NaV1.2 variants

For expression in mammalian cells, hNaV1.2 R850P, V1282 and S1656P variants were generated based on WT human NaV1.2 in a modified pCMV6-XL5 vector by site-directed mutagenesis using Q5 Hifi DNA Polymerase (NEB, Ipswich, MA, USA) in Epi400 bacteria. Constructs were verified by commercial DNA sequencing (Eurofins, Germany).

2.2 HEK cell culture

HEK293T cells (Sigma-Aldrich, St. Louis, MO, USA) were grown in an incubator at 37 °C with 5% CO2 and passaged with Accutase (Sigma-Aldrich, St. Louis, MO, USA) twice a week, after reaching 70% - 80% confluence. Cells were kept in Dulbecco's modified eagle medium (DMEM) /F12 medium (Gibco, Germany) with 10% FBS.

Transient transfection of HEK293T cells with human NaV1.2 WT or any of the three variants was done using jetPEI (Polyplus transfection, Illkirch, France), in 35 mm^2 petri dishes with 2 ml of freshly changed medium, when cells were 40% -50% confluent. For transfection we used 0.7 µg of DNA (0.5 µg NaV DNA and 0.2 µg enhanced green fluorescent protein, eGFP, DNA) and 4 µl of jetPEI. After 12 h incubation, cells were split into plastic petri dishes. Cells were given 2-3h to recover before patch-clamp experiments. Only green fluorescent cells were recorded.

2.3 Reprogramming of the PBMCs / Generation of iPS cells

Patients were selected based on potential fMRI markers of NMDAR dysfunction by Jun.-Prof. Dr. Arnim Gaebler.

Blood samples were collected from one female and one male patient with schizophrenia, both suspected of having NMDAR dysfunction, after obtaining written informed consent. CD34+ peripheral blood mononuclear cells (PBMCs) were isolated from these samples. Blood was first filtered through a 70 µm filter. A volume of 9 mL of Ethylenediaminetetraacetic acid (EDTA) -treated blood was diluted with 3.5 mL of Dulbecco's phosphate-buffered saline (D-PBS, Gibco, Germany) containing 2 mM EDTA (Invitrogen, Waltham, USA). The diluted blood was carefully layered on Pancoll (PAN-Biotec, Aidenbach, Germany) at a 1:1 ratio at room temperature and centrifuged at 2000 rpm for 20 minutes without using the brake. The PBMC layer was collected, diluted in Ca^{2+}- and Mg^{2+}-free D-PBS with 2 mM EDTA, and centrifuged again at 1500 rpm for 10 minutes at room temperature.

The resulting cell pellet was resuspended in 10 mL of Ca^{2+}- and Mg^{2+}-free D-PBS with 2 mM EDTA, counted using a Neubauer chamber, and separated into portions for freezing and reprogramming. For reprogramming, 500,000 cells were seeded in the center of a 24-well plate in supplemented StemPro medium (Gibco) containing the following cytokines: murine SCF 200x CHO (kindly provided by Institute of Cell Biology, University Hospital RWTH Aachen, Germany), human Flt3L (Peprothech, USA), TPO (Miltenyi Biotec, Bergisch Gladbach, Germany), and Hyper IL-6 (kindly provided by Dr. Rose-John, Kiel, Germany).

Cells were reprogrammed with Oct3/4, Sox2, Klf4, and c-Myc in Sendai virus vectors (CytoTune™ 2.0 iPS Sendai Reprogramming Kit, ThermoFisher Scientific) (Sontag et al. 2017). Sixteen iPSC clones per donor were picked as colonies at day 23 of reprogramming and expanded on irradiated mouse embryo fibroblast (MEF) feeder. Quality assessment was performed using immunofluorescence staining of Oct4, Lin28, Nanog, and Sox2. After having stable colonies on MEF layer, iPSCs were split on Geltrex™ LDEV-Free Reduced Growth Factor Basement Membrane Matrix (Termofisher Scientific). Then they were adapted to MEF-free culture on Vitronectin (ThermoFisher Scientific) in Miltenyi iPS brew medium (Miltenyi Biotec), expanded and cryopreserved. IPSCs of two healthy gender-matched controls were obtained from B2T project.

After reprogramming, iPS cells were maintained at 37 °C with 95% O2—5% CO2. They were cultivated on 0.1% Vitronectin or on 0.1% Geltrex for the differentiation. They were supplied daily with StemMACS™ iPS-Brew XF (consisting of Basal Medium and Supplement, Miltenyi Biotech).

2.4 Differentiation of iPS cells into CNS neurons

Two different neural differentiation protocols were tested. The first one, which mainly aimed at the generation of glutamatergic cortical neurons, was a protocol described in (Qi et al. 2017) with only slight modifications. Briefly, iPS cells were plated on Geltrex-coated dishes at a density of 2.5 × 10^5 cells per cm². For the first 7 days, cells were cultured in Knockout Serum Replacement (KSR) medium: DMEM/F12 + Glutamax, 15% KSR, 1% Minimum Essential Medium non-essential amino acids, 100 µM β-mercaptoethanol (all Gibco, USA). From day 4 onwards, the medium was gradually replaced with N2/B27 medium: 50% DMEM/F12 (Gibco) + Glutamax (Life Technologies), 50% Neurobasal (Gibco), 1% Minimum Essential Medium non-essential amino acids (Gibco), 1 × N2 supplement (Gibco), 1 × B27 with RA (Gibco). Differentiation medium changes occurred daily, and small molecule inhibitors were added every two days according to the schedule in Table 3.

After day 7, cortical neuron differentiation continued in N2/B27 medium supplemented with (in µM) 8 PD0325901, 10 SU5402, 10 DAPT, 3 Chir99021, 0.02 BDNF, 500 dbcAMP, and 200 Ascorbic Acid; with regular medium changes every 3-4 days. Cells were observed daily for morphology, and neuron-like cells with processes appeared in the periphery of cell clusters around day 6-7. On day 8, cells were counted and passaged on coverslips for further experiments. Small molecule administration was stopped at day 30.

Table 3. Medium composition schedule for the glutamatergic differentiation

Day	Medium	Small Molecules		Abbreviation of Small Molecule composition
d0 and d1	100% KSR-Medium	LDN193189[1] SB431542[2] XAV939[3]	250nM 10µM 5µM	LSBX
d2 and d3	100% KSR-Medium	LDN193189 SB431542 XAV939 PD0325901[2] SU5402[1] DAPT[3]	250nM 10µM 5µM 1 µM 5 µM 10 µM	LSBX+ P1S5D
d4 and d5	2/3 KSR-Medium + 1/3 N2/B27-Medium	LDN193189 SB431542 XAV939 PD0325901 SU5402 DAPT	250nM 10µM 5µM 1 µM 5 µM 10 µM	LSBX+ P1S5D
d6 and d7	1/3 KSR-Medium + 2/3 N2/B27-Medium	PD0325901 SU5402 DAPT	1 µM 5 µM 10 µM	P1S5D

[1]: Sigma Aldrich

[2]: Stem Cell Technologies, Vancouver, Canada

[3]: Tocris, Wiesbaden-Nordenstadt, Germany

The second protocol aimed at the generation of GABAergic interneurons and was modified from (Maroof et al. 2013): neural induction was started in KSR-medium supplemented with small molecules, that was gradually replaced with N2-medium from day 2 to day 10. From day 10, N2-B27 medium was used. Cells were passaged on day 10. The media change schedule was as follow:

Table 4. Medium composition schedule for the GABAergic differentiation

Day	Medium	Small Molecules	
d0 and d1	100% KSR-Medium	LDN193189 SB431542 XAV939	250nM 10µM 5µM
d2 and d3	100% KSR-Medium	LDN193189 SB431542 XAV939	
d4 and d5	3/4 KSR-Medium + 1/4 N2/B27-Medium	LDN193189 SB431542 XAV939	

d6 and d7	1/2 KSR-Medium + 1/2 N2/B27-Medium	LDN193189 SB431542 XAV939	
d8 and d9	1/4 KSR-Medium + 3/4 N2/B27-Medium	LDN193189 SB431542 XAV939	
d10 – d18	N2/B27-Medium	SHH[1] Purmorphamin[2]	5nM 1µM
[1]: Peprotech [2]: Miltenyi Biotec			

After day 10, we tested the medium with and without the SHH, to test its ability to promote GABAergic identity of the iPSC-derived neurons .

2.5 Electrophysiology

Whole-cell patch-clamp experiments were performed at room temperature using an EPC-10 USB amplifier and PatchMasterNext software (HEKA Elektronik, Lambrecht, Germany). Glass pipettes (Bio-medical Instruments, Zöllnitz, Germany) were pulled with a DMZ puller (Zeitz Instruments, Martinsried, Germany) to a resistance of 0.8 to 1.5 MΩ and filled with intracellular solution (ICS). The sampling rate for the recordings was set to 50 kHz, with a 10 kHz low-pass filter applied. Series resistance, maintained below 5.0 MΩ, was compensated by at least 80%. Leak currents were subtracted in real-time using the P/4 protocol.

2.5.1 Voltage clamp recordings in HEK cells

The ICS contained 140 mM CsF, 1 mM EGTA, 10 mM 4-(2-hydroxyl)-1-piperazineethanesulfonic acid (HEPES) and 10 mM NaCl, and 18 mM sucrose. The ICS was adjusted to pH 7.33 with CsOH and to an osmolarity of 310 mOsm with additional sucrose. The extracellular solution (ECS) contained 40 mM NaCl, 100mM CholineCl, 3 mM KCl, 1 mM CaCl2, 1 mM MgCl2, 10 mM HEPES, 20 mM glucose, and 0.2% Dimethyl sulfoxide (Sigma-Aldrich). The ECS was adjusted to pH 7.4 with NaOH and to an osmolarity of 305 mOsm with glucose. The non-physiologically low NaCl concentration in the ESC was chosen to avoid high voltage error caused by large sodium currents.

Series resistance was compensated by at least 80%. Only cells with a series resistance below 5 MΩ were recorded. For all protocols, the holding potential (Vhold) was set at −120 mV unless otherwise stated. A liquid-liquid junction potential of +10.8 mV (calculated with swharden.com) was adjusted in all experiments before the recording. After establishing the whole-cell configuration and after cancellation of the capacitive transients and compensation of the series resistance, cells were put Vhold = -120 mV and a test IV-protocol was run to ensure sufficient clamp quality and current. The test IV protocol was followed by 5 min of

monitor protocol consisting of step depolarisations to -10 mv for 100 ms to make sure that sodium current had reached stable values.

The voltage-dependence of activation was measured using a series of 40 ms pulses from -100 mV to +50 mV in 10 mV increments, with a 5-second interval at -120 mV between sweeps. Steady-state fast inactivation was assessed with a two-step protocol: a 500 ms pre-pulse at potentials ranging from -130 mV to -40 mV in 10 mV steps, followed by a 40 ms test pulse at -10 mV to determine the remaining available channels.

Ramp currents were elicited by depolarizing voltage ramps from -120 mV to +20 mV at 1.19 mV/ms over 117 ms. Ramp current values were expressed as a percentage of the transient peak current obtained during initial I-V families, measured 5 minutes after breaking into the cell.

The use-dependence protocol involved 20 test pulses of 5 ms applying a depolarization to 0 mV at 10, 25, 50, and 100 Hz, respectively.

Recovery from fast inactivation was measured using a two-pulse protocol with varying inter-pulse durations. Cells were first depolarized to -10 mV for 500 ms, followed by an inter-pulse to -120 mV with durations increasing from 1 ms to 1024 ms. This was followed by a 40 ms test pulse at -10 mV to assess channel recovery.

2.5.2 Current clamp recordings in iPSC-derived neurons

Current clamp recordings were performed on iPSC-derived neurons starting from day 15 of differentiation and were repeated every 15 days. The extracellular solution contained (in mM): 140 NaCl, 3 KCl, 1 MgCl2, 1 CaCl2, 10 Hepe, 20 glucose; pH 7.4, 300-310 mOsm. The intracellular solution contained (in mM): 4 NaCl, 135 K-gluconate, 3 MgCl2, 5 EGTA, 5 HEPES, 2 Na2GTP, 0.3 NaGTP, (pH 7.25; 290-300 mOsm).

The resting membrane potential (RMP) was recorded for 2 seconds immediately after achieving whole-cell configuration, without any current injection. To examine action potential (AP) characteristics, the holding current was adjusted to maintain a membrane voltage of -70 mV ± 5 mV. APs were triggered using incremental square current injections (ranging from 5 to 400 pA over 200 ms, with step sizes of 5 or 10 pA, depending on the necessary current for RMP adjustment) to determine the rheobase, which is the minimal current required to generate an AP. Liquid junction potential was corrected by 14.3 mV. Subsequently, a second protocol was performed, with current injection at 1x rheobase over 1s followed by 5 s of rest and another 1s injection at 2x rheobase to assess the maturity of the neuron and additionally detect synaptic events. APs were considered mature if they surpassed 0 mV and the frequency of firing increased during the second current injection.

2.5.3 Voltage clamp recordings in iPSC-derived neurons

For voltage clamp experiments, the same ICS was used, along with the initial ECS. After completing the current clamp analysis, the setup was switched to voltage clamp mode. A voltage step protocol was applied, lasting 10 seconds at potentials ranging from -140 to +60

mV. Each step was followed by an automated perfusion of ECS (either with or without magnesium ions) containing 100 mM NMDA, which was introduced 2 seconds after the start of the step and continued for 5 seconds.

2.6 Data analysis

Data analysis was performed using Igor Pro 6.37 (WaveMetrics, Lake Oswego, OR, USA), Microsoft Excel (Microsoft, USA) and Prism 10 (GraphPad Software, San Diego, CA, USA). For manual patch-clamp, cells with a voltage error of more than 2 mV or a leak current of more than 500 pA or 30% of maximum current were excluded from analysis. Statistical significance threshold was set to $p < .05$. Histograms and QQ-plots were generated to verify normal distribution of the data. Since not all of the datasets were normally distributed, Kruskal-Wallis test was used when more than two groups were compared. In that case, Dunn's post hoc tests were used for pairwise comparisons. The numbers are presented as Mean ± Standard deviation (SD).

Voltage error was calculated as:

$$V_{err} = \left(R_{ser} - R_{comp}\right) * I_{max},$$

Initially, a 5 mV exclusion criterion was set for the voltage error. However, correlation analysis revealed a dependence of $V_{1/2}$ on the V_{err} ($p = 0.041$, Pearson coefficient = -0.171). To eliminate the correlation between the V_{err} value and the $V_{1/2,}$, the exclusion criterion was adjusted to 2 mV.

Current density was obtained by dividing the maximum peak current (pA) by the cell capacitance (pF) (as a proxy for the area of the cell membrane). For the activation analysis, conductance (G) was calculated at each voltage (V) using the equation:

$$G = I/(V - V_{rev}),$$

with V_{rev} being the reversal potential for sodium and I being the peak inward current at the respective voltage (V). Conductance–voltage curves were fitted using a Boltzmann equation:

$$\frac{G}{G_{max}} = \frac{1}{1+e^{\left(V_m - V_{1/2}\right)/k}},$$

where G_{max} is the maximum sodium conductance, V_m is the membrane voltage, $V_{1/2}$ is the potential at half maximum conductance and k is the slope factor.

For the inactivation analysis, inward current measured during the test-pulse to -10 mV was normalized to the cell's maximum pre-pulse inward current. The normalized peak inward current amplitude at each test-pulse is displayed as a function of pre-pulse potential and fitted using the Boltzmann equation:

$$\frac{I}{I_{max}} = \frac{1}{1+e^{\frac{V - V_{1/2}}{k}}},$$

where k is the slope.

For the recovery from fast inactivation protocol, the current amplitude at the test-pulse I_{test} was normalized to the current amplitude measured at the pre-pulse I_{pre} and plotted against inter-pulse duration and fit with a monoexponential:

$$Y = Y_0 + A * (1 - e^{-K*x}),$$

or a double exponential equation:

$$Y = Y_0 + A_{fast} * (1 - e^{-K_{fast}*x}) + A_{slow} * (1 - e^{-K_{slow}*x}),$$

where Y_0 is the current amplitude at time 0, A_{fast} and A_{slow} represent the amplitude coefficient for the fast and the slow time constants, K_{fast} and K_{slow} represent the two rate constants and X is the time. The time constants τ_{fast} and τ_{slow} are the reciprocals of the respective rate constant K.

2.7 Immunostaining

Cells were grown on Vitronectin-coated cover slips, fixed with 4% paraformaldehyde for 15 min, permeabilized with 0.1% Triton-X-100 for 10 min, blocked in PBS+5% bovine serum albumin for 60 min (all at room temperature) and incubated with primary antibodies (Table 5) on 4 °C overnight. Secondary antibody (Alexa Fluor 594 goat anti-rabbit, 1:500; Alexa Fluor 488 goat anti-mouse, 1:1000; Life Technologies, catalog numbers: A-11037 and A-11001) staining was performed for 60 min at room temperature. Antibodies were diluted in PBS+5% goat serum.

Table 5. Primary antibodies used for the immunocytochemistry of iPSCs and iPSC-derived neurons.

Antigen	Dilution	Host species	Company	Catalog number
Oct4	1:100/1:500	rabbit	Cell signaling	2840
Lin28	1:800	mouse	Cell signaling	5930
Nanog	1:300	rabbit	Cell signaling	4903
Sox2	1:400	mouse	Cell signaling	4900
Nestin	1:200	mouse	Millipore	MAB5326
Pax6	1:1000	rabbit	Life Technologies	MAB532409
Nkx2.1	1:50	1:50	Biomol	ABE-12-1259-100
Foxg1	1:50	rabbit	Life Technologies	702554
βIII tubulin (Tuj1)	1:400	mouse	R&D Systems	MAB1195
Tuj1	1:400	rabbit	Sigma-Aldrich	T3952
Vglut1	1:100	mouse	Abcam	ab134283
GluN1	1:200	rabbit	Huabio	ET1703-75
GAD67	1:1000	mouse	Millipore	MAB5406

Nuclei were counterstained with DAPI (Thermo Fisher Scientific). Three to five random regions of interest were investigated for each cover slip using an LSM700 confocal microscope (Carl Zeiss, Oberkochen, Germany) with 10x or 40x or 63x oil immersion objective. ImageJ-win64 software was used to adapt contrast brightness/background (same settings were used in case a comparison was needed).

2.8 Real-time polymerase chain reaction

Primers were designed using the following guidelines to ensure optimal performance for Polymerase Chain Reaction (PCR) amplification. The desired amplicon length was set between 100-150 bp, and primer lengths were kept within 18-22 bases. GC content was maintained within the 40-60% range to ensure stability and specificity. To avoid potential issues with polymerase slippage, runs of identical nucleotides were minimized, specifically allowing no more than two consecutive G residues. The melting temperature (Tm) of the primers was controlled within 58-62°C, with a maximum difference of 1°C between the forward and reverse primers. Additionally, the 3' end of each primer was designed to contain no more than two G or C bases within the last five nucleotides. Amplicons were designed to span one or more introns to prevent amplification of genomic DNA during quantitative PCR (qPCR). Primer sequences are listed in Table 6

Table 6. List of forward and reverse primers used for the RT-qPCR experiments.

Gene	Forward primer	Reverse primer	Function
GADPH	AGC CAC ATC GCT CAG ACA C	GCC CAA TAC GAC CAA ATC C	Housekeeping
HMBS	CCT GCC AGA GAA GAG TGT GG	ATG GCA CTG AAC TCC TGC TG	Housekeeping
PSMB4	CAT TCC GTC CAC TCC CGA TT	CGA ACT TAA CGC CGA GGA CT	Housekeeping
C1orf43	CCG TTC CTT AAT GGG CAA GAA	CAA AGA CCC CTG TCC CAT AGC	Housekeeping
Oct4	GGG GGT TCT ATT TGG GAA GGT A	ACC CAC TTC TGC AGC AAG GG	Pluripotency
Vglut1	AGG AGG AGC GCA AGT ACA TC	GAC TGG CAT AGA CGT GAA GAA G	Glutamatergic marker
Grin1	ACC CGC ATG TCC ATC TAC T	CGC TGA CCA GCA GGA TGA T	NMDAR
Gria1	GGG ACC AGA CAA CCA GTG AC	AGG TGA AGA ACC ACC AGA CG	AMPA receptor
Grik1	ATG AAA CAG CCG CTG AAA TCC	GAA ACC CGG TCA TGT TTA CGC	Kainate receptor

Cells were collected using Accutase and centrifuged at 200 g for 5 min. RNA was isolated using the Nucleospin® RNA kit (Macherey-Nagel) according to the manufacturer's instructions. After elution with RNAse-free water, RNA was reverse transcribed using the SensiFAST cDNA Synthesis Kit (Bioline). The RNA and DNA concentration and purity were

determined with the NanoDrop 2000c (Thermo Fisher Scientific). qPCR was performed with Quantitect SYBR-Green on a Rotor-Gene Q real-time cycler (Qiagen). A 10-min preincubation period at 95 °C was followed by an amplification cycle: at 95 °C for 15 s, at 60 °C for 1 min, repeated 40 times. Data were calculated based on the $2^{-\Delta\Delta Ct}$ method: data were normalized to the Ct-value of the housekeeping gene GAPDH of the same sample and depicted relative to the respective gene expression of iPSCs at day 0. Mean and standard deviation of technical triplicates are shown.

2.9 Calcium imaging

Images were captured using a Hamamatsu Orca Flash 4.0 LT Plus camera with 340/380 nm illumination from a CoolLED pE340 Fura system, reflected by a T400lp dichroic mirror and emitted through an ET510/80m emission filter (Chroma Technology). A Zeiss Axio Vert microscope with a Fluar 20x objective (Zeiss) was used. Acquisitions were controlled via µManager v2.0 (Edelstein et al., 2014) at a rate of 1 Hz, using a 50 ms exposure time, with 1-20 second intervals between frames during baseline and compound addition, and 20-second intervals during compound wash-out.

Each coverslip containing iPSC-derived neurons was incubated with freshly prepared Fura 2-AM (Life Technologies) in bath solution (2 µM) for 15–20 minutes at room temperature in the dark. The Mg-free bath solution contained (in mM): 140 NaCl, 3 KCl, 1 CaCl2, 10 HEPES, 20 glucose, pH 7.4. Coverslips were mounted in an RC-25 Open Diamond Bath Imaging Chamber (Warner Instruments) secured in a PH-3 chamber (Warner Instruments) and perfused with bath solution for 20–30 minutes before acquisition.

Light intensities for 340 and 380 nm, as well as image thresholds, were adjusted to optimize signal-to-noise ratio while minimizing photobleaching prior to acquisition. Experiments involved recording baseline ratio for 5 minutes during bath perfusion, followed by the addition of NMDA (100 µM for 1 minute), NMDA + Ketamine (100 µM and 5 µM, respectively, for 12 minutes), and a wash step. 100 mM KCl was applied as a control at the end of each experiment.

3 Results

3.1 Effect of schizophrenia-associated mutations in NaV1.2

In order to assess the effect of the mutations on NaV1.2 properties, we conducted whole-cell patch-clamp recordings on HEK293T cells expressing either one of the mutants or the wild-type (WT) NaV1.2 co-transfected with eGFP. The extracellular sodium concentration was lowered compared to the physiological values (40 mM instead of 140 mM NaCl) to prevent large current and subsequent voltage errors in all subsequent experiments.

3.1.1 R850P and V1282F alter voltage dependence of activation, S1656P abolishes the activation current

Activation analysis is used to determine voltage dependence and kinetics of channel opening, allowing to calculate the potential, at which half of the sodium channels are activated ($V_{1/2}$), etc. The peak currents are measured at different voltages and the I-V curve is plotted. Using this plot, the conductance is calculated, normalized to the maximum conductance and plotted against the corresponding voltage. The data is fitted with a Boltzmann function, which allows to extract $V_{1/2}$ and slope values.

Cells were maintained at a holding potential of -120 mV and then depolarized using 40 ms voltage steps of 10 mV up to 50 mV (Fig. 10a). WT, R850P and V1282F mutants responded to voltage steps with rapid inward currents followed by a slower decay in a voltage-dependent manner (Fig. 10b). The maximum peak current density was the largest for WT (-0.245±0.127 nA/pF), then followed by V1282F (-0.185±0.118 nA/pF) and R850P (-0.180±0.074 nA/pF) had the smallest value. Comparison of the current densities revealed a significant decrease for both mutants (Fig. 10c, Table 7). In contrast, S1656P exhibited no current in response to the applied voltage changes, indicating a complete LoF effect that remained unaffected by post-transfectional incubation at 30°C (data not shown). This temperature is commonly used to promote proper folding and trafficking of mutant ion channels, but it failed to restore S1656P function (Rusconi et al. 2007). The mean voltage error was not significantly different between groups

Table 7. Statistics of the activation results. Values are given as mean ± standard deviation. Adjusted p-values refer to the post-hoc comparison between the mutant and the wild-type.

	WT, n=57	P850R, n=53		V1282F, n=24		Kruskal-Wallis test: 3 conditions, 134 values	
	mean±SD	mean±SD	adj. p-value	mean±SD	adj. p-value	stat.	p-value
Current dens., nA/pF	-0.245 ±0.127	-0.180 ±0.074	0.0303	-0.185 ±0.118	0.0181	9.24	0.0098
Activation $V_{1/2}$, mV	-38.3±4.3	-29.3±5.1	<0.0001	-36.2±4.7	0.2345	62.82	<0.0001
Activation slope	8.2±0.7	10.0±1.0	<0.0001	9.5±1.3	<0.0001	69.55	<0.0001
Time to peak at -40 mV, ms	0.58±0.10	0.91±0.28	<0.0001	0.64±0.16	0.4935	44.12	<0.0001
Decay at -40 mv, s^{-1}	1.3±0.5	2.2±0.9	<0.0001	1.5±0.6	0.7857	49.90	<0.0001

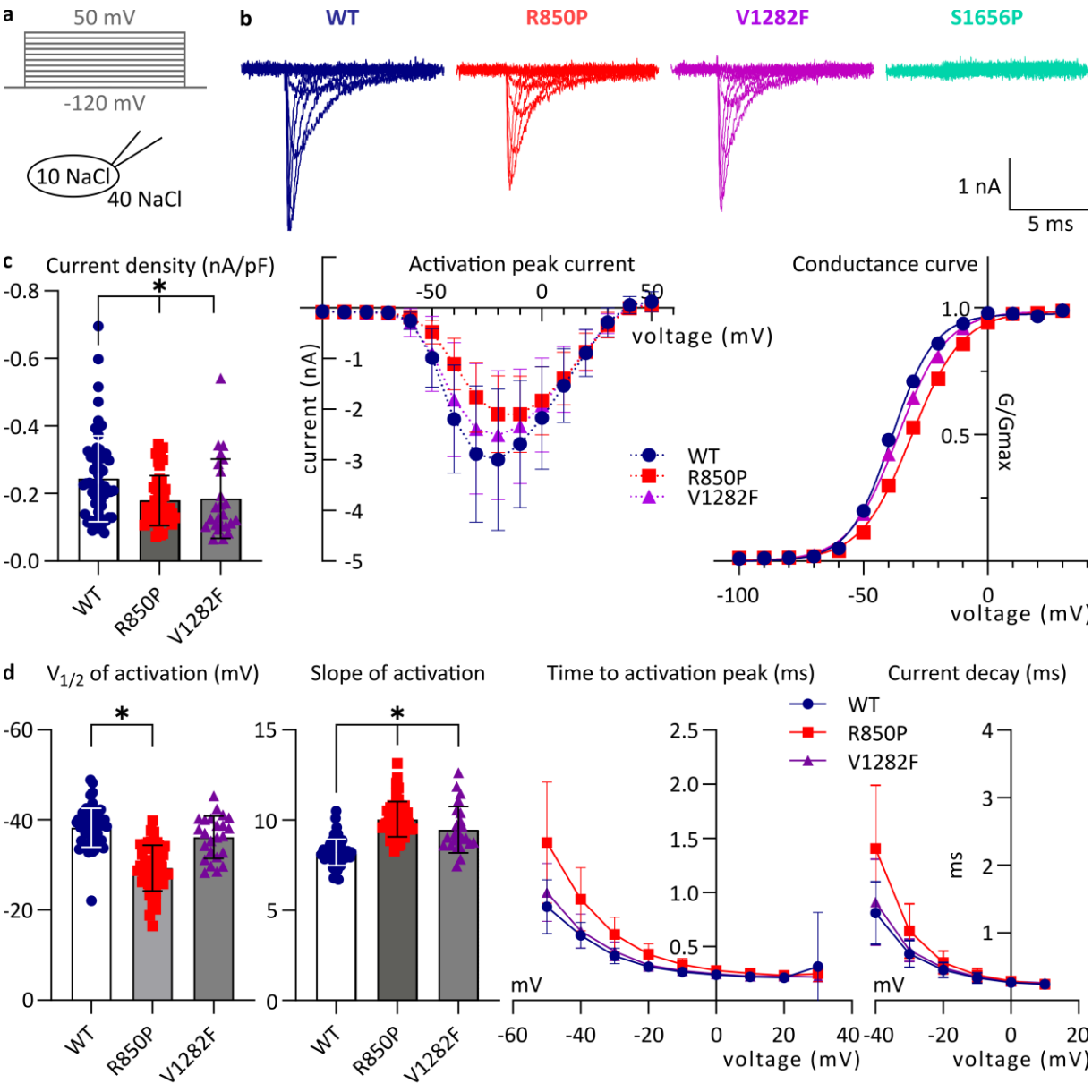

Figure 10. Activation analysis of HEK293T cells expressing NaV1.2 WT (n=57), R850P (n=53), V1282F (n=24) or S1656P (n=21): ***(a)*** *Schematic voltage protocol (top). Cells were depolarized by rectangular voltage steps from the holding potential of -120 mV with a 10 mV increment up until +50 mV. Extracellular solutions with reduced Na^+ concentration (bottom) were used to avoid large currents.* ***(b)*** *Representative current traces for each construct tested.* ***(c)*** *Statistical comparison to the WT NaV1.2 of the current density (left): WT in blue circles, R850P in red squares, and V1282F in purple triangles. Kruskal-Wallis test was used, asterisk reflects p-value < 0.05 and error bars indicate the standard deviation. Peak currents of the activation plotted against the respective potentials (middle). Voltage dependence of conductance (right), the lines are derived from Boltzmann fit.* ***(d)*** *Statistical comparison of the $V_{1/2}$ and slope values (derived from a Boltzmann fit of the conductance curve of each individual cell) between the mutants and the WT, respectively (left). Voltage dependence of the time to activation peak and current decay (right). Line connects the mean values.*

The conductance curve showed a slight depolarized shift of V1282F activation and more pronounced one for R850P (Figure 10c). Activation analysis data are summarized in Table 7. The $V_{1/2}$ value for WT NaV1.2 was -38.3±4.3 mV, with a depolarized shift observed due to the use of patch solutions with reduced Na^+ concentration. Compared to WT, R850P had a further significantly depolarized $V_{1/2}$ of -29.3±5.1 mV. For V1282F, the shift was only 3.1 mV with a $V_{1/2}$ value of -36.2±4.7 mV, and the difference did not reach the significance level (Fig. 10c). Both mutants caused significant alterations of the activation slope (WT: 8.2±0.7, R850P: 10.0±1.0, V1282F: 9.5±1.3; Fig. 10d). Moreover, R805P was activating and inactivating more slowly, as indicated by an increased time to peak current and prolonged current decay (Fig 10d).

3.1.2 R850P alters voltage dependence of inactivation

Inactivation experiments involved a two-pulse voltage clamp protocol. Cells were maintained at a holding potential of -120 mV, then a conditioning 500 ms pre-pulse to a range of steps from -130 to -40 mV was applied. After each conditioning pulse, a 50 ms test-pulse to -10 mV was applied, where sodium channels have near to maximum conductance (Fig. 11a). The test pulse peak current normalized to the pre-pulse peak current indicates the fraction of channels that were not inactivated by the conditioning pulse (Fig. 11b). The data are summarized in Table 8.

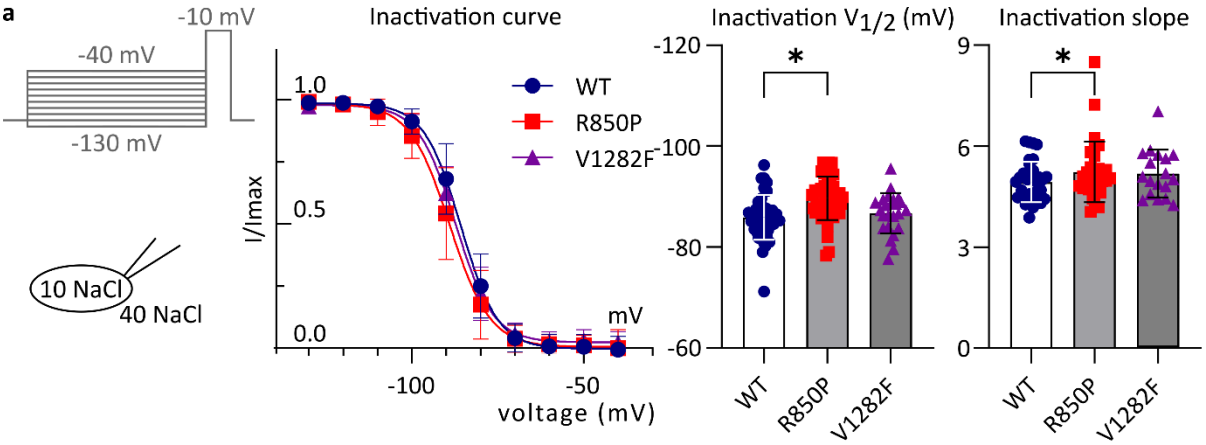

*Figure 11. Inactivation analysis of HEK293T cells expressing NaV1.2 WT (n=40), R850P (n=33) or V1282F (n=19): **(a)** Schematic voltage protocol (top). Cells were depolarized by pre-pulse starting from -130 mV with a 10 mV increment followed by a test-pulse to -10 mV. Extracellular solutions with reduced Na^+ concentration (bottom) were used to avoid large currents. **(b)** Voltage dependence of steady-state fast inactivation: peak current obtained from the test-pulse was normalized to a maximum pre-pulse current and plotted against the pre-pulse potential. WT in blue circles, R850P in red squares, and V1282F in purple triangles. Line represents Boltzmann fit of the mean values and error bars indicate the standard deviation. **(c)** Statistical comparison of the inactivation $V_{1/2}$ and slope. Kruskal-Wallis test was used, asterisk reflects p-value < 0.05.*

WT, R850P and V1282F showed decrease in the test pulse peak current along the pre-pulse depolarization. The inactivation $V_{1/2}$ of WT was measured at -85.6±4.2 mV. R850P demonstrated a significant hyperpolarized 3.4 mV shift of the inactivation curve (Fig. 11c).

V1282F also had a 1.4 mV hyperpolarized shift, which, however, failed statistical significance. The inactivation slope of the R850P also showed a statistically significant difference. (4.9±0.6 for WT vs 5.3±0.9 for R850P).

Table 8. Statistics of the inactivation results. Values are given as mean ± standard deviation. Adjusted p-values refer to the post-hoc comparison between the mutant and the wild-type.

	WT, n=40	P850R, n=33		V1282F, n=19		Kruskal-Wallis test: 3 conditions, 92 values	
	mean±SD	mean±SD	adj. p-value	mean±SD	adj. p-value	stat.	p-value
Inactivation $V_{1/2}$, mV	-85.6±4.2	-89.0±4.4	0.0006	-87.0±3.2	0.2645	13.11	0.0014
Inactivation slope	4.9±0.6	5.3±0.9	0.0362	5.2±0.7	0.1295	6.634	0.0363

3.1.3 R850 affects subthreshold depolarization

Ramp current protocols for subthreshold depolarization are designed to study the properties of sodium channels that contribute to neuronal excitability, synaptic integration and the initiation of action potentials under conditions that do not reach the threshold for action potential firing.

Cells were depolarized from -120 mV to 20 mV with a slow ramp of 117 ms (Fig. 12a). The area under the current curve was measured and normalized to the maximum current obtained from the activation protocol, serving as an indirect measure of channel open time. This value provides insight into the overall efficiency and duration of ion flow through the channel. In addition to this, the time to peak, current amplitude, and normalized amplitude were calculated and compared between different variants (Fig. 12b-e). The results are summarized in Table 9.

The voltage application resulted in a 70-600 pA bell-shaped inward current with a mean peak at 54±3.8 ms for WT NaV1.2. R850P had current peak delayed for 2 ms (Fig. 12b). Normalized amplitudes were indistinguishable between proteins. On a descriptive level, R850P and V1282F had a tendency towards higher normalized integrals, but also exhibited higher variance, accordingly group differences did not reach the significance level (Fig. 12e).

Table 9 Statistics of the ramp-elicted current results. Values are given as mean ± standard deviation. Adjusted p-values refer to the post-hoc comparison between the mutant and the wild-type.

	WT, n=35	P850R, n=29		V1282F, n=22		Kruskal-Wallis test: 3 conditions, 61 values	
	mean±SD	mean±SD	adj. p-value	mean±SD	adj. p-value	stat.	p-value
Norm. integral, 10^{-3} ms	1.3±0.39	1.6±0.62	0.1671	1.7±0.87	0.2112	3.965	0.1377
Time to peak, ms	54±3.8	56±3.8	0.0182	54±3.9	0.8031	6.878	0.0321
Norm. amplitude	0.10±0.036	0.10±0.049	>0.9999	0.10±0.045	>0.9999	0.3018	0.8599
Amplitude, nA	-0.26±0.11	-0.21±0.11	0.0540	-0.27±0.16	>0.9999	5.056	0.0798

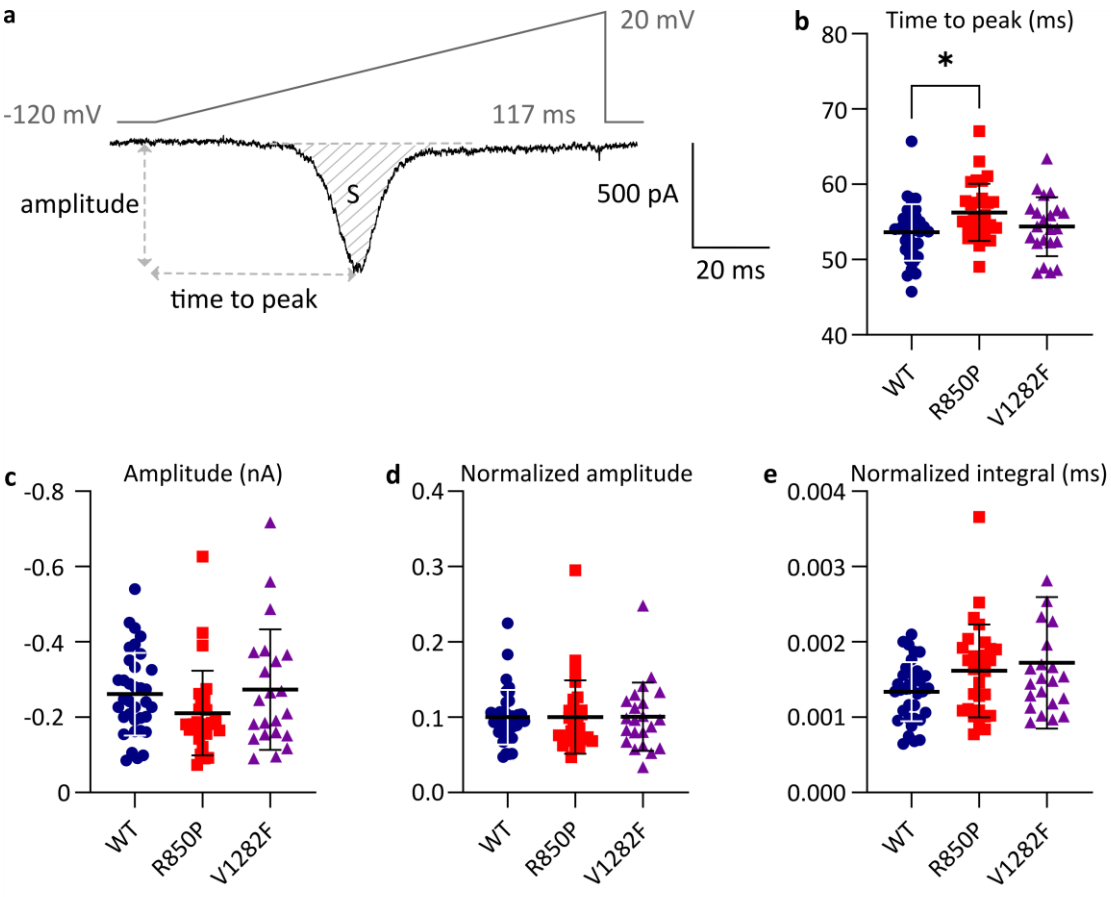

*Figure 12. Subthreshold depolarization analysis of HEK293T cells expressing NaV1.2 WT (n=35), R850P (n=29) or V1282F (n=22): **(a)** Schematic voltage protocol (top). Cells were slowly depolarized by a triangular ramp. Representative recording (bottom), highlighting the analyzed parameters. **(b)-(e)** Statistical comparison of the time to peak, amplitude, amplitude normalized to the maximum current of the activation and normalized integral. WT in blue circles, R850P in red squares, and V1282F in purple triangles. Kruskal-Wallis test was used, asterisk reflects p-value < 0.05. Black line illustrates the mean value and error bars indicate the standard deviation.*

3.1.4 R850P modifies the use-dependent block

To investigate how the activity of sodium channels changes in response to repetitive stimulation, we used the use-dependence (UD) protocol. This protocol allows for the measurement of use-dependent block, i.e., a reduction in sodium channel current in response to repetitive activation, mimicking conditions of repetitive neural firing.

Cells were repetitively depolarized from the holding potential of -120 mV to 0 mV (Fig.13a). The pulse duration was 5 ms, and the interpulse duration was varied to have following pulse frequencies: 10, 25, 50 and 100 Hz. For each sweep, the peak current average of the last three pulses was normalized to the first pulse peak current. The data are summarized in Table 10.

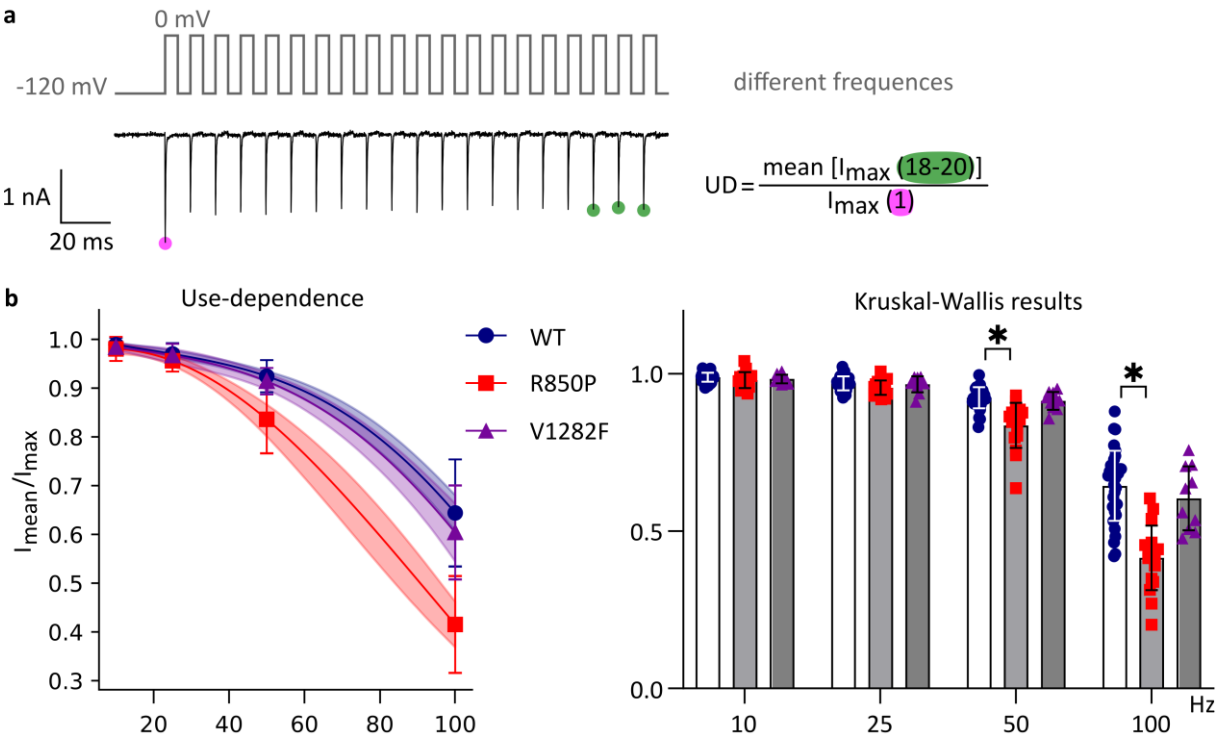

Figure 13. Use-dependence analysis of HEK293T cells expressing NaV1.2 WT (n=34), R850P (n=17), or V1282F (n=10): ***(a)*** *Schematic voltage protocol (top). Cells were depolarized by 5 ms pulses at different frequencies. Representative recording (bottom), highlighting the first current peak and the last three, which were used to calculate the use dependence (bottom right).* ***(b)*** *Use-dependence plotted against the pulses frequencies. WT in blue circles, R850P in red squares, and V1282F in purple triangles, representing the mean values ± standard deviation. Solid lines represent the bootstrapped mean of non-parametric fits, and shaded area show bootstrapped 95% confidence intervals for those fits. Non-overlapping confidence intervals indicate a significant difference between the curves starting from 38 Hz.* ***(c)*** *Statistical comparison of the use-dependence utilizing the Kruskal-Wallis test. Asterisk reflects p-value < 0.05.*

At 10 Hz, only slight reduction in the current was observed for all of the constructs. At 25 Hz frequency, reduction of 3-5% was measured for all three NaV constructs, without statistical difference yet. At 50 Hz, difference in reduction became significant, resulting in 8%, 16% and 9% for WT, R850P and V1282F, respectively. Finally, with pulses applied at 100 Hz resulted in 36% current reduction for WT, 58% reduction for R850P and 40% reduction for V1282F (Fig.13b).

Table 10. Statistics of the use-dependence results. Values are given as mean ± standard deviation.

I_{mean}/I_{max}:	WT, n=34	P850R, n=17		V1282F, n=10		Kruskal-Wallis test: 3 conditions, 61 values	
	mean±SD	mean±SD	adj. p-value	mean±SD	adj. p-value	stat.	p-value
at 10 Hz	0.99±0.014	0.98±0.025	0.1032	0.98±0.014	0.4820	4.228	0.1208
at 25 Hz	0.97±0.023	0.96±0.023	0.0929	0.97±0.025	>0.9999	4.634	0.0986
at 50 Hz	0.92±0.033	0.84±0.072	<0.0001	0.91±0.029	0.8049	24.77	<0.0001
at 100 Hz	0.64±0.11	0.42±0.10	<0.0001	0.60±0.10	0.9461	21.51	<0.0001

3.1.5 R850P impacts recovery from fast inactivation

To investigate why the R850P variant shows a stronger current reduction to repetitive stimulation, we analyzed the rate at which it transitions from an inactivated state back to a state where it can open again (recovery), compared to the WT. The protocol begins with a voltage step (pre-pulse) that depolarizes the membrane, causing sodium channels to open and then quickly inactivate. Following the inactivation phase, the membrane potential is returned to a hyperpolarized or resting level for varying durations (Fig. 14a). This allows the channels to transition from the inactivated state back to the closed (but activatable) state. After the recovery period, a test depolarization is applied to assess the fraction of channels that have recovered from inactivation and are available to open. Peak current of the test pulse is then normalized to the pre-pulse current (Fig. 14b) and plotted as a function of the recovery interval duration. The recovery from inactivation is then fitted using a mono- or bi-exponential equation (Fig. 14c), which provides insights into the kinetics of the recovery process. Knowing how quickly sodium channels can recover from inactivation is crucial for understanding their role in repetitive firing of neurons.

Since the recovery potential can affect the speed of channel recovery and the occurrence of recovery from slow inactivation, we investigated recovery interpulses at -100 mV and -120 mV in this series of experiments. For the -100 mV interpulse, we observed that the test pulse to pre-pulse ratio, when plotted against the interpulse duration, could be fit with a monoexponential function. The data are summarized in Table 11. R850P displayed delayed recovery process with a time constant of 24±9.9 ms (K = 0.049±0.017 ms^{-1}), while WT had time constant of 14±4.0 ms (K = 0.076±0.019 ms^{-1}).

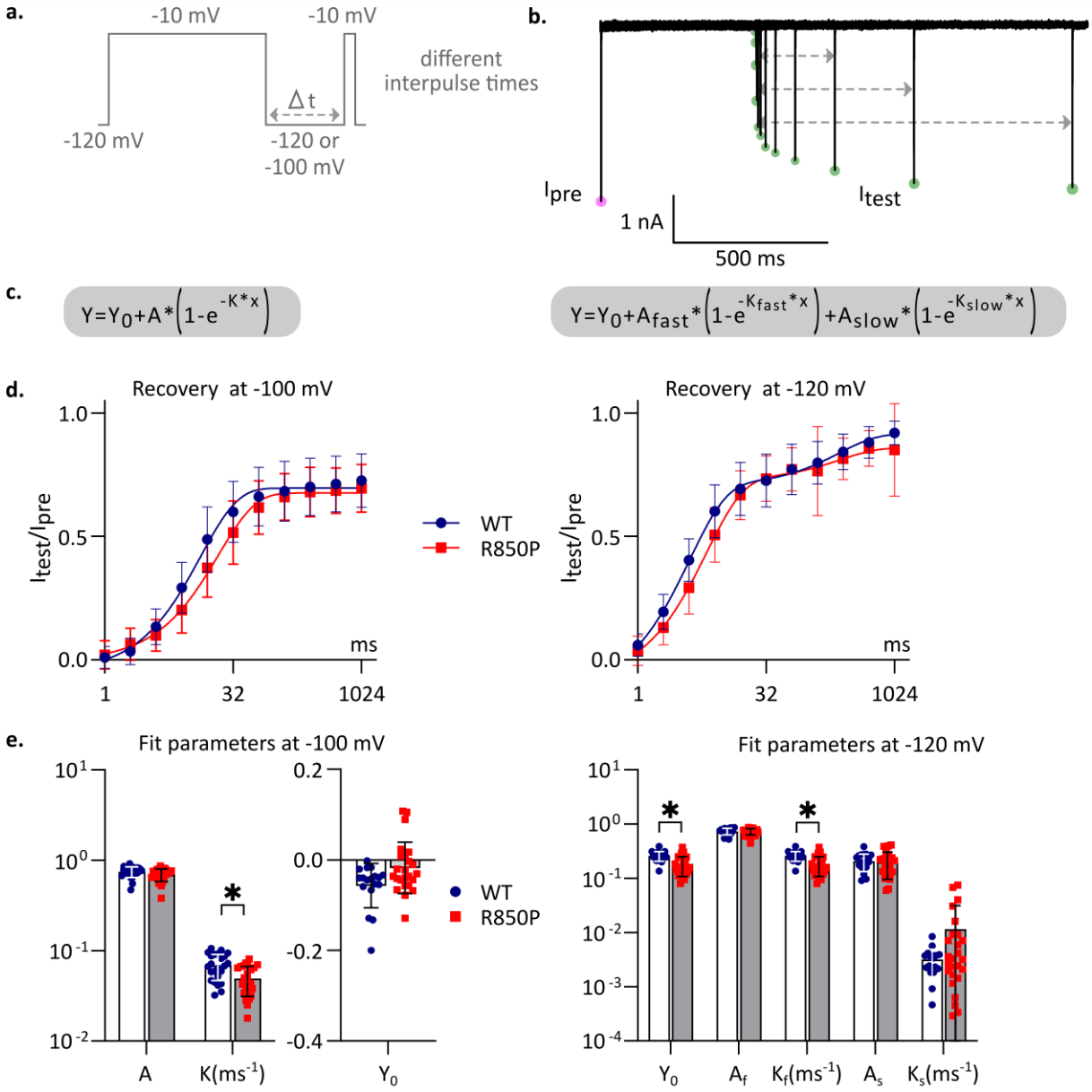

Figure 14: Recovery from fast inactivation analysis of HEK293T cells expressing NaV1.2 WT or R850P: ***(a)*** *Schematic voltage protocol.* ***(b)*** *Representative recording indicating varying sodium inward currents in response to depolarization after different inter-pulse times.* ***(c)*** *Fitting formula used for recovery inter-pulse at -100 mV (mono-exponential function) and -120 mV (bi-exponential function).* ***(d)*** *Time course of recovery from fast inactivation with -100 mV inter-pulse (left) and with -120 mV (right) inter-pulse. Peak current at the test-pulse is normalized to the pre-pulse peak current and plotted against the time of the inter-pulse. WT in blue circles, R850P in red squares. Circles represent the mean of individual recordings ± standard deviation. The line illustrates the curve fitted to these mean values.* ***(e)*** *Fit parameters of individual cells.*

At a -120 mV interpulse, the recovery pattern displayed a biexponential component. This change likely indicates that recovery from slow inactivation is occurring in addition to the fast inactivation recovery. In this scenario, the R850P variant demonstrated a decreased initial value (Y_0) and an increased fast time constant (Tau_{fast}) by 2.4 ms.

Table 11. Statistics of the fit parameters of individual cells subjected to recovery from fast inactivation protocol. Values are given as mean ± standard deviation

	WT, n=18 mean±SD	P850R, n=24 mean±SD	Mann Whitney test		
			Sum of ranks	M-V U	p-value
At -100 mV recovery interpulse					
Y_0	-0.057±0.049	-0.018±0.057	319, 584	148	0.0851
A	0.75±0.11	0.70±0.11	464, 439	139	0.0511
K (ms^{-1})	0.076±0.019	0.049±0.017	534, 369	69	<0.0001
Tau (ms)	14±4.0	24±9.9	240, 663	69	<0.0001
At -120 mV recovery interpulse					
Y_0	0.26±0.053	0.18±0.072	593.5, 441.5	90.50	0.0002
A_{fast}	0.74±0.10	0.73±0.096	456, 579	228	0.6738
K_{fast} (ms^{-1})	0.26±0.053	0.18±0.072	593.5, 441.5	90.50	0.0002
A_{slow}	0.21±0.074	0.20±0.10	468, 567	216	0.4836
K_{slow} (ms^{-1})	0.0032±0.0018	0.012±0.020	410, 625	220	0.5463
Tau_{fast} (ms)	4.0±1.0	6.4±2.4	280.5, 754.5	90.50	0.0002

3.2 Two new iPS cell lines of patients with schizophrenia

One male and one female patient were selected by Jun.-Prof. Dr. Gaebler based on their resting state fMRI functional connectivity profiles that indicated a likely NMDAR dysfunction. Jun.-Prof. Dr. Gaebler also collected their blood samples. The reprogramming process is summarized in Tables 12 and 13.

PBMCs were isolated and reprogrammed using Sendai virus and placed on a MEF layer. Within 7 to 14 days, the initially single cells grow into visible colonies (Fig. 15a,b). On day 23, colonies were considered big enough to pick 16 clones for each patient. A variety of colonies showed distinct morphologies, with some having diffuse edges, inclusions, or sharp edges (Fig. 15c). After picking, the colonies were transferred to feeder-free conditions on Geltrex and later to Vitronectin-coated plates for further expansion and characterization. The time course for each clone is reflected in Tables 12 and 13. Of the clones picked, five for the first patient and six for the second patient were lost during the process. However, multiple clones successfully reached later stages of freezing at passage 8-10 in feeder-free conditions. To assess their pluripotency, the cells were stained for pluripotency markers Oct4, Sox2, Nanog and Lin26 (Fig. 15c,d).

In summary, the reprogramming process yielded four viable iPSC lines per patient, despite several clones lost or contaminated with differentiated cells. The iPSC lines were then tested for their ability to differentiate into neuronal cells.

Table 12: Summary of Reprogramming and Characterization of iPSC Clones Derived from Patient 1 PBMCs

Clone:	P1, Colony picked 28.10.22, day 23	P2, transfer to 6-well	Transferred to feeder-free	Transferred to Vtn	Staining Oct4, Sox2, Nanog, Lin26
NR1_1	Round, dense, 1.2 mm	Lost			
NR1_2	Edgy, dense, 0.8 mm	Lost			
NR1_3	Diffused edges, dense, 2 mm		25.11.22 P4 frozen on MEF	29.12.22 P8-9 frozen of Vtn, “dirty” iPS	
NR1_4	Diffused edges, dense, 1.2 mm		27.11.22 P4 frozen on MEF	12.12.22 frozen of Vtn, good iPS	good
NR1_5	Round, small, 0.8 mm		28.11.22 P4 frozen on MEF	12.01.22 frozen of Vtn, ok iPS	
NR1_6	Round, diffused edges, 1.5 mm		28.11.22 P4 frozen on MEF	Lost	
NR1_7	Round, sharp edges, dense inclusion, 1mm		27.11.22 P4 frozen on MEF	06.01.22 frozen of Vtn, ok iPS	Too few cells
NR1_8	Round, formation in the center, 2 mm		25.11.22 P4 frozen on MEF	24.12.22 frozen of Vtn, ok iPS	ok
NR1_9	Diffused edges, dense, inclusions, 2 mm		25.11.22 P4 frozen on MEF	24.01.22 frozen of Vtn, “dirty” iPS	ok
NR1_10	No data	Lost			
NR1_11	Long, defined but jagged edges, dense, 1.5 mm		25.11.22 P4 frozen on MEF	02.12.22 frozen of Vtn, good iPS	good
NR1_12	Round, homogeneous, defined but jagged edges, 1 mm		25.11.22 P4 frozen on MEF	07.12.22 frozen of Vtn, ok iPS	good
NR1_13	Long, homogeneous, defined but jagged edges, 1 mm		27.11.22 P4 frozen on MEF	30.12.22 frozen of Vtn, good iPS	Differentiated cells present
NR1_14	Long, defined but jagged edges, dense, 1 mm		25.11.22 P4 frozen on MEF	02.12.22 frozen of Vtn, good iPS	Differentiated cells present
NR1_15	Round, defined edges, dense with inclusions	Lost			
NR1_16	Round, dense with inclusions, 1.2 mm	Lost			

Table 13: Summary of Reprogramming and Characterization of iPSC Clones Derived from Patient 2 PBMCs

Clone:	Colony picked	P2, transfer to 6-well	Transferred to feeder-free	Transferred to Vtn	Staining Oct4, Sox2, Nanog, Lin26
NR2_1	Triangular, homogeneous, 1mm		06.12.22 P5 frozen on MEF	Frozen on Vtn, many differentiated	
NR2_2	Round with inclusions, 1.5 mm	Lost			
NR2_3	Round, homogeneous, 1.5 mm		06.12.22 P6 frozen on MEF	Frozen on Vtn, many differentiated	Inconsistent staining
NR2_4	Round, very dense, 1mm		Lost on MEF, kept on Geltrex	26.12.22 frozen of Vtn, good iPS	good
NR2_5	Not round, homogeneous, 1mm		28.11.22 P4 frozen on MEF	26.12.22 frozen of Vtn, ok iPS	Differentiated cells present
NR2_6	Oval, dense, 1mm		Lost		
NR2_7	Triangular, different inclusions, 1.5 mm		27.11.22 P4 frozen on MEF	24-30.12.22 P8-10 frozen of Vtn, good iPS	ok
NR2_8	Jagged edges, homogeneous, 1mm		01.12.22 P4 frozen on MEF	01.12.22 frozen of Vtn, few cells	
NR2_9	Round, dense, 1 mm	Lost			
NR2_10	Round, dense, diffused edges 2mm	Lost			
NR2_11	No data	Lost			
NR2_12	Jagged edges, inclusions, “cap”, 1 mm	Lost			
NR2_13	Round, diffused edges, 2 mm		01.12.22 P5 frozen on MEF	24-29.12.22 P9 frozen of Vtn, good iPS	good
NR2_14	Round, homogeneous, 1.5 mm		06.12.22 P6 frozen on MEF	30.12.22 P8 frozen of Vtn, good iPS	Differentiated cells present
NR2_15	No data	Lost			
NR2_16	Oval, 1.5 mm		25.11.22 P4 frozen on MEF	15.12.22 P8 frozen of Vtn, good iPS	good

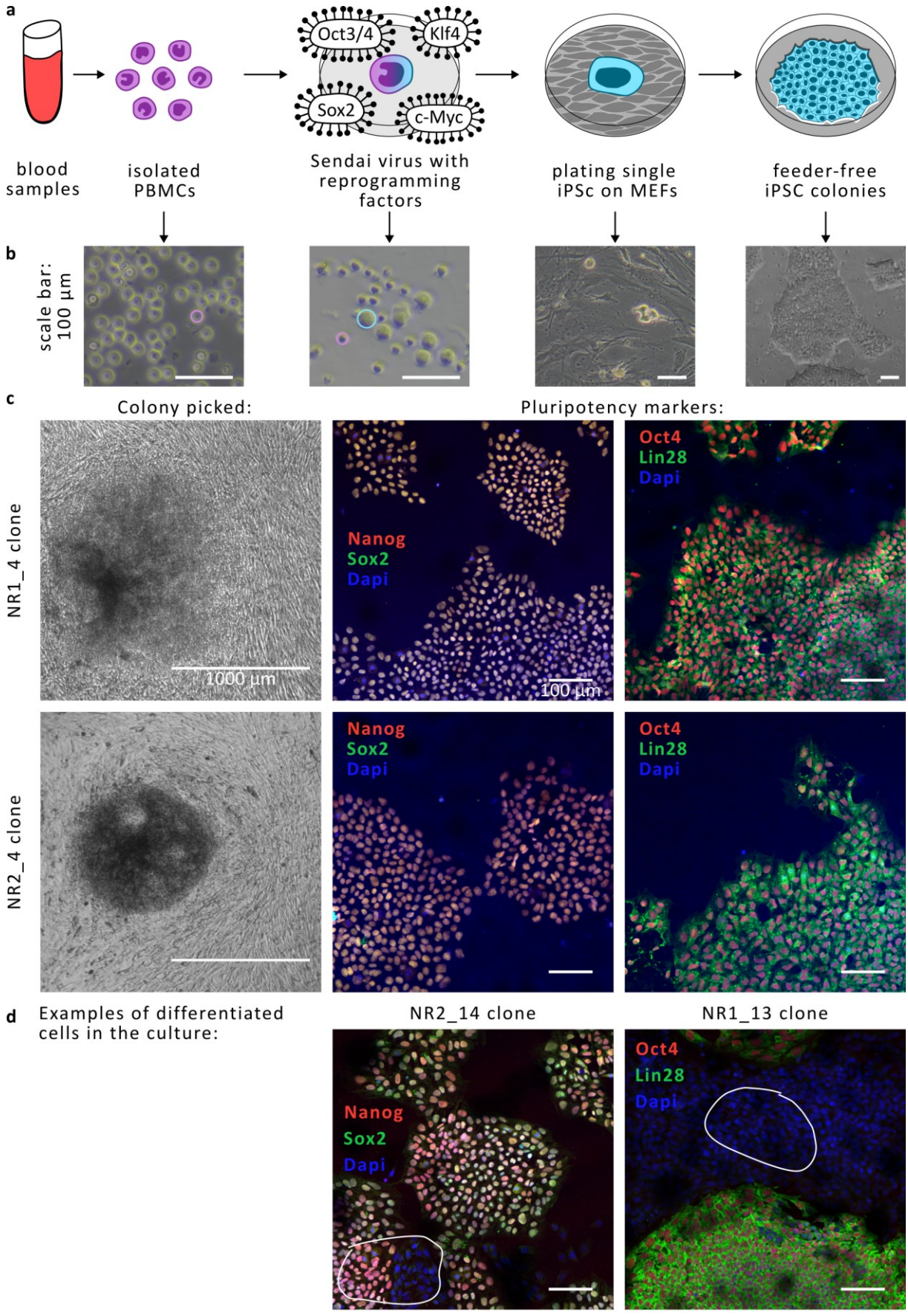

Figure 15: Reprogramming of PBMCs of two patients with SZ: ***(a)*** Schematic depiction of the reprogramming process. **(b)** Optical microscopy pictures of the cells undergoing

reprogramming with notable changes of the cell size; **(c)** Left column: Depiction of a representative colony picked on day 23, Right column: Immunostaining for pluripotency markers Oct4 (red), Sox2 (green), Nanog (red), and Lin28 (green), DAPI is stained blue; **(d)** example of iPSCs contaminated with differentiated cells.

3.3 Testing glutamatergic neuronal differentiation on iPS cells

For glutamatergic cortical differentiation, we followed a modified protocol based on(Qi et al. 2017) which employed dual SMAD inhibition to drive iPSCs towards a neural fate (Fig. 16a). Initially, the cells were transferred onto Geltrex and allowed to reach 90–100% confluency. At this stage, differentiation media containing small molecules were applied to promote neural lineage specification. Immunostaining performed on day 0 confirmed the expression of Oct4, a pluripotency marker, with no detection of neuronal markers, indicating the cells were still in an undifferentiated state.

By day 8, many cells exhibited visible neurites, characteristic of early neuronal development. Nearly all cells were positive for Nestin, a marker of neural progenitor cells, and some cells began to express Tuj1, an early marker of post-mitotic neurons (Fig. 16b,c). After passaging on day 8, the cells continued to differentiate, with longer neurites extending and forming early neuronal clusters.

Finally, by day 34, immunostaining revealed the presence of Vglut1, a specific marker for glutamatergic neurons (Fig. 16c), confirming successful differentiation into cortical neurons with a glutamatergic identity. This result demonstrates that the reprogrammed iPSCs were capable of efficiently differentiating into neurons that align with cortical excitatory cell types.

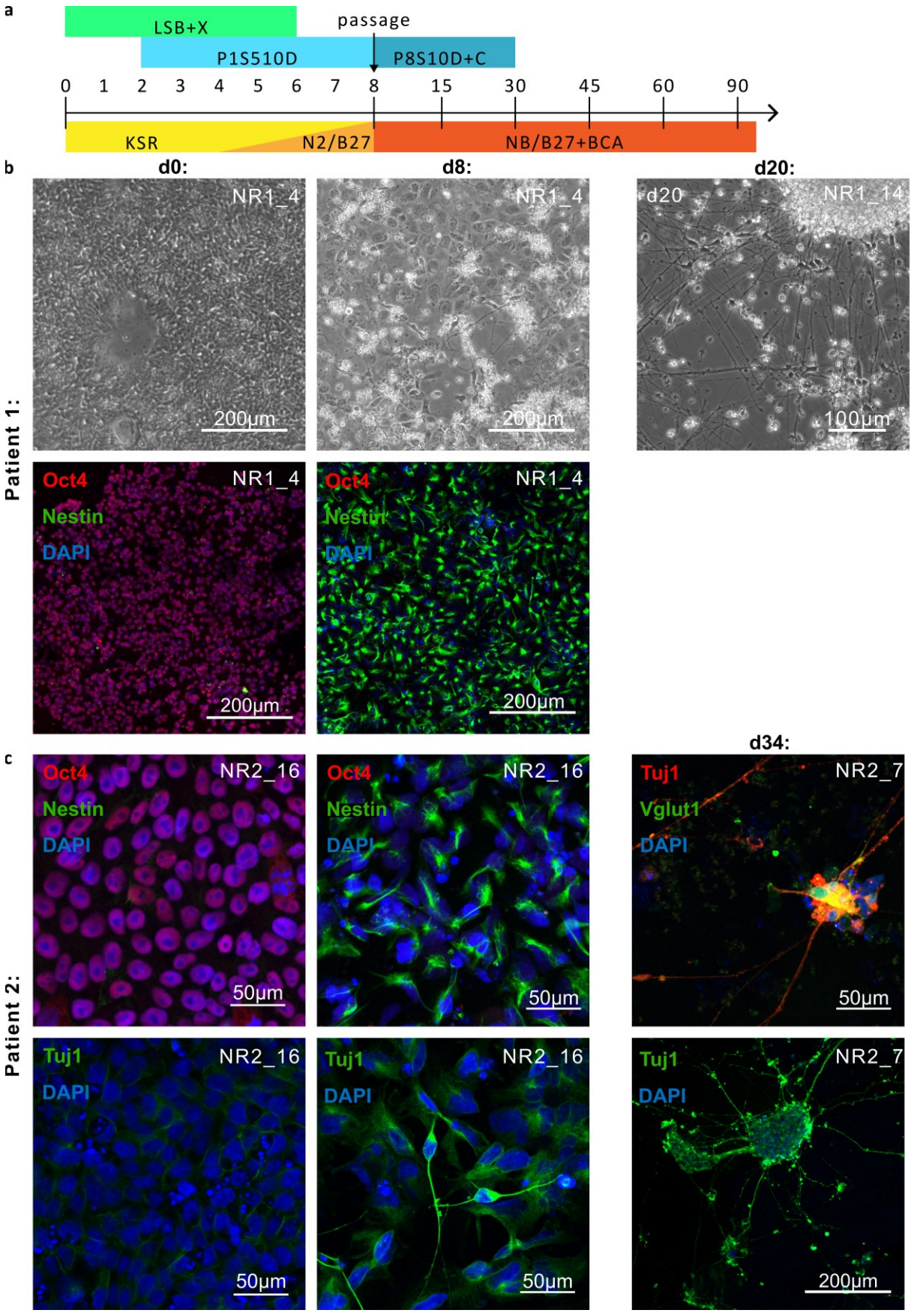

Figure 16. Cortical differentiation of reprogrammed iPSCs: ***(a)*** *Schematic representation of the modified dual SMAD inhibition protocol for cortical differentiation, adapted from Qi et al. (2017).* ***(b)*** *Top: Phase contrast microscopy images of differentiation*

stages; Bottom: Immunostaining of cells on day 0 and 8 for pluripotency markers Oct4 (red), neural progenitor marker Nestin (green), indicating successful differentiation of iPSCs from Patient 1. DAPI (blue) was used for nuclear counterstaining. ***(c)*** *Immunostaining of cells from patient 2 on day 0, 8, and 34 for Oct4 (red), Nestin (green), post-mitotic neuronal marker Tuj1 (green), and glutamatergic marker Vglut1 (green).*

3.4 Proof of principle of NMDAR recordings in iPSC-derived neurons

To test the NMDAR dysfunction hypothesis in iPSC-derived neurons, we differentiated a control cell line until d60 and further. We aimed to characterize mature neurons in their expression profile, electrophysiological properties and NMDAR function specifically. The same differentiation protocol was applied (Fig. 17a). Cells developed visible processes by day 8 and formed cluster with strong neural connections from around day 30 (Fig. 17b). Immunostaining and qPCR revealed Oct4 expression on day 0, that was not detected on day 8 and further. On day 8, cells were positive for Tuj1, Nestin, and glutamatergic progenitor marker Pax6. By day 60, cells were expressing both Vglut and GluN1 (NMDAR subunit1), which was confirmed by immunostaining and qPCR (Fig. 17c, d).

For the functional characterization of iPSC-derived neurons, the current clamp technique was employed using internal and external solutions that mimicked physiological ion composition. We measured the resting membrane potential and assessed the rheobase using a 200 ms pulse protocol. Additionally, a longer protocol was utilized, which involved injecting a rheobase current followed by a second pulse with double rheobase current (Fig. 18a).

We considered neurons mature when their action potentials were spike shaped, overshooting above the 0 mV level, and the neurons were able to fire repetitively with the frequency of firing correlating with the injected current. The neurons were able to fire immature action potentials already on day 15. Multiple APs were detected on day 30, however, most of them were rather immature. On day 45, multiple mature APs were detected, and by day 60 the neurons fired repetitively with a prominent overshoot (Fig. 18b). With the long-pulse protocol, we detected some synaptic events on day 30, and steady firing frequency increase was observed on day 60 (Fig. 18c). Examples of patched neurons are shown on Figure 18d. On day 113, we also noticed very prominent excitatory postsynaptic potentials (Fig 18e).

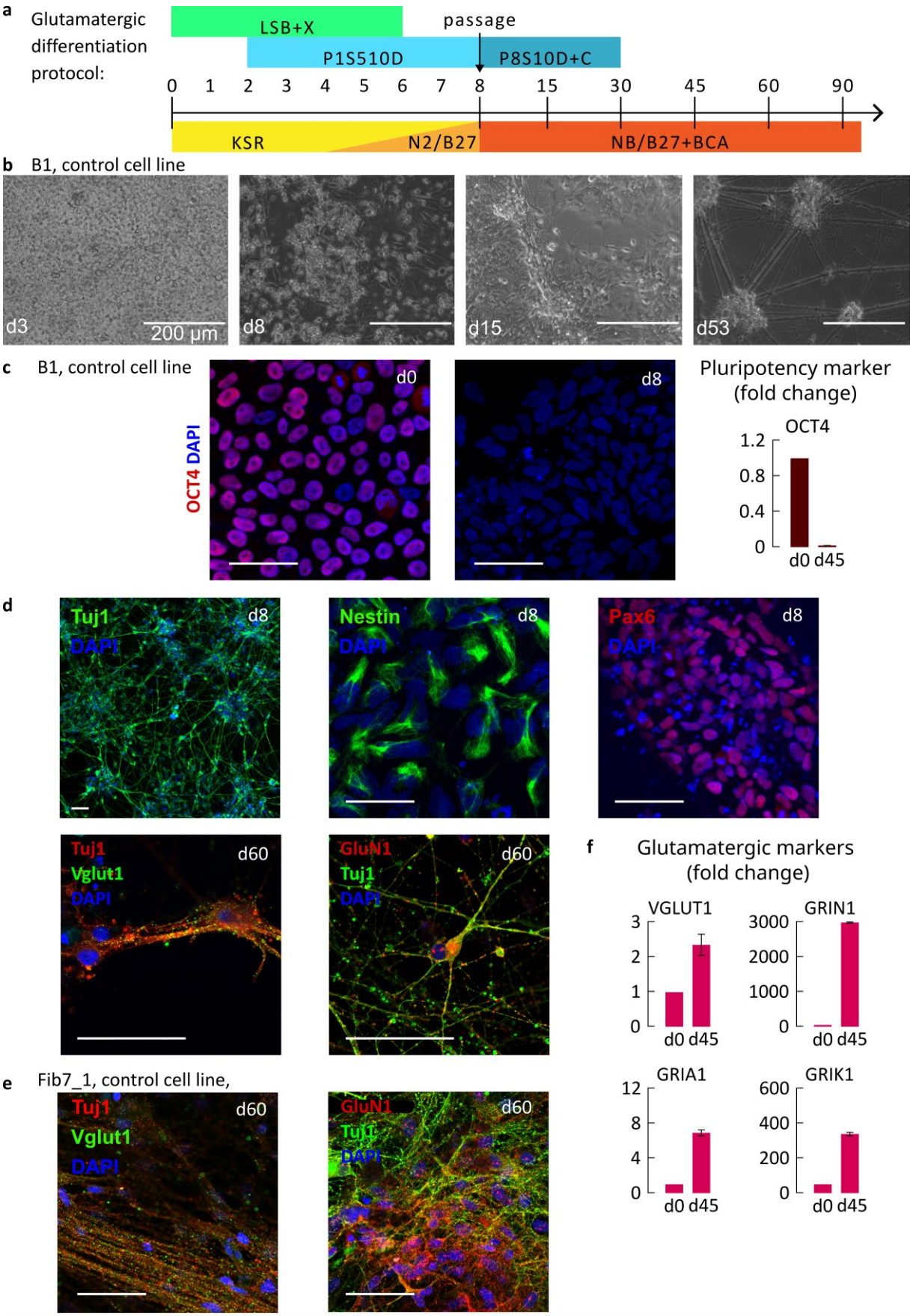
a
Glutamatergic differentiation protocol:
LSB+X
passage
P1S10D
P8S10D+C
0 1 2 3 4 5 6 7 8 15 30 45 60 90
KSR
N2/B27
NB/B27+BCA
b B1, control cell line
d3
200 µm
d8
d15
d53
c B1, control cell line
d0
d8
OCT4 DAPI
Pluripotency marker (fold change)
OCT4
1.2
0.8
0.4
0
d0 d45
d
Tuj1
DAPI
d8
Nestin
DAPI
d8
Pax6
DAPI
d8
Tuj1
Vglut1
DAPI
d60
GluN1
Tuj1
DAPI
d60
f
Glutamatergic markers (fold change)
VGLUT1
3
2
1
0
d0 d45
GRIN1
3000
2000
1000
0
d0 d45
GRIA1
12
8
4
0
d0 d45
GRIK1
600
400
200
0
d0 d45
e Fib7_1, control cell line,
Tuj1
Vglut1
DAPI
d60
GluN1
Tuj1
DAPI
d60

Figure 17. iPS-derived neurons express glutamatergic markers and GluN1: ***(a)*** *Schematic representation of the modified dual SMAD inhibition protocol for cortical differentiation, adapted from Qi et al. (2017).* ***(b)*** *Phase contrast microscopy images of differentiation stages from the control cell line B1.* ***(c)*** *Pluripotency marker assessment for B1 cell line: Immunostaining of cells on day 0 (left) and 8 (right) for Oct4 (red), DAPI (blue) was used for nuclear counterstaining; mRNA expression of OCT4 quantified using qPCR technique (right). Glutamatergic marker assessment for cell lines B1* ***(d)*** *and Fib7_1* ***(e)****: Immunostaining of cells on day 8 and 60 for post-mitotic neuronal marker Tuj1 (left, green on top, red on bottom), neural progenitor marker Nestin (middle, green), glutamatergic progenitor marker Pax6 (right, red), glutamatergic marker Vglut1 (left, green), and the NMDAR subunit GluN1 (middle, red).* ***(f)*** *qPCR results of cells from control cell line B1 on day 0, and 45 for Vglut1, GRIN1 (NMDAR subunit 1), GRIA1 (AMPA receptor subunit 1), and GRIK1 (Kainate receptor subunit 1).*

We subsequently assessed the functional status of NMDA receptors in the differentiated neurons through voltage clamp analysis. This involved a stepwise application of voltage for 10 seconds, ranging from -140 mV to +60 mV, combined with an automated perfusion of an NMDA solution initiated 2 seconds after the voltage application. We conducted experiments using external solutions both with and without magnesium ions.

After four months of differentiation, the neurons displayed a notable response to the application of 100 µM NMDA, exhibiting an inward current of 1-2 nA at negative voltages in the absence of magnesium (Fig. 18e). As expected from the literature, the reversal potential was detected at around 0 mV. In the presence of magnesium, currents were only vaguely discernible for highly depolarized voltages at around +60 mV. The characteristic response pattern in magnesium-free solutions confirms the presence of functional NMDA receptors in the iPSC-derived neurons. The ability to elicit this current highlights the efficacy of our differentiation protocol, establishing it as a reliable method for testing NMDA receptor functionality in neurons derived from induced pluripotent stem cells.

Next, we tested whether our model could be applied to a technique more suitable for high-throughput experiments, such as drug screening, by using calcium imaging in magnesium-free conditions. After establishing a baseline fluorescence ratio, we administered NMDA, followed by a combined application of NMDA and ketamine. To confirm cell viability during the experiment, we performed a washout step and then perfused the cells with KCl.

The application of NMDA resulted in a significant calcium influx into the neurons, evidenced by an increase in fluorescence ratio (Fig. 18g). Notably, this influx decreased upon the administration of ketamine, suggesting an antagonistic effect on NMDA receptor-mediated calcium entry. This finding underscores the potential of our model not only for studying NMDA receptor function but also for investigating the pharmacological effects of compounds that modulate excitatory neurotransmission.

Our approach demonstrates the ability of iPSC-derived neurons to serve as a platform for drug screening and understanding the mechanisms underlying schizophrenia pathophysiology. Overall, these results indicate that our differentiation protocol provides a

robust foundation for future studies exploring therapeutic interventions in conditions characterized by NMDA receptor dysregulation.

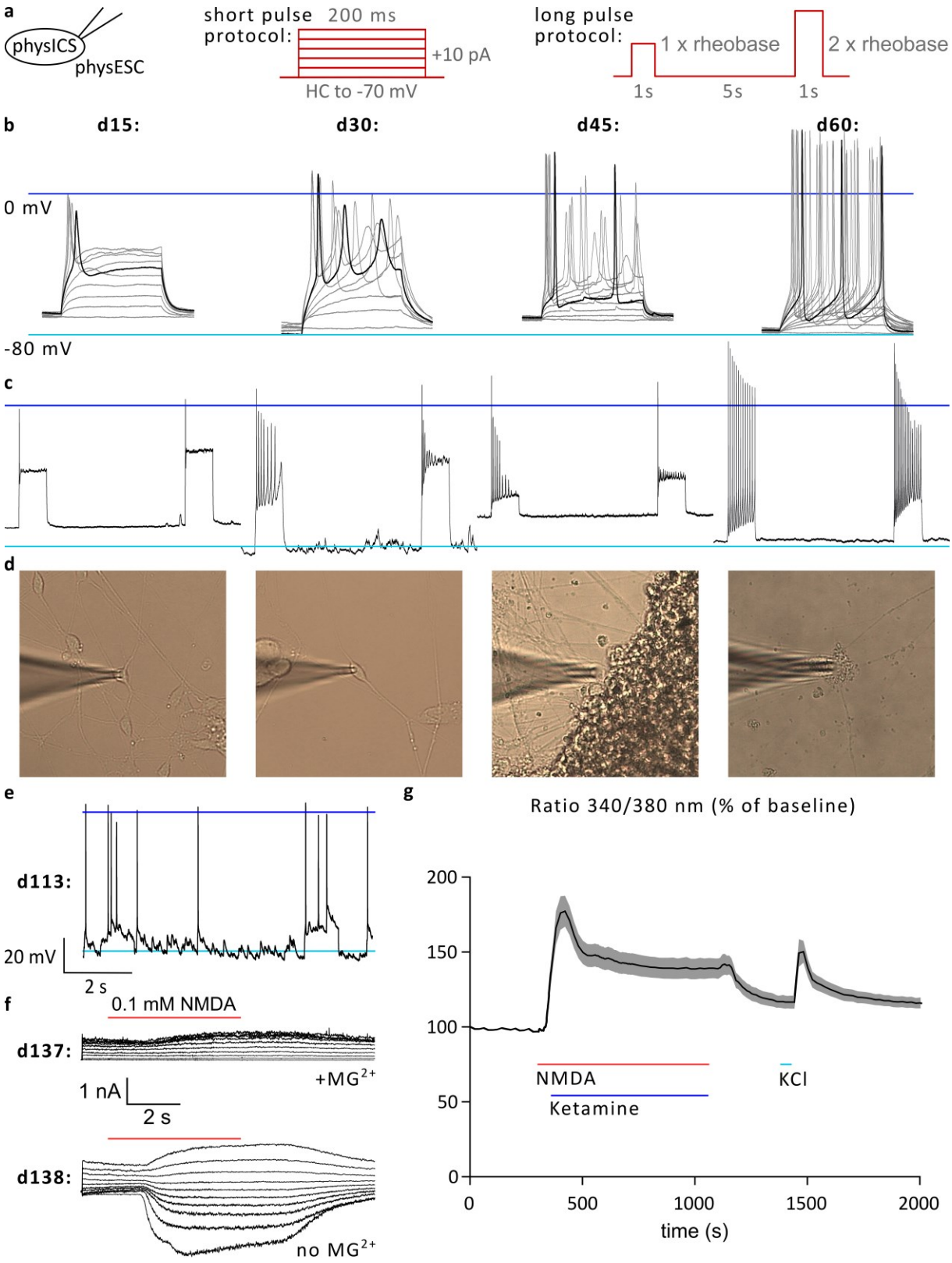

Figure 18. Functional characterization of iPSC-derived neurons from control cell lines: ***(a)*** *Patch solutions (left) and voltage protocols (middle and right) used for the current clamp and voltage clamp experiments. Maturation of action potentials over time, measured using a*

*short pulse protocol **(b)** and a long pulse protocol **(c)**. Blue line indicates 0 mV and cyan line – 80 mV. **(d)** Phase contrast image of neurons selected for recordings, corresponding to the data shown in (b). **(e)** Spontaneous action potentials and excitatory postsynaptic transmission recorded on day 113. **(f)** Voltage clamp recordings of NMDA-evoked currents in Mg^{2+}-containing (top) and Mg^{2+}-free (bottom) solution. The red line indicates the time of NMDA application. **(g)** Calcium imaging recording of day 97 iPSC-derived neurons, n=16. The black line represents the mean value, with the shaded area indicating the standard error of the mean. The red line marks the time of NMDA application, while the blue line corresponds to the Ketamine application, and the cyan line indicates the KCl application.*

3.5 Testing GABAergic differentiation on iPS cells

To generate cortical interneurons, we followed the protocol by (Maroof et al. 2013). This method allows for the directed differentiation of iPSCs into neural progenitor cells (NPCs) using dual SMAD inhibition, followed by patterning these cells into GABAergic interneurons. Initially, we employed LDN and SB for 10 days to push iPSCs towards an NPC fate. After this period, Sonic Hedgehog (SHH) activation was introduced until day 18 (Fig. 19a). As a control, a parallel group of cells was maintained without SHH activation. On day 18, the cells were passaged for further differentiation.

The results showed a clear distinction in cell fate between the SHH-treated group and the control. In the SHH-activated condition, a majority of day 18 NPCs expressed Nkx2.1, a marker of GABAergic progenitors, indicating a ventral forebrain identity. In contrast, over half of the cells in the control group expressed Pax6, a marker of glutamatergic progenitors, suggesting a dorsal telencephalic fate (Fig. 19b). Notably, there was no co-expression of Nxk2.1 and Pax6 in single cells, confirming distinct differentiation pathways for each population. Furthermore, all cells expressed Foxg1, a transcription factor associated with forebrain development (Fig. 19c), confirming that they had adopted a forebrain fate.

By day 35, the cells exhibited robust expression of GAD1, a key enzyme for GABA synthesis, and GluN1 (Fig. 19d), making them a promising model for studying NMDA receptor (NMDAR) dysfunction of iPSC derived GABAergic interneurons obtained from patients with schizophrenia.

We further analyzed the electrophysiological properties of the resulting GABAergic neuronal culture. Recordings of the resting membrane potential (RMP) revealed an abundance of inhibitory synaptic events (see Fig. 19e), confirming the presence of functional GABAergic synapses. Moreover, the cells were able to fire multiple action potentials (APs), and the firing rate increased with higher current injection (Fig. 16f,g), suggesting that the culture, despite being only one month old, had reached a relatively mature state.

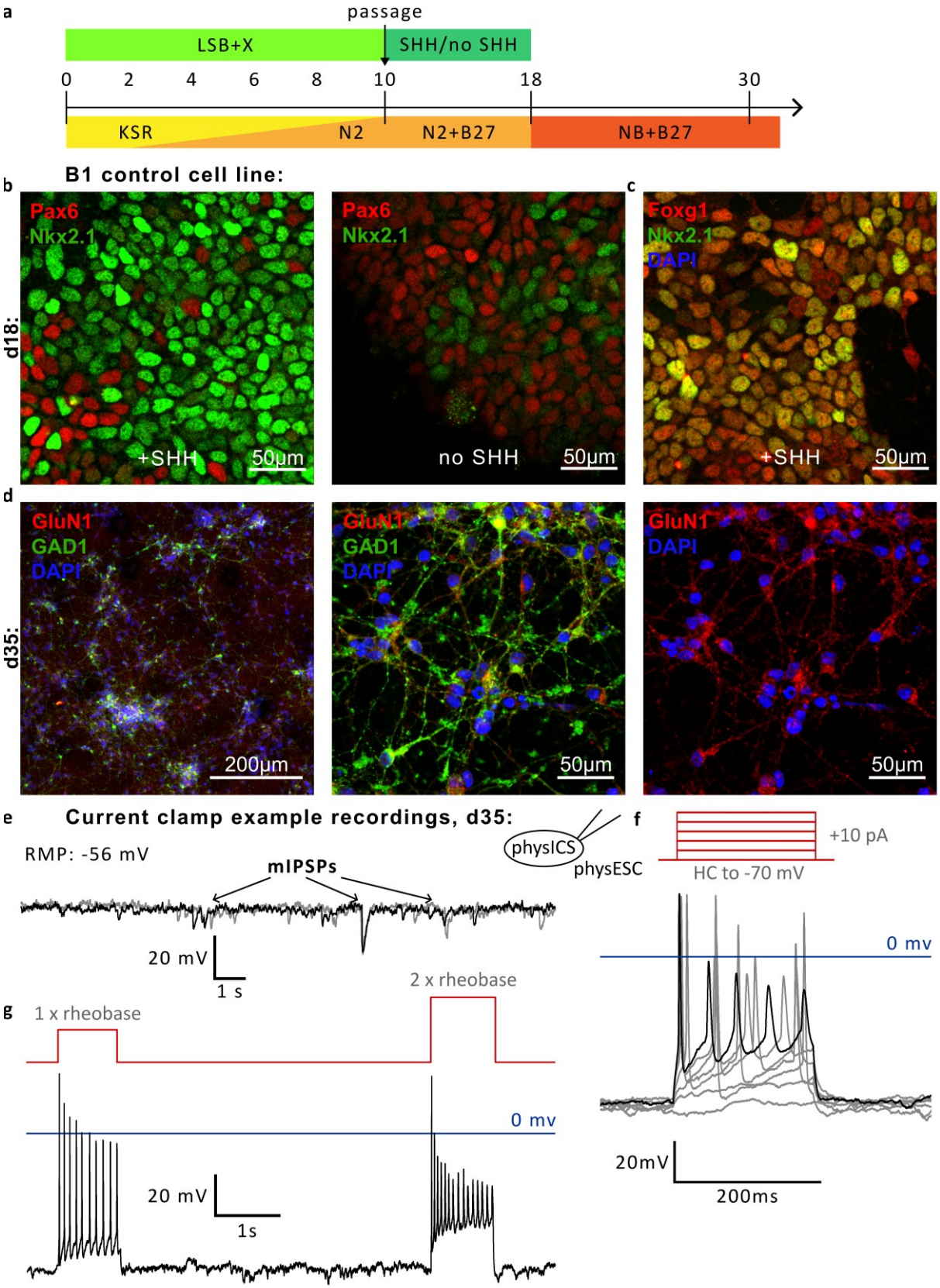

Figure 19. GABAergic differentiation of control iPSCs: ***(a)*** *Schematic representation of the modified protocol for cortical interneuronal differentiation from* (Maroof et al. 2013). ***(b)*** *Immunostaining of cells differentiated in media with SHH (left) and without (middle) on day*

18 for glutamatergic progenitor marker PAX6 (red) and GABAergic progenitor marker Nkx2.1 (green). DAPI (blue) was used for nuclear counterstaining. ***(c)*** *Immunostaining of cells differentiated in media with SHH on day 18 for GABAergic progenitor marker Nkx2.1 (green) and forebrain progenitor marker Foxg1 (red).* ***(d)*** *Immunostaining of cells on day 35 for GABAergic marker GAD1 (green) and NMDAR (red) on different magnifications.* ***(e)-(g):*** *Functional characterization of the cortical interneurons using current clamp:* ***(e)*** *Inhibitory postsynaptic potentials (IPSPs) observed on day 35 without any current injection.* ***(f)*** *Schematic representation of the short pulse protocol (top) and a respective membrane potential trace (bottom).* ***(f)*** *Schematic representation of the long pulse protocol (top) and a respective membrane potential trace (bottom) containing inhibitory postsynaptic potentials.*

4 Discussion

This study provides insights into the molecular and cellular mechanisms underlying schizophrenia. By examining the impact of NaV1.2 mutations on the excitatory/inhibitory (E/I) balance, it advances our understanding of the fundamental pathophysiological processes involved in the disorder. Moreover, it provides a foundation for studying the NMDAR dysfunction in iPSC-derived neurons from patients with schizophrenia.

4.1 Effect of NaV1.2 variants

Genetic studies have shown that SCN2A gene variants are more common among patients with schizophrenia, ASD, epileptic encephalopathy, and intellectual disability compared to the general population (J. Li et al. 2016). This broad clinical spectrum likely results from the diverse ways these variants disrupt NaV1.2 channel function. While truncating mutations generally yield non-functional channels, missense mutations can cause both gain-of-function (GoF) and loss-of-function (LoF) effects. However, this binary classification is often insufficient, as NaV1.2 mutations impact various electrophysiological parameters, creating further challenges for categorization. Patients also exhibit diverse seizure onset patterns, with some experiencing seizures that resolve with age. Although most cases of NaV1.2-related diseases are identified early in life, schizophrenia typically presents in young adulthood, hindering the collection of schizophrenia-relevant clinical cases.

(Wolff et al. 2017) identified two distinct patient groups with epilepsy: an early-onset group (before 3 months) with GoF mutations responsive to sodium channel blockers and a late-onset group with LoF mutations benefiting from conventional antiepileptic drugs. Similarly, (Begemann et al. 2019) examined six SCN2A variants, showing that LoF variants with no conductance were linked to ID and ASD without seizures, while modest GoF effects were associated with benign epilepsy. Epileptic encephalopathy cases demonstrated profound GoF effects, leading to neuronal hyperexcitability.

In our study, we found that schizophrenia-associated SCN2A variants largely exhibit a range of LoF effects. These graded LoF responses suggest that subtle functional losses may contribute to the phenotypic heterogeneity seen in schizophrenia, offering deeper insights into the genetic basis of this complex disorder.

4.1.1 R850P variant causes diverse LoF effects on NAV1.2 electrophysiology

Overall, the R850P variant caused significant disturbances in NaV1.2 electrophysiology. The loss-of-function effect of the R850P variant on NaV1.2 function was evident in all the protocols we applied. Given that it reduces the positive charge of the voltage sensor, it is likely that the voltage-sensing domain movement in response to depolarization is slower or less energetically favourable. Moreover, a substitution to a proline might introduce a kink into the S4 helix, reducing its stability (Visiers, Braunheim, and Weinstein 2000). Additionally, altered trafficking of the channel may contribute to the reduced current amplitude and density.

Altogether, we observed a 9 mV depolarized activation shift and a shallower slope of the conductance curve. The peak of the activation current at -40 mV was delayed by a factor of 1.5, and the current decay was also slower. However, these changes in both parameters can likely be attributed to the overall depolarizing shift in the current gating. Inactivation analysis revealed a 3.5 mV hyperpolarized shift of the inactivation curve with a similarly shallower slope. Ramp currents displayed a delayed current peak and approximately a 20% increase in the normalized integral. Furthermore, the R850P variant was significantly more affected by repetitive activation in the use-dependence protocol, with the difference becoming more pronounced as the frequency increased. Follow-up experiments demonstrated a slower recovery from fast inactivation as a potential explanation of this finding.

To our knowledge, the R850P variant has not been characterized before. However, other mutations involving gating charges such as R850Q/C, R853Q, R856Q, K859Q, and K862Q mutations, are described in the literature, providing an intriguing contrast to the R850P variant. R853Q is found in several patients with West syndrome, later-onset developmental epileptic encephalopathy and developmental delay (Berecki et al. 2018; Nakamura et al. 2013; Samanta and Ramakrishnaiah 2015). R856P is associated with severe cases of early-infantile epilepsy. Other substitutions were generated to study the effect gating charge reduction (Cestèle et al. 2001).

While R850P leads to distinct alterations in channel kinetics and current properties, R850Q and R853Q mutations have been shown to induce K^+-selective inward current at resting states, which is blocked upon activation (Sokolov, Scheuer, and Catterall 2005). R853Q alone has been shown to reduce transient current amplitude and open probability, shift the inactivation voltage dependence, but not the activation, towards hyperpolarization (Berecki et al. 2018; Mason et al. 2019). R856P showed a hyperpolarized shift of both activation and inactivation (Berecki et al. 2022). In contrast, R850P caused a depolarized shift of activation and hyperpolarized shift of inactivation. Moreover, it caused a slower recovery from fast inactivation. One possible explanation is that an arginine to glutamine substitution mainly removes the charge from the residue, whereas a substitution to a proline – in addition - likely disrupts a protein alpha helix, introducing a kink (Visiers, Braunheim, and Weinstein 2000).

Interestingly, an R850P mutation in the SCN8A gene, which encodes another CNS sodium channel, NaV1.6, has been shown to exhibit a gain-of-function effect (Pan and Cummins 2020). This mutation is also associated with epilepsy, underscoring the significance of this residue across different sodium channels. However, the contrasting functional outcomes between NaV1.2 and NaV1.6 suggest a structural explanation. In NaV1.2, R850 is the first charged residue within the S4 helix, positioned closest to the extracellular side. In NaV1.6, by contrast, R850 is the third charged residue on the same helix, placing it closer to the intracellular side. This positional difference likely alters the movement and role of the corresponding gating charge during depolarization, which could explain the opposing effects of the R850P mutation in these two sodium channel subtypes. This comparison suggests that

even subtle differences in the spatial arrangement of gating charges in sodium channels can result in markedly different physiological outcomes.

4.1.2 V1282F variant has a moderate effect on NaV1.2 function

In most of our experiments, the V1282F variant displayed a tendency toward similar functional effects as R850P, though its differences from the WT rarely reached statistical significance. Nevertheless, it showed significantly reduced current density and a shallower slope of inactivation. This aligns with findings from (Kohlnhofer et al. 2021), who demonstrated a reduction in current amplitude for the V1282F variant in HEK cells. However, their study only analyzed the activation properties of the channel, with no further electrophysiological characteristics examined (Kohlnhofer et al. 2021).

Kohlnhofer et al. also reported that membrane expression of the V1282F variant was unaffected. This finding, however, should be interpreted with caution, as distinguishing between membrane insertion and submembrane localization of the channel can be quite challenging. The potential for submembrane accumulation without proper integration into the plasma membrane could explain the functional deficits observed.

Interestingly, Kohlnhofer et al. also introduced the V1282F mutation into iPSC-derived neurons and performed voltage-clamp experiments. The reduced current density in mutated neurons is consistent with our findings, but we observed a shallower slope as well. The authors do not provide details regarding pipette resistance or voltage errors. Our stringent selection criteria and treatment of voltage errors potentially allowed for detection of this more subtle effect.

The position of V1282 relative to the pore makes it unlikely to affect single-channel conductance. However, the possible van der Waals interaction between V1282F and the nearby gating charge residue R1315 (based on the PDB structure 6J8E) could provide a plausible explanation for the altered kinetics. The bulkier phenylalanine residue may spatially hinder the movement of the S4 segment, which is crucial for channel gating. Such structural disruptions could affect transition rates, leading to the observed reduction in current density, while leaving activation or inactivation curves largely unaffected in voltage-clamp assays. However, due to the lower number of cells recorded for this mutant in this project, these results should be interpreted with caution.

4.1.3 S1656P variant results in a non-functional sodium channel

The S1656P variant was reported in a patient with the full known phenotypic spectrum of SCN2A mutations, encompassing infantile-onset seizures, ASD, episodic ataxia, and schizophrenia spectrum disorder (SSD) (Suddaby, Silver, and So 2019). This patient is the first reported to exhibit the full range of symptoms, with SSD being diagnosed at age 38. This suggests that SSD could be a late-onset manifestation of SCN2A-related neurodevelopmental disorders. It is possible that more patients may develop the full phenotypic spectrum as they age, highlighting the need for longitudinal studies to track the progression of SCN2A-linked conditions.

We detected no sodium current in HEK cells expressing the NaV1.2 S1656P variant, regardless of whether solutions with reduced sodium concentration or physiological extracellular solutions were used. It is known that incubating transfected cells at lower temperatures can sometimes facilitate proper protein folding and trafficking by slowing down these processes. To test this, cells were incubated at 30°C after transfection. However, despite this approach, no sodium current was observed, indicating that the S1656P mutation significantly impairs the functional expression or proper trafficking of NaV1.2.

This variant has not yet been previously characterized by means of patch clamp. However, an opposing substitution at a nearby position, P1658S, was described as a complete LoF mutation (Miao et al. 2020). It was identified in a patient with epilepsy and choreoathetosis whose seizures were unresponsive to sodium channel blockers, consistent with the loss-of-function nature of this mutation.

Additionally, a patient with epilepsy was reported to have S1656F mutation in the SCN2a gene (Wolff et al. 2017). The patient was also suffering from hypotonia, crouched gait and agitation. At the time of the last follow-up, the patient was 12 years old, an age at which additional symptoms, such as those related to schizophrenia, may not yet have manifested. To our knowledge, the electrophysiological impact of this mutation has not been described.

Proline is known to be a rigid amino acid, critical for proper protein folding. Introducing a proline into the channel may disrupt its folding, potentially preventing the channel from being properly inserted into the membrane. On the other hand, when exploring NaV1.2 structure in the inactivated state with Ring software, we found that the serine at position 1656 forms a hydrogen bond with A1659, which in turn has Van der Waals interactions with both F1489 and M1490 of the IFM motif—critical for channel inactivation. The substitution of S1656 with proline could alter the conformation of the α-helix, disrupting key interactions with the IFM motif and resulting in a complete LoF. Removing the inactivation gate through the IFM/QQQ mutation could help determine whether the S1656P mutant is properly inserted into the membrane but fails to conduct current due to its altered interaction with the inactivation particle.

The identification of specific NaV1.2 variants (R850P, V1282F, S1656P) associated with schizophrenia underscores the potential of sodium channel modulators as therapeutic agents. Sodium channel blockers, commonly used for epilepsy, could potentially be repurposed to address the altered excitability caused by SCN2A mutations in schizophrenia. However, this approach should be pursued with caution, as it could potentially worsen symptoms in patients with NaV1.2 LoF variants. Furthermore, developing selective NaV1.2 modulators would improve therapeutic precision and minimize off-target effects that broader sodium channel inhibitors might cause. Sodium channel blockers have already been shown to alleviate PCP-induced cognitive symptoms in rat models of schizophrenia (Large et al. 2011). This suggests that these drugs might hold promise for treating cognitive symptoms in humans with schizophrenia. Translating these findings to clinical settings is a promising avenue for improving treatment.

4.1.4 Other findings, implicating NaV1.2 in pathogenesis of schizophrenia or psychosis

While a patient with a point variant (S1656P) was reported to have a full SCN2A phenotype, one with an early truncating variant (E169X) was reported to have treatment-resistant schizophrenia. E169X may behave similarly to other truncating mutations in SCN2A. For instance, the R102X mutation, when co-expressed with wild-type WT NaV1.2 in HEK cells, exhibited a dominant-negative effect, while heterozygous knockout mice with only one functional NaV1.2 allele showed no major behavioral abnormalities or seizures (Kamiya et al. 2004). This suggests that the E169X mutation could also exert a dominant-negative influence. The difference between S1656P and E169X may be explained by the fact that S1656P unlikely undergoes nonsense-mediated RNA decay and may result in a full production of a non-functional protein. For NaV1.1, truncating mutations are generally linked to a severe phenotype, but exceptions have been reported (Takaori et al. 2017).

Another patient with schizophrenia was reported to have an intronic SNP (Fromer et al. 2014), making it challenging to model its effects in HEK cells, as intronic mutations cannot be reflected in transfected cDNA. The altered splicing caused by the intronic SNP may modify NaV1.2 function and contribute to abnormal neuronal excitability in the patient.

Two intronic SNPs in the SCN2A gene, rs10182570 and rs10174400, have been reported in schizophrenia patients. RNA sequencing showed reduced expression of alternative SCN2A transcripts in dorsolateral prefrontal cortex. These reduced mRNA expression levels correlated with diminished cognitive abilities in affected individuals (Ph et al. 2014). Interestingly, the SNP rs10174400 has been associated with an opposite effect on mRNA expression and cognitive function in healthy individuals. Research indicated that this genetic variant may confer a cognitive advantage, potentially mediated by enhanced information processing capabilities between the dorsolateral prefrontal cortex and the dorsal anterior cingulate cortex, which are critical for higher cognitive functions (American Psychological Association 2017).

(Howrigan et al. 2020) identified two *de novo* SNP variants in SCN2a gene in schizophrenia patients, rs551347418 and rs2105255398. The first one resulted in R15C substitution. Another variant, R379H, was found in a patient with childhood-onset schizophrenia (Rees et al. 2021). This variant was previously reported in three ASD patients; however, unlike the ASD cases, the schizophrenia patient did not exhibit intellectual disability or autism. Patch-clamp studies by (Ben-Shalom et al. 2017) demonstrated that the R379H mutation leads to a complete LoF effect. When viewed in the broader context of E/I imbalance, it is interesting that the same study by Rees et al. reported a missense variant in the SLC6A1 gene, encoding GABA transporter-1, in another schizophrenia patient.

Although not diagnosed with schizophrenia, another patient with a truncating W1716X variant exhibited moderate intellectual disability and psychosis (Wolff et al. 2017). Her seizures worsened with the sodium channel blocker carbamazepine but were completely controlled by valproate, which, while also inhibiting sodium currents, enhances GABA transmission. This variant truncates the C-terminal region of the protein, removing A1718 of

the selectivity filter, a part of the pore-forming S6 helix in domain IV and the C-terminus. In HEK cells, it was shown that this mutation results in the absence of sodium current. Moreover, in cardiac NaV1.5 it was demonstrated that a truncating mutation positioned later in the amino acid sequence, G1642X, has a dominant-negative effect on WT NaV1.5 through coupled gating with the wild-type protein (Zheng et al. 2021). Interestingly, the effect of W1716X mutation was investigated in patient-derived iPS cells (Asadollahi et al. 2023). Mutated neurons showed lower NaV1.2 protein levels with normal mRNA expression, suggesting no nonsense-mediated mRNA decay, but channel dysfunction. Patch clamp experiments demonstrated lower sodium current density and reduced AP firing.

4.1.5 Implication of NaV1.1, 1.3, and 1.6 in schizophrenia

Other VGSC isoforms expressed in the central nervous system have been sparsely studied in the context of schizophrenia.

A variant in the SCN1A gene has been identified in a boy with childhood-onset schizophrenia (Papp-Hertelendi et al. 2018). This same variant has also been reported in patients with Dravet syndrome, many of whom exhibit psychotic symptoms (Wolff, Cassé-Perrot, and Dravet 2006). The variant, 4793A>T (p.Tyr1598Phe), is predicted to occur within the intracellular loop between the S2 and S3 transmembrane segments of the fourth homologous domain, involving a substitution from a polar to a non-polar residue. Given the psychotic features observed in Dravet patients, this variant may contribute to similar symptoms.

Further evidence of SCN1A's involvement in schizophrenia includes findings from a common target PPI network analysis, which revealed SCN1A downregulation in schizophrenia (X. Wang et al. 2024) fMRI/behavioral studies have also demonstrated NaV1.1's critical role in short-term memory—a cognitive function frequently disrupted in schizophrenia (Papassotiropoulos et al. 2011). Additionally, the sodium channel activator Lu AE98134 has been shown to enhance NaV1.1 current in HEK cells and restore fast-spiking interneuron activity in a Dlx5/6+/- mouse model of schizophrenia (von Schoubye et al. 2018).

SCN3A may also be relevant, as one schizophrenia patient was reported to have potentially disruptive variants in both copies of the SCN3A gene (paternal R1510H and maternal S540F), though their role in disease remains unclear (Balakrishna and Curtis 2020). More broadly, (Rees et al. 2019) examined LoF variants in 187 genes associated with schizophrenia, identifying several variants in voltage-gated sodium channels in a large cohort. Among these, three variants introduced stop codons in NaV1.6, three in NaV1.4, and one splice variant in NaV1.3. Stop codons were also identified in NaV1.5 and NaV1.7-9 in both schizophrenia patients and controls. Variants were found in sodium channel beta-subunits as well, including three stop codons in SCN1B (one in a control individual) and two splice variants in SCN2B.

Wang et al, 2010 identified three genetic polymorphisms in NaV1.6 that were statistically significant in schizophrenia patients with suicide attempts compared to controls

(rs10506302, P=0.024; rs1601012, P=0.004; rs12581041, P=0.004) (Y. Wang et al. 2010). The atypical antipsychotic risperidone has been shown to inhibit peak current in NaV1.6, leading to a use-dependent block, suggesting NaV1.6 may play a critical role in schizophrenia pathophysiology (Brauner et al. 2014). Similarly, the antipsychotic aripiprazole inhibits the cardiac VGSC NaV1.5 in a state-dependent manner (Föhr et al. 2022). It would be of interest to further elucidate the effect of antipsychotics on sodium channels.

The reason why NaV1.2, among all CNS sodium channel isoforms, is particularly implicated in schizophrenia may lie in its predominant expression in excitatory neurons of the cerebral cortex and hippocampus—regions critical for cognitive functions that are often impaired in schizophrenia. In contrast, NaV1.1 is primarily found in inhibitory neurons, and NaV1.6, while involved in excitability, has a more ubiquitous distribution across various brain regions.

Mutations in the SCN2A gene, which encodes NaV1.2, have been associated with a broad spectrum of neurodevelopmental disorders, including autism, intellectual disability, and schizophrenia. This pleiotropy has led to more targeted studies, potentially creating a bias towards finding more associations with this gene compared to SCN1A or SCN8A.

Future research may yet reveal associations between Nav1.1 or Nav1.6 mutations and schizophrenia, especially given the growing understanding of shared genetic risk factors across neurodevelopmental and psychiatric disorders (Rees, O'Donovan, and Owen 2015).

4.1.6 NaV1.2 loss-of-function implication in E/I imbalance

LoF mutations in NaV1.2 can contribute to E/I imbalance in neural networks, paradoxically leading to neuronal overexcitation despite reduced sodium currents in several ways. In a study on SCN2a-related epilepsy, from 21 patients with complete LoF mutations, 13 developed seizures and 7 had only ASD symptoms (Berg et al. 2024).

One important mechanism is linked to impaired action potential generation in pyramidal neurons due to reduced NaV1.2-mediated sodium currents at the AIS during early development. While other sodium channels, particularly NaV1.6, can compensate at the AIS and nodes of Ranvier in adult neurons, they may not provide adequate compensation at synaptic terminals. This deficiency in synaptic excitability could lead to abnormal downstream signaling, particularly in inhibitory neurons. Impaired firing in excitatory pyramidal neurons impacts inhibitory thalamic reticular nucleus neurons, which fail to suppress thalamocortical relay neurons. These excited thalamocortical neurons may then generate hyper-synchronous oscillations, contributing to seizure activity or other excitability-related dysfunctions like the circuitry disturbances seen in schizophrenia (Ogiwara et al. 2018).

Furthermore, Ogiwara et al. suggested a role of basal ganglia in NaV1.2 Lof-mediated hyperexcitability. The basal ganglia play a critical role in modulating activity within the thalamocortical circuits, especially in regulating motor control and behavior. Studies using NaV1.2 LoF mouse models have revealed prominent epileptiform discharges in the striatum. It receives excitatory inputs from both the cortex and thalamus and, in turn, projects back to

the thalamus. The loss of NaV1.2 function in excitatory neurons affects the cortico-basal ganglia-thalamic loop, disrupting this feedback system, which is crucial for normal movement and cognitive control. When the basal ganglia are disrupted due to NaV1.2 dysfunction, they may fail to properly modulate the thalamocortical oscillations responsible for maintaining balanced network excitability. This failure allows synchronized epileptic discharges to propagate more easily through cortical-basal ganglia circuits, further exacerbating network hyperexcitability. Interestingly, hyperconnectivity between the thalamus and cortex, as well as between the basal ganglia and cortex, is a consistent finding in fMRI studies on schizophrenia and ketamine (Gaebler et al. 2023).

In addition, rebound hyperexcitability may occur within the cortex itself. Excitatory neurons in the cortex form complex reciprocal networks with inhibitory neurons, and the reduced excitatory input into inhibitory neurons can lead to disinhibition of downstream excitatory neurons. This disinhibition further enhances excitatory activity, potentially leading to runaway network excitation across cortical-thalamic circuits (Ogiwara/Meeren 2002).

There is also evidence from mouse models that NaV1.2 channels play a role in the functioning of interneurons. Loss of NaV1.2-mediated currents at the proximal AIS of SST-expressing interneurons, which are crucial for maintaining inhibitory control within cortical circuits, leads to increased recurrent network activity (T. Li et al. 2014).

Furthermore, computational models suggest that NaV1.2 LoF impairs potassium channel-mediated repolarization between action potentials, contributing to heightened excitability (P. Spratt et al. 2021). A similar effect was observed in mice, where NaV1.2 knock out led to heightened neuronal excitability due to the downregulation of multiple potassium channels, including KV1.1 (J. Zhang et al. 2021).

Finally, the decreased neuronal activity caused by NaV1.2 deficits could have profound impacts on neural network formation during brain development. Scn2a mutations might interfere with the maturation, migration, or connectivity of both inhibitory and excitatory neurons, ultimately altering the balance of global brain network excitability. This imbalance could disrupt the proper development of synaptic networks, leading to long-term consequences for brain function.

These findings provide a potential explanation for how, despite the predominantly loss-of-function nature of schizophrenia-associated SCN2A mutations, they may still contribute to increased excitation—consistent with models of E/I imbalance in schizophrenia.

4.2.1 Modulation of NaV1.2 as a potential mechanism of E/I imbalance

An important aspect of NaV1.2's involvement in schizophrenia pathology is its modulation by acidosis. *Postmortem* studies of schizophrenia patients have shown a decreased brain pH, which may stem from increased lactate levels due to impaired energy metabolism and mitochondrial dysfunction (H. J. Park, Choi, and Leem 2021). Low pH affects NaV1.2 function by reducing current amplitude, slowing fast inactivation, and decreasing channel availability (Vilin, Peters, and Ruben 2012). Moreover, acidic conditions lead to

increased use-dependent block of NaV1.2, a phenomenon observed in R850P mutations as well, which shows heightened vulnerability to repetitive firing.

Another effect of NaV1.2 in the E/I imbalance schizophrenia may be linked to its modulation by serotonin (5-HT) receptors, particularly 5-HT1A receptors. *Postmortem* studies have consistently shown that patients with schizophrenia exhibit increased 5-HT1A receptor density in the prefrontal and temporal cortices, regions involved in cognitive and emotional processing (Bantick et al., 2001; Maćkowiak et al., 2000; Tauscher et al., 2002). On the other hand, decreased 5-HT1A receptor binding in the amygdala has been associated with negative and depression/anxiety symptoms in schizophrenia (Yasuno et al., 2005). 5-HT1A receptors are known to modulate sodium channels, particularly by inhibiting Na^+ currents at the AIS by a depolarizing shift of the activation curve and a facilitation of slow inactivation. Interestingly, NaV1.2 channels, specifically located at the AIS, are selectively inhibited by 5-HT1A activation, while NaV1.6 channels in the axon trunk remain unaffected (Yin et al. 2017). This selective inhibition of NaV1.2 is comparable to the effect of R850P variant and could contribute to altered excitability in neurons and potentially explain some of the cognitive and emotional disturbances associated with schizophrenia.

Dysregulation of NaV1.2 function in schizophrenia may be also linked to disturbances in CaMKII signaling, a pathway crucial for synaptic plasticity and neuronal excitability. Notably, six CaMKIIα variants identified in schizophrenia patients demonstrated impaired function, particularly R396stop and R8H, which compromised CaMKII activity (Brown et al. 2021). Given that CaMKII inhibition has been shown to attenuate gain-of-function effects of mutant NaV1.6 channels, thereby reducing neuronal excitability (Zybura et al. 2022), similar interactions may exist for NaV1.2. Taken together, these findings suggest that NaV1.2 dysfunction in schizophrenia may be multifactorial and not only relevant to patients with rare coding variants.

4.1.7 Interactions between sodium channels and NMDARs

It has been shown that NMDARs in cerebellar stellate cells can induce intrinsic plasticity by modulating NaV channel activation and inactivation through a Ca^{2+}- and CaMKII-dependent pathway (Alexander and Bowie 2021). This pathway leads to a hyperpolarizing shift in NaV channel gating, lowering the action potential threshold and altering neuronal excitability. Given that similar Ca^{2+}- and CaMKII-mediated mechanisms may operate in other neuronal populations, NMDAR dysfunction in schizophrenia could impact NaV channel function, contributing to the altered excitability and E/I imbalances observed in the disorder.

Conversely, NaV1.2 channels are critical for action potential backpropagation, which directly influences NMDAR function. When an AP backpropagates into the dendrites, it acts as a global signal that relays information about the neuron's output to synaptic input sites, inducing long-term changes in synaptic efficacy. This process, known as spike-timing dependent plasticity, depends on coincident pre- and postsynaptic activity and is strongly influenced by calcium influx through NMDARs, as shown in hippocampal pyramidal cells and cortical neurons (Nevian and Sakmann 2006).

In neurons, the close temporal proximity of excitatory postsynaptic potentials and backpropagating action potentials often leads to a supralinear increase in dendritic calcium concentrations, especially at synaptic spines. This calcium influx activates signaling pathways essential for synaptic plasticity, with the timing and frequency of backpropagating APs further modulating NMDAR activation. These processes underlie plasticity mechanisms such as long-term potentiation and long-term depression (Sjöström and Nelson 2002).

Thus, NaV1.2 dysfunction could arise upstream or as a downstream consequence of NMDAR abnormalities, contributing to impaired synaptic plasticity and further linking voltage-gated sodium channels to the pathophysiology of schizophrenia. This underscores how E/I imbalances in schizophrenia may result from both direct receptor or channel mutations and disrupted intracellular signaling pathways.

4.2 Modelling schizophrenia using iPSCs

NMDA receptors have been implicated in the pathophysiology of schizophrenia by various studies (Hyun, Inoue, and Hayashi-Takagi 2020). The use of iPSC-derived neurons provides a valuable tool to validate the NMDAR dysfunction hypothesis. By comparing iPSC-derived neurons from patients with NMDAR-related endophenotypes to those without respective endophenotypes and with healthy controls, we could gain deeper insight into distinct disease mechanisms. This approach would also allow for the testing of pharmacological compounds, enabling us to identify treatments that specifically restore function in patients with likely NMDAR dysfunction, while exploring alternative therapies for those without this dysfunction. Despite the strong theoretical foundation, research into NMDAR function at the cellular level has been limited, with only a single published study to date that electrophysiologically evaluated NMDAR function in iPSC-derived neuronal models (Zhang et al. 2016).

4.2.1 Establishment of schizophrenia patient iPS cell lines

In this project, we selected two schizophrenia patients based on their fMRI functional connectivity profiles suggesting NMDAR hypofunction. Then, we successfully reprogrammed PBMCs from these patients into iPSCs. Using a Sendai virus-based method, we were able to isolate and expand several viable clones from both patients. While some clones were lost during expansion, the successful reprogramming was confirmed through immunostaining for pluripotency markers (Oct4, Sox2, Nanog, Lin26), with 4 viable clones from each patient. This allowed us to move forward with differentiation protocols.

4.2.2 Glutamatergic neuronal differentiation and schizophrenia pathology

The differentiation of the iPSCs into glutamatergic cortical neurons using a modified dual SMAD inhibition protocol yielded promising results. Early neural markers (Nestin, Tuj1) were detected by day 8, and by day 34, the neurons exhibited characteristics of mature glutamatergic cells, expressing Vglut1, a specific marker for cortical excitatory neurons. This outcome suggests that our iPSCs can be directed towards a neural lineage, with a potential to mature into excitatory neurons.

Glutamatergic neurons are particularly relevant in the context of schizophrenia, as disruptions in glutamatergic transmission have been implicated in the disorder, potentially causing E/I imbalance. Our ability to generate these neurons from schizophrenia patients provides a platform for examining the functional deficits associated with glutamatergic signaling in schizophrenia.

4.2.3 Electrophysiological characterization of iPSC-derived neurons

To assess NMDA receptor function, we differentiated a control iPSC line into neurons and evaluated their electrophysiological properties over a 60-day period. The neurons matured gradually, with repetitive action potentials and synaptic events detected by day 60. Functional NMDA receptors were confirmed by voltage clamp experiments, where neurons responded to NMDA application with a significant inward current, confirming the successful differentiation into neurons expressing NMDAR (Fig. 18).

Therefore, we demonstrated the possibility of using iPSC-derived neurons to study NMDAR function. This system also allows for pharmacological testing, as demonstrated by the calcium imaging experiments. The administration of ketamine, an NMDA receptor antagonist, reduced the calcium influx induced by NMDA, highlighting the potential of this model for drug screening and testing compounds targeting excitatory neurotransmission.

4.2.4 GABAergic differentiation in iPSCs

We used the Maroof et al. (2013) protocol to generate GABAergic interneurons from iPSCs. Dual SMAD inhibition guided the cells toward a neural progenitor state, followed by SHH activation to promote ventral forebrain identity. At the NPC stage, SHH-treated cells predominantly expressed Nkx2.1, a marker of GABAergic progenitors, confirming their ventral telencephalic identity. The absence of Nkx2.1 and Pax6 co-expression further validated that SHH activation drove a clear GABAergic differentiation pathway (Fig. 19b). Moreover, all cells expressed Foxg1, underscoring their forebrain identity. By day 35, the cells showed strong expression of GAD1 and NMDA receptors, making them a relevant model for studying GABAergic function and NMDA receptor dysregulation in schizophrenia. Electrophysiology revealed inhibitory synaptic events and mature action potentials, indicating the neurons had achieved functional maturity (Fig. 19e-g).

Our findings establish a robust foundation for investigating E/I imbalance and NMDAR dysfunction using patient-derived iPSCs. Moving forward, the next steps will involve comparing the electrophysiological properties of neurons derived from schizophrenia patients with those from healthy controls.

4.2.5 Possible origins of NMDAR dysfunction in schizophrenia

Recent study has shown that schizophrenia-associated GRIN2A variants (encoding the NMDAR subunit GluN2A) predominantly exhibit loss-of-function phenotypes, while other disorders, such as epilepsy and developmental delay/intellectual disability, are characterized by both gain- and loss-of-function mutations in the same receptor (Shepard et al. 2024). While coding variants in the NMDAR complex are enriched in schizophrenia patients, they are found

in only a relatively small fraction of cases. Interestingly, NMDAR-related endophenotypes, such as mismatch negativity or prepulse inhibition, are fairly common among SZ patients (Taylor et al. 2017), suggesting that NMDAR dysfunction may arise through mechanisms other than coding variants. Indeed, genome wide association studies have consistently documented a set of common intronic variants of GRIN2A associated with schizophrenia (Ripke et al., 2014, Trubetskoy et al., 2022). Besides GRIN2A, also other common variants have been identified affecting genes which are relevant for NMDAR functioning such as serine racemase (SRR), the enzyme converting L-serine in the NMDAR co-agonist D-serine. Other implicated enzymes include DAO (D-amino acid oxidase, degrades D-serine), and DAOA (G72, an activator of DAO). Additionally, genes like DTNP1 (dysbindin), NRG1, NRG2, and ERBB4 regulate NMDAR and synaptic plasticity. Reduced DTNP1 levels have been found in schizophrenia patients and animal models, linking it to decreased NMDAR expression and cognitive deficits. Increased NRG1–ErbB4 signaling has also been observed in patients with schizophrenia, which inhibits NMDAR activity, especially via GluN2B subunits (Bygrave et al. 2019).

Another schizophrenia-associated gene, DISC1, has been linked to NMDA receptor dysfunction through its interaction with SRR. Ma et al. (2012) demonstrated in mice that mutant DISC1 leads to the degradation of SRR. This degradation results in a D-serine deficiency, which is associated with behavioral changes suggestive of impaired NMDAR signaling (Ma et al. 2013).

Apart from genetic alterations, NMDAR downregulation could be caused by environmental factors, such as oxidative stress, excess of kynurenic acid, and hypoxia (Nakazawa and Sapkota 2020). Altered NMDAR expression was also demonstrated in animal studies, modelling schizophrenia via maternal stress induction (Espana et al. 2021).

Proteins like PSD-95 and SAP102 anchor NMDARs to the postsynaptic membrane and regulate their function. Disruptions in these scaffolding proteins or signaling pathways (e.g., CaMKII or Src-family kinases) can impair NMDAR function, leading to reduced synaptic efficacy.

4.2.6 iPSC-based models of schizophrenia

The use of iPSC-derived models to investigate E/I imbalance in schizophrenia offers unique insights into the cellular mechanisms underlying this complex disorder. By modelling synaptic or neural circuity disruptions in patient-derived neurons, iPSC-based studies provide a valuable platform for dissecting the contributions of genetic and molecular factors to this imbalance.

(Heider et al. 2024) conducted research on iPSC-derived excitatory/inhibitory cocultures, finding that SZ clones exhibited enhanced network activity compared to the more regular pacing of the control clones. This increased network communication may stem from heightened excitatory input into GABAergic neurons, impacting co-culture dynamics. While altered network burst behavior has been associated with SZ in several iPSC studies, the direction of these changes remains ambiguous. Supporting these findings, a mutation model

of the SZ risk gene SETD1A showed improved network connectivity in mutant cultures with induced NGN2 and AD2 neurons (S. Wang et al. 2022). Conversely, two studies involving patient-derived iPSCs (Kathuria et al. 2019) and 16p11.2 duplication iPSCs (Parnell et al. 2023) demonstrated reduced network bursting in SZ cultures, linked to deficits in interneurons and glutamatergic neurons, respectively. Thus, the relationship between synaptic deficits and network activity in SZ remains unclear. One possible explanation is that iPSC-derived neuronal cultures may exhibit altered dynamics during maturation. As a result, the observed differences could stem from the cultures being at different developmental stages, with impairments either improving or worsening due to compensatory mechanisms over time.

(Sawada et al. 2020) provided another perspective by examining iPSC-derived neurons from twin pairs discordant for schizophrenia and schizoaffective disorder (SAD). For SAD, at later neurodevelopment stages, there was an altered E/I-balance; while soma size and dendritic arborization of 120-day-old neurons did not differ between twins, SAD neurons exhibited more dendritic protrusions, suggesting accelerated maturation. There were no notable differences in the frequency or amplitude of synaptic currents, but a decrease in the density of SYN1+Homer1+ excitatory synapses and an increase in SYN1+Gephyrin+ inhibitory puncta were observed. The proportion of GABAergic neurons was markedly higher, and treatment with LiCl reduced both the density of inhibitory synapses and the GABAergic population. SZ NPCs showed upregulation of 35 genes, including those encoding both pre- and postsynaptic GABA receptor subunits and ion channels. The discussion highlights dysregulation in neuronal development, emphasizing that deficits in the WNT signaling pathway precede reduced proliferation and a significant dorsal-ventral fate shift, tilting the E/I balance toward GABAergic interneuron differentiation. The findings emphasize the importance of studying both excitatory and inhibitory synapse development in understanding how E/I balance is disrupted in schizophrenia.

These findings collectively underscore the utility of iPSC-derived models in capturing the E/I imbalance observed in schizophrenia. While the exact nature of network disruptions remains unresolved, the ability to model these processes using patient-derived neurons allows for a detailed examination of the pathways involved. iPSCs provide a unique platform to study neuronal development, synaptic function, and the impact of genetic mutations in a human-relevant system, offering unparalleled insights into the cellular mechanisms of schizophrenia. However, the variability in findings across different studies highlights the need for further research to reconcile these discrepancies and to more precisely define the nature of E/I dysregulation in schizophrenia.

In conclusion, iPSC-based models have proven to be an invaluable resource for studying the intricate E/I dynamics in schizophrenia, offering a human-based system to explore genetic and molecular contributions to the disorder. Given their ability to recapitulate disease-relevant phenotypes, more studies employing iPSCs are warranted to further elucidate the mechanisms driving E/I imbalance and to uncover novel therapeutic targets for this debilitating condition.

4.3 Limitations

There are several limitations to our study. First, while HEK cells are widely used to study the biophysics of ion channels, they represent a highly simplified model. HEK cells lack the complex cellular architecture and specialized compartments of neurons, such as dendrites and axons, which are critical for the functional context of NaV1.2 in native neuronal networks. The membrane composition and intracellular environment of HEK cells may also differ from those of neurons, potentially impacting channel trafficking, localization, and modulation. As a result, the electrophysiological data obtained from HEK cells might not fully recapitulate the behavior of NaV1.2 in a more physiologically relevant environment.

Moreover, HEK cells are not capable of firing action potentials, a key function of neurons. Therefore, while we were able to assess biophysical properties of the channel variants, we were unable to evaluate their impact on neuronal excitability. To address this limitation, future studies could involve incorporating these NaV1.2 mutations into more complex models, such as iPSC-derived neurons or genetically engineered mice, which would allow for a more comprehensive analysis of their functional effects within a neuronal network.

Additionally, to maintain precise measurements and allow for comparative analyses between different constructs, we used a reduced extracellular solution, which is not entirely reflective of physiological conditions. While this approach facilitated controlled comparisons, the deviation from native conditions may influence how well the results translate to in vivo scenarios.

The limitations of using iPSC-derived neurons for studying schizophrenia are multifaceted. One key issue is the potential loss of the patient's original epigenetic signature during the reprogramming process. While this could help remove medication effects and other confounding factors, it also eliminates the influence of environmental exposures, which are critical for understanding disease pathology in real-world contexts. Furthermore, correlating the age of the cultured cells to the actual developmental stage of neurons in the human brain is challenging, as maturation criteria can vary from study to study.

Another limitation is that 2D iPSC-derived neuron cultures fail to fully replicate the complex 3D architecture and signaling interactions that occur in the human brain. This simplified system may overlook critical cell-cell interactions and network dynamics essential for a complete understanding of schizophrenia mechanisms. To mitigate this, co-cultures that include various neuronal subtypes and glial cells can be employed, although achieving precise control over the differentiation into specific neuronal subtypes remains difficult. The exact identity of neurons derived from iPSCs can vary, making it hard to ensure reproducibility across experiments.

Moreover, a lack of standardized protocols and validation criteria for iPSC-derived neurons across different research groups contributes to inconsistency in results. This variability makes it difficult to directly compare findings from separate studies and hinders the establishment of robust disease models.

Finally, the short-term nature of most iPSC cultures limits the ability to study the long-term progression of schizophrenia. These cultures primarily represent early developmental stages of the disease, which may occur far before the disorder manifests clinically. Addressing these limitations, such as through long-term cultures and the use of 3D systems or organoids, will be critical for improving the translational relevance of iPSC-based models for psychiatric research.

5 Conclusion and outlook

This project focused on understanding the excitation/inhibition (E/I) imbalance characteristic of schizophrenia, a neuropsychiatric disorder linked to neural circuit dysregulation. Two complementary model systems were employed to explore distinct aspects of this imbalance.

First, by utilizing heterologous expression in HEK cells, we investigated schizophrenia-associated variants in the voltage-gated sodium channel NaV1.2. Our findings revealed a loss-of-function effect to varying degrees for all tested variants, indicating their potential to disrupt the E/I-balance in neurons — a mechanism that may contribute to schizophrenia pathophysiology. Future studies should incorporate these findings into computational models of neurons to better understand how these variants might affect excitability. Additionally, implementing these variants in iPSC-based neurons to assess their excitability directly would provide further insights.

Second, we generated two iPSC lines from schizophrenia patients exhibiting NMDAR-related phenotypes and successfully differentiated them into neurons. We established a protocol to explore the NMDAR hypofunction hypothesis of schizophrenia using these iPSC-derived neurons, offering a valuable platform for investigating how NMDAR dysfunction may drive disease mechanisms. Moving forward, we plan to measure NMDA receptor function in neurons derived from schizophrenia patients and compare this to healthy controls. This will enable us to confirm the presence of NMDAR hypofunction in patients with relevant fMRI phenotypes, deepening our understanding of schizophrenia's molecular basis and potentially improving the diagnostics efficiency. We then aim to assess the effects of various NMDAR and GABA receptor agonists and antagonists on these cultures, ultimately to inform better therapeutic strategies.

6 References

Ahmad, Ruhel et al. 2018. “Tracing Early Neurodevelopment in Schizophrenia with Induced Pluripotent Stem Cells.” *Cells* 7(9).

Alexander, Ryan P.D., and Derek Bowie. 2021. “Intrinsic Plasticity of Cerebellar Stellate Cells Is Mediated by NMDA Receptor Regulation of Voltage-Gated Na+ Channels.” *Journal of Physiology* 599(2): 647–65.

American Psychological Association. 2017. “Clinical Practice Guideline for the Treatment of Posttraumatic Stress Disorder (PTSD).” *Washington, DC: APA, Guideline Development Panel for the Treatment of Posttraumatic Stress Disorder in Adults.*: 139. https://www.apa.org/ptsd-guideline/ptsd.pdf%0Ahttps://www.apa.org/about/offices/directorates/guidelines/ptsd.pdf.

Asadollahi, R. et al. 2023. “Pathogenic SCN2A Variants Cause Early-Stage Dysfunction in Patient-Derived Neurons.” *Human Molecular Genetics* 32(13): 2192–2204.

Bagal, Sharan K. et al. 2015. “Voltage Gated Sodium Channels as Drug Discovery Targets.” *Channels* 9(6): 360–66.

Balakrishna, Thivia, and David Curtis. 2020. “Assessment of Potential Clinical Role for Exome Sequencing in Schizophrenia.” *Schizophrenia Bulletin* 46(2): 328–35.

Begemann, Anaïs et al. 2019. “Further Corroboration of Distinct Functional Features in SCN2A Variants Causing Intellectual Disability or Epileptic Phenotypes.” *Molecular medicine (Cambridge, Mass.)* 25(1): 6.

Belforte, Juan E. et al. 2010. “Postnatal NMDA Receptor Ablation in Corticolimbic Interneurons Confers Schizophrenia-like Phenotypes.” *Nature Neuroscience* 13(1): 76–83.

Ben-Shalom, Roy et al. 2017. “Opposing Effects on NaV1.2 Function Underlie Differences Between SCN2A Variants Observed in Individuals With Autism Spectrum Disorder or Infantile Seizures.” *Biological Psychiatry* 82(3): 224–32. http://dx.doi.org/10.1016/j.biopsych.2017.01.009.

Berecki, Géza et al. 2018. “Dynamic Action Potential Clamp Predicts Functional Separation in Mild Familial and Severe de Novo Forms of SCN2A Epilepsy.” *Proceedings of the National Academy of Sciences of the United States of America* 115(24): E5516–25.

———. 2022. “Functional Correlates of Clinical Phenotype and Severity in Recurrent SCN2A Variants.” *Communications Biology* 5(1): 1–13.

Berg, Anne T. et al. 2024. “Expanded Clinical Phenotype Spectrum Correlates with Variant Function in SCN2A-Related Disorders.” *Brain* 147(8): 2761–74. https://doi.org/10.1093/brain/awae125.

Brauner, Jan M. et al. 2014. “Risperidone Inhibits Voltage-Gated Sodium Channels.” *European Journal of Pharmacology* 728(1): 100–106. http://dx.doi.org/10.1016/j.ejphar.2014.01.062.

Brennand, Kristen J. et al. 2011. “Modelling Schizophrenia Using Human Induced Pluripotent Stem Cells.” *Nature* 473(7346): 221–25.

Brown, Carolyn Nicole et al. 2021. “Characterization of Six CaMKIIα Variants Found in Patients with Schizophrenia.” *iScience* 24(10): 103184. https://doi.org/10.1016/j.isci.2021.103184.

Bygrave, Alexei M. et al. 2019. “Can N-Methyl-D-Aspartate Receptor Hypofunction in Schizophrenia Be Localized to an Individual Cell Type?” *Frontiers in Psychiatry* 10(November): 1–23.

Cannon, Stephen C. 2017. Handbook of experimental pharmacology *Voltage-Gated Sodium Channels: Structure, Function and Channelopathies*.

Cantrell, Angela R., Jenny Y. Ma, Todd Scheuer, and William A. Catterall. 1996. “Muscarinic Modulation of Sodium Current by Activation of Protein Kinase C in Rat Hippocampal Neurons.” *Neuron* 16(5): 1019–26.

Carroll, Liam S. et al. 2016. “Mutation Screening of SCN2A in Schizophrenia and Identification of a Novel Loss-of-Function Mutation.” *Psychiatric Genetics* 26(2): 60–65.

Catterall, William A. 2000. “From Ionic Currents to Molecular Mechanisms: The Structure and Function of Voltage-Gated Sodium Channels.” *Neuron* 26(1): 13–25.

Catterall, William A. 2023. “Voltage Gated Sodium and Calcium Channels: Discovery, Structure, Function, and Pharmacology.” *Channels* 17(1): 1–23. https://doi.org/10.1080/19336950.2023.2281714.

Cestèle, Sandrine et al. 2001. “Neutralization of Gating Charges in Domain II of the Sodium Channel α Subunit Enhances Voltage-Sensor Trapping by a β-Scorpion Toxin.” *Journal of General Physiology* 118(3): 291–301.

Clairfeuille, Thomas et al. 2019. “Structural Basis of A-Scorpion Toxin Action on Na v Channels.” *Science* 363(6433).

Correll, Christoph U., and Nina R. Schooler. 2020. “Negative Symptoms in Schizophrenia: A Review and Clinical Guide for Recognition, Assessment, and Treatment.” *Neuropsychiatric Disease and Treatment* 16: 519–34.

Dalmau, Josep et al. 2019. “An Update on Anti-NMDA Receptor Encephalitis for Neurologists and Psychiatrists: Mechanisms and Models.” *The Lancet Neurology* 18(11): 1045–57.

Das, Dhanjit K. et al. 2015. “Genetic and Morphological Features of Human IPSC-Derived Neurons with Chromosome 15q11.2 (BP1-BP2) Deletions.” *Complex Psychiatry* 1(2): 116–23.

Dong, Bin, Yang Yue, Han Dong, and Yuehui Wang. 2023. “N-Methyl-D-Aspartate Receptor Hypofunction as a Potential Contributor to the Progression and Manifestation of Many Neurological Disorders.” *Frontiers in Molecular Neuroscience* 16(June).

Duncan, Gary E. et al. 2004. “Deficits in Sensorimotor Gating and Tests of Social Behavior in a Genetic Model of Reduced NMDA Receptor Function.” *Behavioural Brain Research* 153(2): 507–19.

Espana, Agnès et al. 2021. “Alteration of NMDA Receptor Trafficking as a Cellular Hallmark of Psychosis.” *Translational Psychiatry* 11(1): 1–11. http://dx.doi.org/10.1038/s41398-021-01549-7.

Föhr, Karl Josef et al. 2022. “Block of Voltage-Gated Sodium Channels by Aripiprazole in a State-Dependent Manner.” *International Journal of Molecular Sciences* 23(21).

Forrest, Marc P. et al. 2017. “Open Chromatin Profiling in HiPSC-Derived Neurons Prioritizes Functional Noncoding Psychiatric Risk Variants and Highlights Neurodevelopmental Loci.” *Cell Stem Cell* 21(3): 305-318.e8. http://dx.doi.org/10.1016/j.stem.2017.07.008.

Friston, Karl, Harriet R. Brown, Jakob Siemerkus, and Klaas E. Stephan. 2016. “The Dysconnection Hypothesis (2016).” *Schizophrenia Research* 176(2–3): 83–94. http://dx.doi.org/10.1016/j.schres.2016.07.014.

Fromer, Menachem et al. 2014. “De Novo Mutations in Schizophrenia Implicate Synaptic Networks.” *Nature* 506(7487): 179–84.

Gaebler, Arnim J. et al. 2023. “Functional Connectivity Signatures of NMDAR Dysfunction in Schizophrenia—Integrating Findings from Imaging Genetics and Pharmaco-FMRI.” *Translational Psychiatry* 13(1).

Gao, Wen Jun, Sha Sha Yang, Nancy R. Mack, and Linda A. Chamberlin. 2022. “Aberrant Maturation and Connectivity of Prefrontal Cortex in Schizophrenia—Contribution of NMDA Receptor Development and Hypofunction.” *Molecular Psychiatry* 27(1): 731–43.

Gazina, Elena V. et al. 2015. “‘Neonatal’ Nav1.2 Reduces Neuronal Excitability and Affects Seizure Susceptibility and Behaviour.” *Human Molecular Genetics* 24(5): 1457–68.

Goldin, A L. 2002. “Evolution of Na+ Channels.” *Journal of Experimental Biology* 584: 575–84. http://jeb.biologists.org/content/jexbio/205/5/575.full.pdf.

Grunwald, Lena Marie et al. 2019. “Comparative Characterization of Human Induced Pluripotent Stem Cells (HiPSC) Derived from Patients with Schizophrenia and Autism.” *Translational Psychiatry* 9(1). http://dx.doi.org/10.1038/s41398-019-0517-3.

Halene, T. B. et al. 2009. “Assessment of NMDA Receptor NR1 Subunit Hypofunction in Mice as a Model for Schizophrenia.” *Genes, Brain and Behavior* 8(7): 661–75.

Hanemaaijer, Naomi A.K. et al. 2020. “Ca2+ Entry through Nav Channels Generates Submillisecond Axonal Ca2+ Signaling.” *eLife* 9: 1–75.

Hansen, Kasper B et al. 2018. “Structure, Function, and Allosteric Modulation of NMDA Receptors.” *Journal of General Physiology* 150(8): 1081–1105.

Harms, Lauren, Gloria G. Parras, Patricia T. Michie, and Manuel S. Malmierca. 2021. “The Role of Glutamate Neurotransmission in Mismatch Negativity (MMN), A Measure of Auditory Synaptic Plasticity and Change-Detection.” *Neuroscience* 456: 106–13. https://doi.org/10.1016/j.neuroscience.2020.01.046.

Harris, Julia J., and David Attwell. 2012. “The Energetics of CNS White Matter.” *Journal of Neuroscience* 32(1): 356–71.

Harvey, Philip D. 2014. “Disability in Schizophrenia: Contributing Factors and Validated Assessments.” *Journal of Clinical Psychiatry* 75(SUPPL. 1): 15–20.

Hashimoto, Takanori et al. 2003. “Gene Expression Deficits in a Subclass of GABA Neurons in the Prefrontal Cortex of Subjects with Schizophrenia.” *Journal of Neuroscience* 23(15): 6315–26.

Heider, Johanna et al. 2024. “Aberrant Neuronal Connectivity and Network Activity of Neurons Derived from Patients with Idiopathic Schizophrenia.” *Neurobiology of Disease* 201(May).

Heinemann, Stefan H. et al. 1992. “Calcium Channel Characteristics Conferred on the Sodium Channel by Single Mutations.” *Nature* 356(6368): 441–43.

Hellier, Jennifer L. 2014. “Sodium Channels.” In *The Brain, the Nervous System, and Their Diseases: Volumes 1-3*, ed. Bernd Fritzsch. Elsevier, 974–78.

Hoischen, Alexander, Niklas Krumm, and Evan E. Eichler. 2014. “Prioritization of Neurodevelopmental Disease Genes by Discovery of New Mutations.” *Nature Neuroscience* 17(6): 764–72.

Hoptman, Matthew J. 2015. “Impulsivity and Aggression in Schizophrenia: A Neural Circuitry Perspective with Implications for Treatment.” *CNS Spectrums* 20(3): 280–86. https://www.cambridge.org/core/journals/cns-spectrums/article/impulsivity-and-aggression-in-schizophrenia-a-neural-circuitry-perspective-with-implications-for-treatment/D1CE7890DB86B39490B9FBAEB3A5A36C.

Howrigan, Daniel P. et al. 2020. “Exome Sequencing in Schizophrenia-Affected Parent–Offspring Trios Reveals Risk Conferred by Protein-Coding de Novo Mutations.” *Nature Neuroscience* 23(2): 185–93. http://dx.doi.org/10.1038/s41593-019-0564-3.

Hribkova, Hana et al. 2022. “Clozapine Reverses Dysfunction of Glutamatergic Neurons Derived From Clozapine-Responsive Schizophrenia Patients.” *Frontiers in Cellular Neuroscience* 16(February): 1–16.

Hu, Wenqin et al. 2009. “Distinct Contributions of Nav1.6 and Nav1.2 in Action Potential Initiation and Backpropagation.” *Nature Neuroscience* 12(8): 996–1002.

Hyun, Jo Soo, Takafumi Inoue, and Akiko Hayashi-Takagi. 2020. “Multi-Scale Understanding of Nmda Receptor Function in Schizophrenia.” *Biomolecules* 10(8): 1–14.

Insel, Thomas R. 2010. “Rethinking Schizophrenia.” *Nature* 468(7321): 187–93.

Ishii, Takaya et al. 2019. “In Vitro Modeling of the Bipolar Disorder and Schizophrenia Using Patient-Derived Induced Pluripotent Stem Cells with Copy Number Variations of PCDH15 and RELN.” *eNeuro* 6(5).

Javitt, Daniel C., and Stephen R. Zukin. 1991. “Recent Advances in the Phencyclidine Model of Schizophrenia.” *American Journal of Psychiatry* 148(10): 1301–8.

Jiang, Daohua, Jiangtao Zhang, and Zhanyi Xia. 2022. “Structural Advances in Voltage-Gated Sodium Channels.” *Frontiers in Pharmacology* 13(June): 1–16.

de Jonge, Jeroen C., Christiaan H. Vinkers, Hilleke E. Hulshoff Pol, and Anouk Marsman. 2017. “GABAergic Mechanisms in Schizophrenia: Linking Postmortem and In Vivo Studies.” *Frontiers in Psychiatry* 8(AUG): 118.

Kahn, René S. et al. 2015. “Schizophrenia.” *Nature Reviews Disease Primers* 1(November).

Kamiya, Kazusaku et al. 2004. “A Nonsense Mutation of the Sodium Channel Gene SCN2A in A Patient with Intractable Epilepsy and Mental Decline.” *Journal of Neuroscience* 24(11): 2690–98.

Kasai, Norio et al. 2001. “Genomic Structures of SCN2A and SCN3A - Candidate Genes for Deafness at the DFNA16 Locus.” *Gene* 264(1): 113–22.

Kathuria, Annie et al. 2019. “Synaptic Deficits in IPSC-Derived Cortical Interneurons in Schizophrenia Are Mediated by NLGN2 and Rescued by N-Acetylcysteine.” *Translational Psychiatry* 9(1). http://dx.doi.org/10.1038/s41398-019-0660-x.

———. 2020. “Transcriptomic Landscape and Functional Characterization of Induced Pluripotent Stem Cell-

Derived Cerebral Organoids in Schizophrenia." *JAMA Psychiatry* 77(7): 745–54.

Kearney, Jennifer A. et al. 2002. "Molecular and Pathological Effects of a Modifier Gene on Deficiency of the Sodium Channel Scn8a (Nav1.6)." *Human Molecular Genetics* 11(22): 2765–75.

Kim, Nam Shik et al. 2021. "Pharmacological Rescue in Patient IPSC and Mouse Models with a Rare DISC1 Mutation." *Nature Communications* 12(1): 1–11. http://dx.doi.org/10.1038/s41467-021-21713-3.

Kim, Yangsik, Esther Yang, and Hyun Kim. 2022. "Impaired Prepulse Inhibition in Mice with IRSp53 Deletion in Modulatory Neurotransmitter Neurons Including Dopamine, Acetylcholine, Oxytocin, and Serotonin." *Biochemical and Biophysical Research Communications* 586: 114–20. https://doi.org/10.1016/j.bbrc.2021.11.049.

Kohlnhofer, B et al. 2021. "The Schizophrenia Variant V1282F in SCN2A Causes Functional Impairment of NaV1.2." *Journal of Schizophrenia Research* 7(1): 1–7.

Kole, Maarten H.P., and Greg J. Stuart. 2012. "Signal Processing in the Axon Initial Segment." *Neuron* 73(2): 235–47. http://dx.doi.org/10.1016/j.neuron.2012.01.007.

Körner, Jannis et al. 2024. "Molecular Architecture of Human Dermal Sleeping Nociceptors." *bioRxiv*. http://biorxiv.org/content/early/2024/12/20/2024.12.20.629638.abstract.

Kostritskii, Andrei Y., and Jan Philipp Machtens. 2023. "Domain- and State-Specific Shape of the Electric Field Tunes Voltage Sensing in Voltage-Gated Sodium Channels." *Biophysical Journal* 122(10): 1807–21. https://doi.org/10.1016/j.bpj.2023.04.013.

Labrie, Viviane, and John C. Roder. 2010. "The Involvement of the NMDA Receptor D-Serine/Glycine Site in the Pathophysiology and Treatment of Schizophrenia." *Neuroscience and Biobehavioral Reviews* 34(3): 351–72.

Lahti, Adrienne C., Bettylou Koffel, David Laporte, and Carol A. Tamminga. 1995. "Subanesthetic Doses of Ketamine Stimulate Psychosis in Schizophrenia." *Neuropsychopharmacology* 13(1): 9–19.

Lakhan, Shaheen E., Mario Caro, and Norell Hadzimichalis. 2013. "NMDA Receptor Activity in Neuropsychiatric Disorders." *Frontiers in Psychiatry* 4(JUN): 1–7.

Large, Charles H. et al. 2011. "The Efficacy of Sodium Channel Blockers to Prevent Phencyclidine-Induced Cognitive Dysfunction in the Rat: Potential for Novel Treatments for Schizophrenia." *Journal of Pharmacology and Experimental Therapeutics* 338(1): 100–113.

Laursen, Thomas Munk, Merete Nordentoft, and Preben Bo Mortensen. 2014. "Excess Early Mortality in Schizophrenia." *Annual Review of Clinical Psychology* 10: 425–48.

Li, Jinchen et al. 2016. "Genes with de Novo Mutations Are Shared by Four Neuropsychiatric Disorders Discovered from NPdenovo Database." *Molecular Psychiatry* 21(2): 290–97.

Li, Tun et al. 2014. "Action Potential Initiation in Neocortical Inhibitory Interneurons." *PLoS Biology* 12(9).

Lisman, John E. et al. 2008. "Circuit-Based Framework for Understanding Neurotransmitter and Risk Gene Interactions in Schizophrenia." *Trends in Neurosciences* 31(5): 234–42.

Ma, T. M. et al. 2013. "Pathogenic Disruption of DISC1-Serine Racemase Binding Elicits Schizophrenia-like Behavior via D-Serine Depletion." *Molecular Psychiatry* 18(5): 557–67.

Malaspina, Dolores et al. 2001. "Advancing Paternal Age and the Risk of Schizophrenia." *Archives of General Psychiatry* 58(4): 361–67.

Maroof, Asif M. et al. 2013. "Directed Differentiation and Functional Maturation of Cortical Interneurons from Human Embryonic Stem Cells." *Cell Stem Cell* 12(5): 559–72. http://dx.doi.org/10.1016/j.stem.2013.04.008.

Marsman, Anouk et al. 2014. "GABA and Glutamate in Schizophrenia: A 7 T 1H-MRS Study." *NeuroImage: Clinical* 6: 398–407. http://dx.doi.org/10.1016/j.nicl.2014.10.005.

Martínez-Hernández, José et al. 2013. "Polarised Localisation of the Voltage-Gated Sodium Channel Na v1.2 in Cerebellar Granule Cells." *Cerebellum* 12(1): 16–26.

Mason, Emily R. et al. 2019. "Resurgent and Gating Pore Currents Induced by De Novo SCN2A Epilepsy

Mutations." *eNeuro* 6(5).

Matas, Emmanuel, Deakin John Francis William, and Carla Tatiana Toro. 2021. "Abnormal Expression of Post-Synaptic Proteins in Prefrontal Cortex of Patients with Schizophrenia." *Neuroscience Letters* 745(January): 135629. https://doi.org/10.1016/j.neulet.2021.135629.

Mattheisen, Glynis B., Timur Tsintsadze, and Stephen M. Smith. 2018. "Strong G-Protein-Mediated Inhibition of Sodium Channels." *Cell Reports* 23(9): 2770–81. https://doi.org/10.1016/j.celrep.2018.04.109.

McCutcheon, Robert A., John H. Krystal, and Oliver D. Howes. 2020. "Dopamine and Glutamate in Schizophrenia: Biology, Symptoms and Treatment." *World Psychiatry* 19(1): 15–33.

McGrath, John J. et al. 2014. "A Comprehensive Assessment of Parental Age and Psychiatric Disorders." *JAMA Psychiatry* 71(3): 301–9.

Merritt, Kate et al. 2016. "Nature of Glutamate Alterations in Schizophrenia a Meta-Analysis of Proton Magnetic Resonance Spectroscopy Studies." *JAMA Psychiatry* 73(7): 665–74.

Mi, Zhen et al. 2019. "Alterations of Electrophysiological Properties and Ion Channel Expression in Prefrontal Cortex of a Mouse Model of Schizophrenia." *Frontiers in Cellular Neuroscience* 13(December): 1–11.

Miao, Pu et al. 2020. "Electrophysiological Features: The next Precise Step for SCN2A Developmental Epileptic Encephalopathy." *Molecular Genetics and Genomic Medicine* 8(7): 1–12.

Molnár, Hajnalka et al. 2024. "A Comparison of Visual and Acoustic Mismatch Negativity as Potential Biomarkers in Schizophrenia." *Scientific Reports* 14(1): 1–11. https://doi.org/10.1038/s41598-023-49983-5.

Moy, Sheryl S., Antonio Perez, Beverly H. Koller, and Gary E. Duncan. 2006. "Amphetamine-Induced Disruption of Prepulse Inhibition in Mice with Reduced NMDA Receptor Function." *Brain Research* 1089(1): 186–94. http://dx.doi.org/10.1016/j.brainres.2006.03.073.

Nakamura, Kazuyuki et al. 2013. "Clinical Spectrum of SCN2A Mutations Expanding to Ohtahara Syndrome." *Neurology* 81(11): 992–98.

Nakazawa, Kazu, and Kiran Sapkota. 2020. "The Origin of NMDA Receptor Hypofunction in Schizophrenia." *Pharmacology and Therapeutics* 205: 107426. https://doi.org/10.1016/j.pharmthera.2019.107426.

Narla, S. T. et al. 2017. "Common Developmental Genome Deprogramming in Schizophrenia — Role of Integrative Nuclear FGFR1 Signaling (INFS)." *Schizophrenia Research* 185: 17–32. http://dx.doi.org/10.1016/j.schres.2016.12.012.

Nevian, Thomas, and Bert Sakmann. 2006. "Spine Ca2+ Signaling in Spike-Timing-Dependent Plasticity." *Journal of Neuroscience* 26(43): 11001–13.

Ni, Peiyan et al. 2020. "IPSC-Derived Homogeneous Populations of Developing Schizophrenia Cortical Interneurons Have Compromised Mitochondrial Function." *Molecular Psychiatry* 25(11): 2873–88. http://dx.doi.org/10.1038/s41380-019-0423-3.

Ogiwara, Ikuo et al. 2018. "Nav1.2 Haplodeficiency in Excitatory Neurons Causes Absence-like Seizures in Mice." *Communications Biology* 1(1).

Pan, Yanling, and Theodore R. Cummins. 2020. "Distinct Functional Alterations in SCN8A Epilepsy Mutant Channels." *Journal of Physiology* 598(2): 381–401.

Papassotiropoulos, A. et al. 2011. "A Genome-Wide Survey of Human Short-Term Memory." *Molecular Psychiatry* 16(2): 184–92.

Papp-Hertelendi, Renáta et al. 2018. "First Report on the Association of SCN1A Mutation, Childhood Schizophrenia and Autism Spectrum Disorder without Epilepsy." *Psychiatry Research* 270(June): 1175–76. https://doi.org/10.1016/j.psychres.2018.07.028.

Park, Hae Jeong, Inyeong Choi, and Kang Hyun Leem. 2021. "Decreased Brain Ph and Pathophysiology in Schizophrenia." *International Journal of Molecular Sciences* 22(16): 8–11.

Park, James M. et al. 2021. "Migratory Cortical Interneuron-Specific Transcriptome Abnormalities in Schizophrenia." *Journal of Psychiatric Research* 137(February): 111–16. https://doi.org/10.1016/j.jpsychires.2021.02.054.

Parnell, Euan et al. 2023. “Excitatory Dysfunction Drives Network and Calcium Handling Deficits in 16p11.2 Duplication Schizophrenia Induced Pluripotent Stem Cell–Derived Neurons.” *Biological Psychiatry* 94(2): 153–63. https://doi.org/10.1016/j.biopsych.2022.11.005.

Paulsen, Bruna da Silveira et al. 2012. “Altered Oxygen Metabolism Associated to Neurogenesis of Induced Pluripotent Stem Cells Derived from a Schizophrenic Patient.” *Cell Transplantation* 21(7): 1547–59.

Payandeh, Jian. 2018. “Progress in Understanding Slow Inactivation Speeds Up.” *Journal of General Physiology* 150(9): 1235–38.

Ph, D et al. 2014. “Schizophrenia Cases and Controls.” 71(6): 647–56.

Pierri, Joseph N., Adil S. Chaudry, Tsung Ung W. Woo, and David A Lewis. 1999. “Alterations in Chandelier Neuron Axon Terminals in the Prefrontal Cortex of Schizophrenic Subjects.” *American Journal of Psychiatry* 156(11): 1709–19.

Preller, Katrin H., Joachim Scholpp, Andreas Wunder, and Holger Rosenbrock. 2024. “Neuroimaging Biomarkers for Drug Discovery and Development in Schizophrenia.” *Biological Psychiatry* 96(8): 666–73. https://doi.org/10.1016/j.biopsych.2024.01.009.

Qi, Yuchen et al. 2017. “Combined Small-Molecule Inhibition Accelerates the Derivation of Functional Cortical Neurons from Human Pluripotent Stem Cells.” *Nature Biotechnology* 35(2): 154–63.

Räsänen, Sami et al. 2000. “Sex Differences in Schizophrenia: A Review.” *Nordic Journal of Psychiatry* 54(1): 37–45.

Rees, Elliott et al. 2019. “Targeted Sequencing of 10,198 Samples Confirms Abnormalities in Neuronal Activity and Implicates Voltage-Gated Sodium Channels in Schizophrenia Pathogenesis.” *Biological Psychiatry* 85(7): 554–62.

———. 2021. “Schizophrenia, Autism Spectrum Disorders and Developmental Disorders Share Specific Disruptive Coding Mutations.” *Nature Communications* 12(1): 1–9. http://dx.doi.org/10.1038/s41467-021-25532-4.

Rees, Elliott, Michael C. O’Donovan, and Michael J. Owen. 2015. “Genetics of Schizophrenia.” *Current Opinion in Behavioral Sciences* 2: 8–14. http://dx.doi.org/10.1016/j.cobeha.2014.07.001.

Ren, Dejian et al. 2001. “A Prokaryotic Voltage-Gated Sodium Channel.” *Science* 294(5550): 2372–75.

Robicsek, O. et al. 2013. “Abnormal Neuronal Differentiation and Mitochondrial Dysfunction in Hair Follicle-Derived Induced Pluripotent Stem Cells of Schizophrenia Patients.” *Molecular Psychiatry* 18(10): 1067–76.

Robicsek, Odile et al. 2018. “Isolated Mitochondria Transfer Improves Neuronal Differentiation of Schizophrenia-Derived Induced Pluripotent Stem Cells and Rescues Deficits in a Rat Model of the Disorder.” *Schizophrenia Bulletin* 44(2): 432–42.

Roussos, Panos et al. 2016. “Activity-Dependent Changes in Gene Expression in Schizophrenia Human-Induced Pluripotent Stem Cell Neurons.” *JAMA Psychiatry* 73(11): 1180–88.

Rühlmann, Annika H. et al. 2020. “Uncoupling Sodium Channel Dimers Restores the Phenotype of a Pain-Linked Nav1.7 Channel Mutation.” *British Journal of Pharmacology* 177(19): 4481–96.

Rusconi, Raffaella et al. 2007. “Modulatory Proteins Can Rescue a Trafficking Defective Epileptogenic Nav1.1 Na+ Channel Mutant.” *Journal of Neuroscience* 27(41): 11037–46.

Samanta, Debopam, and Raghu Ramakrishnaiah. 2015. “De Novo R853Q Mutation of SCN2A Gene and West Syndrome.” *Acta Neurologica Belgica* 115(4): 773–76. http://dx.doi.org/10.1007/s13760-015-0454-8.

Sawada, Tomoyo et al. 2020. “Developmental Excitation-Inhibition Imbalance Underlying Psychoses Revealed by Single-Cell Analyses of Discordant Twins-Derived Cerebral Organoids.” *Molecular Psychiatry* 25(11): 2695–2711. http://dx.doi.org/10.1038/s41380-020-0844-z.

Schlief, Thomas, Roland Schönherr, Keiji Imoto, and Stefan H. Heinemann. 1996. “Pore Properties of Rat Brain II Sodium Channels Mutated in the Selectivity Filter Domain.” *European Biophysics Journal* 25(2): 75–91.

von Schoubye, Nadia Lybøl et al. 2018. “The Sodium Channel Activator Lu AE98134 Normalizes the Altered Firing Properties of Fast Spiking Interneurons in Dlx5/6+/− Mice.” *Neuroscience Letters* 662(October 2017): 29–35.

Shen, Huaizong et al. 2017. “Structure of a Eukaryotic Voltage-Gated Sodium Channel at near-Atomic Resolution.” *Science* 355(6328).

Sheng, Shaohu et al. 2000. “Characterization of the Selectivity Filter of the Epithelial Sodium Channel.” *Journal of Biological Chemistry* 275(12): 8572–81. http://dx.doi.org/10.1074/jbc.275.12.8572.

Shepard, Nate et al. 2024. “Differential Functional Consequences of GRIN2A Mutations Associated with Schizophrenia and Neurodevelopmental Disorders.” *Scientific Reports* 14(1): 1–10. https://doi.org/10.1038/s41598-024-53102-3.

Singh, Tarjinder et al. 2022. “Rare Coding Variants in Ten Genes Confer Substantial Risk for Schizophrenia.” *Nature* 604(7906): 509–16.

Sjöström, Per Jesper, and Sacha B. Nelson. 2002. “Spike Timing, Calcium Signals and Synaptic Plasticity.” *Current Opinion in Neurobiology* 12(3): 305–14.

Snyder, Melissa A., and Wen Jun Gao. 2013. “NMDA Hypofunction as a Convergence Point for Progression and Symptoms of Schizophrenia.” *Frontiers in Cellular Neuroscience* 7(MAR): 1–12.

Snyder, Solomon H. 1980. “Phencyclidine.” 285(June): 355–56.

Sokolov, Stanislav, Todd Scheuer, and William A. Catterall. 2005. “Ion Permeation through a Voltage-Sensitive Gating Pore in Brain Sodium Channels Having Voltage Sensor Mutations.” *Neuron* 47(2): 183–89.

Sontag, Stephanie et al. 2017. “Modelling IRF8 Deficient Human Hematopoiesis and Dendritic Cell Development with Engineered IPS Cells.” *Stem Cells* 35(4): 898–908.

Spratt, Perry et al. 2021. “Paradoxical Hyperexcitability from NaV1.2 Sodium Channel Loss in Neocortical Pyramidal Cells.” *Cell Reports* 36(5): 109483. https://doi.org/10.1016/j.celrep.2021.109483.

Spratt, Perry W.E. et al. 2019. “The Autism-Associated Gene Scn2a Contributes to Dendritic Excitability and Synaptic Function in the Prefrontal Cortex.” *Neuron* 103(4): 673-685.e5. https://doi.org/10.1016/j.neuron.2019.05.037.

Stephan, Klaas E., Karl J. Friston, and Chris D. Frith. 2009. “Dysconnection in Schizophrenia: From Abnormal Synaptic Plasticity to Failures of Self-Monitoring.” *Schizophrenia Bulletin* 35(3): 509–27.

Suddaby, Jessica S., Josh Silver, and Joyce So. 2019. “Understanding the Schizophrenia Phenotype in the First Patient with the Full SCN2A Phenotypic Spectrum.” *Psychiatric Genetics* 29(3): 91–94.

Sun, Ye Ming, Isabelle Favre, Laurent Schild, and Edward Moczydlowski. 1997. “On the Structural Basis for Size-Selective Permeation of Organic Cations through the Voltage-Gated Sodium Channel: Effect of Alanine Mutations at the DEKA Locus on Selectivity, Inhibition by Ca2+ and H+, and Molecular Sieving.” *Journal of General Physiology* 110(6): 693–715.

Suzuki, Toshimitsu et al. 2024. “Inversed Effects of Nav1.2 Deficiency at Medial Prefrontal Cortex and Ventral Tegmental Area for Prepulse Inhibition in Acoustic Startle Response.” *Molecular Neurobiology* 61(2): 622–34. https://doi.org/10.1007/s12035-023-03610-6.

Takahashi, Kazutoshi, and Shinya Yamanaka. 2006. “Induction of Pluripotent Stem Cells from Mouse Embryonic and Adult Fibroblast Cultures by Defined Factors.” *Cell* 126(4): 663–76.

Takaori, Toru et al. 2017. “Two Mild Cases of Dravet Syndrome with Truncating Mutation of SCN1A.” *Brain and Development* 39(1): 72–74. http://dx.doi.org/10.1016/j.braindev.2016.07.006.

Tatsukawa, Tetsuya et al. 2019. “Scn2a Haploinsufficient Mice Display a Spectrum of Phenotypes Affecting Anxiety, Sociability, Memory Flexibility and Ampakine CX516 Rescues Their Hyperactivity.” *Molecular Autism* 10(1): 1–15.

Taylor, J. A. et al. 2017. “Auditory Prediction Errors as Individual Biomarkers of Schizophrenia.” *NeuroImage: Clinical* 15(February): 264–73. https://doi.org/10.1016/j.nicl.2017.04.027.

Topol, Aaron et al. 2015. “Altered WNT Signaling in Human Induced Pluripotent Stem Cell Neural Progenitor Cells Derived from Four Schizophrenia Patients.” *Biological Psychiatry* 78(6): e29–34.

Trubetskoy, Vassily et al. 2022. “Mapping Genomic Loci Implicates Genes and Synaptic Biology in Schizophrenia.” *Nature* 604(7906): 502–8.

Vargas, Ernesto et al. 2012. “An Emerging Consensus on Voltage-Dependent Gating from Computational Modeling and Molecular Dynamics Simulations.” *Journal of General Physiology* 140(6): 587–94.

Vilin, Yury Y., Colin H. Peters, and Peter C. Ruben. 2012. “Acidosis Differentially Modulates Inactivation in Nav1.2, Nav1.4, and Nav1.5 Channels.” *Frontiers in Pharmacology* 3 JUN(June): 1–21.

Visiers, Irache, Benjamin B. Braunheim, and Harel Weinstein. 2000. “Prokink: A Protocol for Numerical Evaluation of Helix Distortions by Proline.” *Protein Engineering* 13(9): 603–6.

Wang, Shan et al. 2022. “Loss-of-Function Variants in the Schizophrenia Risk Gene SETD1A Alter Neuronal Network Activity in Human Neurons through the CAMP/PKA Pathway.” *Cell Reports* 39(5): 110790. https://doi.org/10.1016/j.celrep.2022.110790.

Wang, Xiuhuan et al. 2024. “Exploration on the Potential Efficacy and Mechanism of Methyl Salicylate Glycosides in the Treatment of Schizophrenia Based on Bioinformatics, Molecular Docking and Dynamics Simulation.” *Schizophrenia* 10(1): 1–20. http://dx.doi.org/10.1038/s41537-024-00484-y.

Wang, Yang et al. 2010. “Genetic Polymorphisms in the SCN8A Gene Are Associated with Suicidal Behavior in Psychiatric Disorders in the Chinese Population.” *The World Journal of Biological Psychiatry* 11(8): 956–63. http://www.tandfonline.com/doi/full/10.3109/15622971003801936.

Weickert, C. S. et al. 2013. “Molecular Evidence of N-Methyl-D-Aspartate Receptor Hypofunction in Schizophrenia.” *Molecular Psychiatry* 18(11): 1185–92.

Westenbroek, Ruth E., Dawn K. Merrick, and William A. Catterall. 1989. “Differential Subcellular Localization of the RI and RII Na+ Channel Subtypes in Central Neurons.” *Neuron* 3(6): 695–704.

Whitaker, William R.J. et al. 2001. “Comparative Distribution of Voltage-Gated Sodium Channel Proteins in Human Brain.” *Molecular Brain Research* 88(1–2): 37–53.

Willner, P. 1997. “The Dopamine Hypothesis of Schizophrenia: Current Status, Future Prospects.” *International Clinical Psychopharmacology* 12(6): 297–308.

Wolff, Markus et al. 2017. “Genetic and Phenotypic Heterogeneity Suggest Therapeutic Implications in SCN2A-Related Disorders.” *Brain* 140(5): 1316–36.

Wolff, Markus, Catherine Cassé-Perrot, and Charlotte Dravet. 2006. “Severe Myoclonic Epilepsy of Infants (Dravet Syndrome): Natural History and Neuropsychological Findings.” *Epilepsia* 47(SUPPL. 2): 45–48.

Xu, Meng Yi, and Albert H.C. Wong. 2018. “GABAergic Inhibitory Neurons as Therapeutic Targets for Cognitive Impairment in Schizophrenia.” *Acta Pharmacologica Sinica* 39(5): 733–53. http://dx.doi.org/10.1038/aps.2017.172.

Yamagata, Tetsushi et al. 2017. “Nav1.2 Is Expressed in Caudal Ganglionic Eminence-Derived Disinhibitory Interneurons: Mutually Exclusive Distributions of Nav1.1 and Nav1.2.” *Biochemical and Biophysical Research Communications* 491(4): 1070–76. http://dx.doi.org/10.1016/j.bbrc.2017.08.013.

Yin, Luping et al. 2017. “Selective Modulation of Axonal Sodium Channel Subtypes by 5-HT1A Receptor in Cortical Pyramidal Neuron.” *Cerebral Cortex* 27(1): 509–21.

Yu, Diana Xuan et al. 2014. “Modeling Hippocampal Neurogenesis Using Human Pluripotent Stem Cells.” *Stem Cell Reports* 2(3): 295–310. http://dx.doi.org/10.1016/j.stemcr.2014.01.009.

Zhang, Wen Bo et al. 2016. “Fyn Kinase Regulates GluN2B Subunit-Dominant NMDA Receptors in Human Induced Pluripotent Stem Cell-Derived Neurons.” *Scientific Reports* 6(March): 1–11. http://dx.doi.org/10.1038/srep23837.

Zheng, Yang et al. 2021. “A Heart Failure-Associated SCN5A Splice Variant Leads to a Reduction in Sodium Current Through Coupled-Gating With the Wild-Type Channel.” *Frontiers in Physiology* 12(March).

Zick, Jennifer L. et al. 2018. “Blocking NMDAR Disrupts Spike Timing and Decouples Monkey Prefrontal Circuits: Implications for Activity-Dependent Disconnection in Schizophrenia.” *Neuron* 98(6): 1243-1255.e5. https://doi.org/10.1016/j.neuron.2018.05.010.

Zuccoli, Giuliana S. et al. 2023. “Mitochondrial, Cell Cycle Control and Neuritogenesis Alterations in an IPSC-Based Neurodevelopmental Model for Schizophrenia.” *European Archives of Psychiatry and Clinical Neuroscience* 273(8): 1649–64. https://doi.org/10.1007/s00406-023-01605-x.

Zybura, Agnes S., Firoj K. Sahoo, Andy Hudmon, and Theodore R. Cummins. 2022. "CaMKII Inhibition Attenuates Distinct Gain-of-Function Effects Produced by Mutant Nav1.6 Channels and Reduces Neuronal Excitability." *Cells* 11(13): 2108. https://www.mdpi.com/2073-4409/11/13/2108.

Websites:

Name	Link	Aim
Basic Local Alignement Search Tool (BLAST)	https://blast.ncbi.nlm.nih.gov/Blast.cgi	To compare the NaV isoforms
The Residue Interaction Network Generator (RING)	https://ring.biocomputingup.it	To assess interactions between amino acids
ChatGPT	https://chatgpt.com	To correct the grammar and get inspiration

7 List of figures

Figure 1. Sodium channel involvement in the action potential generation11
Figure 2. VGSC topology model, highlighting selectivity filter in yellow, pore-forming helixes in pink, and voltage-sensing helixes in blue.12
Figure 3. VGSC structure and activation schemes13
Figure 4. Inactivation particle reception cite and the IFM-motif of VGSCs14
Figure 5. Topological scheme of the NaV1.2 with marked positions of the 3 schizophrenia-associated variants18
Figure 6. Subunit arrangement and 3D structure of GluN1/2 NMDA receptors19
Figure 7. Scheme of E/I imbalance induced by NMDAR hypofunction in inhibitory neurons20
Figure 8. Key signaling pathways define neuronal fate along the anterior-posterior and dorsal-ventral axes24
Figure 9. Scheme of differentiation utilizing dual SMAD inhibition25
Figure 10. Activation analysis of HEK293T cells expressing NaV1.2 WT, R850P, V1282F or S1656P38
Figure 11. Inactivation analysis of HEK293T cells expressing NaV1.2 WT, R850P or V1282F39
Figure 12. Subthreshold depolarization analysis of HEK293T cells expressing NaV1.2 WT, R850P or V1282F41
Figure 13. Use-dependence analysis of HEK293T cells expressing NaV1.2 WT, R850P, or V1282F42
Figure 14: Recovery from fast inactivation analysis of HEK293T cells expressing NaV1.2 WT or R850P44
Figure 15: Reprogramming of PBMCs of two patients with SZ48
Figure 16. Cortical differentiation of reprogrammed iPSCs50

Figure 17. iPS-derived neurons express Glutamatergic markers and GluN153
Figure 18. Functional characterization of iPSC-derived neurons from control cell lines54
Figure 19. GABAergic differentiation of control iPSCs.56

8 List of tables

Table 1: Voltage-gated sodium channel isoforms – protein name, gene name, protein size and predominant tissue expression15
Table 2. Locations of the variants in the Nav1.2 channel in patients with the schizophrenia phenotype18
Table 3. Medium composition schedule for the glutamatergic differentiation30
Table 4. Medium composition schedule for the GABAergic differentiation30
Table 5. Primary antibodies used for the immunocytochemistry of iPSCs and iPSC-derived neurons.34
Table 6. List of forward and reverse primers used for the RT-qPCR experiments.35
Table 7. Statistics of the activation results.37
Table 8. Statistics of the inactivation results40
Table 9 Statistics of the ramp-elicted current results40
Table 10. Statistics of the use-dependence results43
Table 11. Statistics of the fit parameters of individual cells subjected to recovery from fast inactivation protocol45
Table 12: Summary of Reprogramming and Characterization of iPSC Clones Derived from Patient 1 PBMCs46
Table 13: Summary of Reprogramming and Characterization of iPSC Clones Derived from Patient 1 PBMCs**Fehler! Textmarke nicht definiert.**

9 Declaration of authorship

I, Mariia Suslova, declare that this thesis and the work presented in it are my own and has been generated by me as the result of my own original research. It was conducted in the Institute of Neurophysiology at the Uniklinik RWTH Aachen between August 2020 and March 2025. I do solemnly swear that:

1. This work was done wholly or mainly while in candidature for the doctoral degree at this faculty and university;

2. Where any part of this thesis has previously been submitted for a degree or any other qualification at this university or any other institution, this has been clearly stated;

3. Where I have consulted the published work of others or myself, this is always clearly attributed;

4. Where I have quoted from the work of others or myself, the source is always given. This thesis is entirely my own work, with the exception of such quotations;

5. I have acknowledged all major sources of assistance;

6. Where the thesis is based on work done by myself jointly with others, I have made clear exactly what was done by others and what I have contributed myself;

7. Some of this work has been published before submission

March 15, 2025

Mariia Suslova

10 Appendix

During my time as a PhD student at RWTH, I contributed to the following publications and presentations:

- **Suslova M**, Gaebler A. Translational investigation of excitatory/inhibitory imbalance in schizophrenia and its relationship with impulsivity. Talk presented in 2023 at the 7th Spring School of the International Research Training Group 2150 “The Neuroscience of Modulating Aggression and Impulsivity in Psychopathology”
- **Suslova M**, Yazdani G, Lampert A, Gaebler A. Electrophysiological characterization of schizophrenia-associated variants in NaV1.2 sodium channel. *In preparation*; presented at the World Congress Of Psychiatry in 2022
- Gaebler A, Fakour N, Stöhr F, **Suslova M**, […], Mathiak K. Brain signatures of the schizophrenia-associated genetic variant of the NMDA receptor suggest excitatory / inhibitory imbalance – An integrative study combining imaging genetics, pharmaco-fMRI and whole brain gene expression data. doi.org/10.1038/s41398-023-02344-2

Acknowledgments

First and foremost, I would like to express my deepest gratitude to my supervisors. To Jun.-Prof. Dr. Arnim Gaebler, for his patience and humorous guidance combined with sometimes intimidatingly wide expertise he was always willing to share throughout this project. Without him I would neither start, nor finish. To Prof. Dr. Angelika Lampert for her neverending enthusiasm in sharing her profound knowledge of NaVs, empathy, and kindness. Every conversation was inspiring and calming, I wish every PhD student could have such experience. To Prof. Dr. Martin Zenke for very friendly attitude and insightful discussions. To Prof. Dr. Marc Spehr, and Prof. Maria Fyta for making my defence take place. To Prof. Dr. Klaus Mathiak, Prof. Dr. Ute Habel and Prof. Dr. Raquel Gur for accepting me into the program and providing me with a great oppotunity to make my experience even more international.

A sincere thank you to my colleagues in the AG Lampert for a nice working atmosphere. Thank you, Anika, for teaching me stem cell culture and tirelessly answering my questions. Thank you, Petra, for helping with all the molecular biology. Thank you, Brigitte, for perfecting my sterile work skills and always greeting me by my name. Thank you, Marina, for always being nice and friendly. Thank you, Raya, for deep discussions about horrible tattoos and the most wild parties. Thank you, Jannis, for dedicating time for explanations and especially for teaching me to try and fix things myself. Thank you Sofie, for crazy 6 AM swims and great sense of humour. Thank you, Fiona, Vishal, Aylin, Andie, Srijeeta, Stas, Marlene, Nina, Lena, Lennart, Markos, Idil, and others, for being nice to be around.

I am also grateful to my family for their undestructable belief in my genius and for motivating me to keep going – especially by taking out loans in the hope that I would one day repay them with my Nobel Prize. To my sister Yulia, for being an ambassador of my most important life choices. To Andrey, for helping me with the thesis corrections while being funny. To Anna and Sergey for taking a great care of my homeless… self, providing both support and much-needed discipline during the writing of this thesis.

Finally, I would like to thank Daniel for always willing to share his intelligence, for his patience in listening to all the whining I did while writing this thesis, and for being my bestie.